To the Graduate Council:

I am submitting herewith a thesis written by Israel Jerome Huff entitled, "Anti-amyloid Antibodies as Probes of Amyloid Fibril Structure." I have examined the final electronic copy of this thesis for form and content and recommend that it be accepted in partial fulfillment of the requirements for the degree of Master of Science, with a major in Biochemistry, Cellular, and Molecular Biology.

Ronald Wetzel

_____

Major Professor

We have read this thesis and recommend its acceptance:

Chris Dealwis

_____

Elizabeth Howell

_____

Stephen Kennel

_____

Accepted for the Council:

Anne Mayhew

_____

Vice Chancellor and Dean of Graduate Studies

(Original signatures are on file with official student records.)

Anti-amyloid Antibodies as Probes of Amyloid Fibril Structure

A Thesis

Presented for the

Master of Science Degree

The University of Tennessee, Knoxville

Israel Jerome Huff

May, 2005

Abstract

Amyloid fibrils have been implicated in numerous human diseases including Alzheimer's disease (AD). The fibrils found in AD are formed by the misfolding and aggregation of the Aβ peptide. Amyloid fibrils are potentially important causative agents, but high-resolution structural information is not yet available. This research analyzes amyloid fibril structure via two different experimental routes. In one approach, ELISA techniques were utilized to study the binding of available anti-amyloid antibodies to single-residue proline and alanine mutant fibrils of Aβ. Binding to some cysteine and modified cysteine mutants was also tested. These data were compared to fibril stability, hydrophobicity change, ThT binding, and changes in fibril protection. There appeared to be no correlation to these, except for weak correlation to ThT binding. The results at specific residues did stand out as significant. WO1 and PGA1 binding appeared to be affected by both charge and structural changes at specific residues. For WO1, mutations at residues 16, 27, and 28 were shown to have the greatest impact on binding. For PGA1, mutations at residues 27, 28, 30, 31, and 36 were shown to do so. Upon closer examination, the enhanced binding to mutants at residues 16 and 36 appeared to be due to structural changes. Binding to mutants at residue 27 could

be due to structural changes, but these results are not entirely clear. Binding to mutants at resides 28, 30, and 31 appeared to be due to charge differences. Binding of WO1 was found to be sensitive to salt and pH conditions suggesting electrostatic interactions are important to binding. Mutations in the Aβ sequence have a strong impact on binding. The basis of these results is still not entirely clear, but they could be important clues to the nature of fibril structure or the fibril epitopes recognized by the antibodies. Since the number of existing antibodies reacting with fibrils is limited, phage display techniques were employed to develop new binding reagents with a larger range of binding properties for fibrils. A library of antibody fragments was constructed in a phage display system and was selected for members with fibril-binding properties. Although the library was validated, to date, no suitable antibodies have been isolated.

Table of Contents

Chapter		Page
I.	**Introduction**	1
	Alzheimer's Disease	1
	Amyloid Fibrils	4
	Other Amyloid Diseases	8
	The Aβ Peptide	11
	Aβ Amyloid	14
	Anti-amyloid Antibodies	18
	Phage Display Principles	22
II.	**Methods**	32
	Section 1. Anti-amyloid Antibodies	32
	Determining Antibody Binding Properties	32
	Determining Antibody Concentration	41
	Antibody Fragmentation	45
	Section 2. Phage Display	47
	The pComb3X Phagemid Vector	47
	PCR Random Mutagenesis	49
	Amplification of Helper Phage	56
	Phage Selection	59
	Phage ELISA	69
	Production of Soluble Fab	74
III.	**Antibody Binding Results and Discussion**	80
	Salt and pH Effects on WO1 Binding to Aβ Fibrils	80
	Binding of rIgM WO2 Fragments to Aβ Fibrils	85
	PGA1 Binding to Aβ Amyloid versus Polyglutamine Aggregates	88
	WO1 and PGA1 Binding to Fibrils of Aβ Proline Mutants	90
	WO1 and PGA1 Binding to Fibrils of Aβ Alanine Mutants	103
	PGA1 Binding to Cysteine and Modified Cysteine Mutants of Aβ	107
	Correlation Analysis	111
	Conclusions	139
IV.	**Phage Display Results and Discussion**	142
	Verification of Phage Production and Anti-M13 Antibody Specificity	143
	Phage Library Production	143

Phage Clone Selection 148
Antibody Clone Sequences 151
Soluble Expression 155
Conclusions 160
List of References 161
Appendices 165
Vita 169

List of Tables

Table		Page
1.	Buffers for salt and pH effects experiments.	38
2.	PCR primers.	53
3.	PGA1 binding to cysteine mutant fibrils.	109
4.	Comparison table of antibody binding to fibril stability.	114
5.	Comparison table of antibody binding to hydrophobicity change.	120
6.	Comparison table of antibody binding to ThT binding.	128
7.	Comparison table of antibody binding to difference in protected residues.	134
8.	Clone heavy chain sequences.	152
9.	Clone light chain sequences.	153

List of Figures

Figure		Page
1.	The cross-β conformation.	7
2.	APP metabolism.	13
3.	The Aβ(1-43) amino acid sequence.	13
4.	Aβ amyloid protofilament model.	17
5.	Major immunoglobulin classes.	19
6.	A diagram of the M13 bacteriophage.	25
7.	A diagram of phagemid display.	28
8.	A diagram of the ELISA protocol.	34
9.	ELISA plate layout.	36
10.	An example of ELISA data.	40
11.	The pComb3X phagemid display vector.	48
12.	Salt effect on WO1 binding.	82
13.	pH effect on WO1 binding.	84
14.	Binding of WO2 rIgM fragments to Aβ fibrils.	87
15.	PGA1 binding to Aβ fibrils versus polyglutamine aggregates.	89
16.	Summary of WO1 binding to proline mutants of Aβ.	92
17.	WO1 binding to proline mutants of Aβ.	93-5
18.	Aβ protofilament cross-section: WO1 and PGA1 binding to mutant fibrils.	97-98
19.	Summary of PGA1 binding to proline mutants of Aβ.	101
20.	Summary of WO1 binding to alanine mutants of Aβ.	104
21.	Summary of PGA1 binding to alanine mutants of Aβ.	106
22.	Comparison plots of antibody binding to fibril stability.	113
23.	WO1 and PGA1 binding to proline and alanine mutant fibrils versus fibril stability.	116-117
24.	Comparison plots of antibody binding to hydrophobicity change.	119
25.	WO1 and PGA1 binding to proline and alanine mutant fibrils versus hydrophobicity change.	121-122
26.	Comparison plots of antibody binding to ThT binding.	127
27.	WO1 and PGA1 binding to proline and alanine mutant fibrils versus ThT binding.	130-131
28.	Comparison plots of antibody binding to difference in protected residues.	133
29.	Two Aβ amyloid protofilament models.	135

30. Verification of anti-M13 Ab specificity. 144
31. Phage pool ELISAs. 147
32. Phage clone binding to Aβ amyloid fibrils. 149
33. Phage clone binding to polyglutamine aggregates. 150
34. Anti-HA western blots. 156-7
35. Anti-human IgG (heavy and light chain specific) western blot. 159

List of Abbreviations

AA	amyloid A
AD	Alzheimer's disease
AFM	atomic force microscopy
APP	amyloid precursor protein
βME	β-mercaptoethanol
BSA	bovine serum albumin
bp	base pair
cDNA	complementary deoxyribonucleic acid
CDR	complementarity determining region
C_H1	heavy chain constant domain 1
C_L	light chain constant domain
CMT	carboxymethylthio
$\Delta\Delta G$	free energy difference
$\Delta\Delta G_{app}$	free energy difference approximation
DNA	deoxyribonucleic acid
EDTA	ethylenediaminetetraacetic acid
ELISA	enzyme-linked immunosorbent assay
EM	electron micrograph
Fab	light chain plus Fd fragment
Fd	heavy chain C_H1 plus V_H domains
FAP	familial amyloid polyneuropathy
fmol	femtomole
HA	hemagglutinin
HD exchange	hydrogen-deuterium exchange
H6	hexahistidine
HRP	horseradish peroxidase
IAA	iodoacetic acid
IAPP	islet amyloid polypeptide
IgG	immunoglobulin G
IgM	immunoglobulin M
IPTG	isopropyl-β-D-thiogalactopyranoside
κ	kappa
kb	kilobase
KCl	potassium chloride
Kd	dissociation constant
kDa	kilodalton
kV	kilovolt
LB	Luria broth
M	molar

MeI	methyl iodide
mg	milligram
mL	milliliter
mM	millimolar
MOPS	3-(N-Morpholino)propanesulfonic acid
MT	methylthio
MW	molecular weight
NaCl	sodium chloride
Na_2HPO_4	sodium phosphate (dibasic)
ng	nanogram
nm	nanometer
OD	optical density
ORF	open reading frame
PAGE	polyacrylamide gel electrophoresis
PBS	phosphate-buffered saline
PCR	polymerase chain reaction
PEG	polyethylene glycol
pfu	plaque-forming unit
pmol	picomole
psi	pounds per square inch
PVDF membrane	polyvinylidene difluoride membrane
rIgM	reduced IgM
rpm	revolution per minute
SAA	serum amyloid A
SB	Super broth
SD	Shine-Dalgarno sequence
SDS	sodium dodecyl sulfate
ssDNA	single-stranded DNA
Taq	polymerase from *Thermus aquaticus*
ThT	thioflavin T
Tris	tris(Hydroxymethyl)aminomethane
TTR	transthyretin
μ	mu (IgM heavy chain)
μF	microfarad
μg	microgram
μL	microliter
V	volt
V_H	heavy chain variable domain
V_L	light chain variable domain

Chapter I
Introduction

Alzheimer's Disease

Amyloid fibrils have been implicated in numerous human diseases. One of the most prominent of these is Alzheimer's disease (AD). AD is a neurodegenerative disorder characterized by progressively worsening dementia. Affected individuals can suffer among other symptoms: memory loss, difficulty in reasoning, disorientation, and personality changes. It is the leading cause of dementia and is the most common neurodegenerative disease [1]. For the most part, it affects people later in life, though some inheritable forms can take effect in mid-life and even earlier. Indeed, age is the greatest risk factor for AD with up to ten percent of people over 65 and up to fifty percent of people over 85 being affected. The symptoms of AD can be attributed to the extensive neuronal cell death associated with the disease. This cell death and corresponding loss of brain function can result in the deaths of affected individuals. An estimated four million Americans are currently afflicted and millions more will follow in the coming years [1]. The costs in human suffering and medical care make AD a grim and far-reaching disease with disastrous socioeconomic consequences. It is of the utmost

importance that we continue to make headway in our efforts to fight the disease. Much is now known about AD, but continuing research will be required before the effects of the disease can be effectively curbed.

The onset and advancement of Alzheimer's disease can be correlated to the accumulation of the Aβ peptide. It is a 39 to 43 amino acid cleavage product from the amyloid precursor protein (APP) that can accumulate in the brain. This relationship is supported by the fact that all genes currently known to be connected to familial AD influence either Aβ production or deposition [2-4]. Moreover, Aβ(1-42) and Aβ(1-40) are cytotoxic peptides [5-7]. Some studies indicate that increasing levels of insoluble Aβ in the brain relative to the soluble form may be directly related to the development of AD [8]. In addition, Aβ cytotoxicity has been linked to the ability of the peptide to aggregate into amyloid fibrils, which can accumulate in deposits in neural tissue [6]. The form of Aβ found primarily in aggressive, early-onset AD, Aβ(1-42), is much more prone to aggregation than the (1-40) species of late-onset AD [6, 9]. This suggests that an enhanced ability to form amyloid fibrils can lead to a more rapidly progressing disease state [6]. Furthermore, amyloid fibrils have been shown to be

toxic to neurons [10]. This connection between amyloid fibrils, the ubiquitous indicators of AD found in affected neural tissues, and AD pathogenesis led to the development of the amyloid hypothesis of AD. This theory states that it is the buildup of Aβ in amyloid fibrils that leads to the neural tissue degeneration and pathogenesis of AD [11]. There is much evidence supporting the amyloid hypothesis of AD, but there is also evidence pointing away from it.

Some studies suggest the fibrils themselves may not be the direct cause of AD pathogenesis [12]. Bearing in mind that insoluble Aβ appears to take part in AD pathogenesis, it may be that other insoluble Aβ species besides amyloid fibrils are at fault. Amyloid fibril intermediates may actually be responsible for AD pathogenesis [13]. These intermediates include spherical particles as well as protofibrils [14-16]. They may be precursors in the formation of amyloid fibrils [14, 16] or they may be the products of distinct assembly pathways [14]. The protofibrils are of particular interest since there is some evidence suggesting these may be the toxic species. For instance, the 'Arctic' APP mutation associated with a particular familial form of AD has been shown to lead to increased protofibril formation and stability, but not increased fibril formation [17]. Because of the possible role of

protofibrils in AD pathogenesis, they will be further explored within a discussion of amyloid fibrils.

Amyloid Fibrils

Amyloid fibrils were first discovered in human neural tissue and reported by Virchow in 1851 [18]. The name amyloid is a misnomer stemming from the fact that a starch staining technique was originally used to stain the fibrils. The word "amyloid" actually means starch-like. Virchow used the iodine and sulfuric acid technique for staining starches and found that the fibrils stained similar to cellulose [19]. Though we now know the fibrils are made up of proteins, the name amyloid remains in use. Since that initial discovery, more refined techniques have been developed for staining and detecting amyloid fibrils.

Congo Red staining was a significant development to that end. This dye was found to be a specific and sensitive detector of amyloid fibrils by Bennhold in 1922, as it stains the fibrils a bright red [20]. It was later discovered by Divry and Florkin that polarizing optics could be used to observe amyloid fibrils [21]. With this technique, otherwise inconspicuous amyloid deposits in tissue samples can be detected

since they show birefringence. That is, the fibrils have a regular, ordered structure capable of altering the phase of incident light passing through them. By combining these two techniques, using polarizing optics on fibrils stained with Congo Red, it was found that amyloid fibrils have a distinctive green birefringence [22]. The red color exhibited by the dye shifts to green under polarizing optics. Other than the obvious utility this technique provides, it also emphasizes that amyloid fibrils are not amorphous aggregates, but rather highly organized structures.

There are many amyloid diseases and conditions in which amyloid fibrils are present. The proteins responsible for the fibrils vary from one disease to the next. In fact, there are at least 20 different proteins found in humans that are reported to form amyloid fibrils [23]. Though the fibrils in each amyloid disease are composed of different proteins, they share many structural characteristics common to all amyloid fibrils. Cohen and Calkins revealed through electron microscopy studies that amyloid fibrils of many different proteins share a number of common characteristics at the macro scale. The fibrils are highly insoluble, rigid, nonbranching, and of variable lengths up to several μm [22, 23]. They are in the vicinity of 8 to 10 nm in

diameter and are likely made up of two or more protofilaments running in parallel and twisted about one another. These are in the range of about 3 nm in diameter. Protofilaments and protofibrils are separate, distinct species. Protofibrils have been found to be curved fibers 3 to 10 nm wide and up to 200 nm in length [14, 16, 24]. They do not approach the lengths reached by amyloid fibrils and are not subunits of these fibrils.

X-ray fiber diffraction studies were later conducted on a number of different amyloid fibrils to probe the amyloid superstructure. These revealed that amyloid fibrils exhibit a cross-β conformation. That is, the fibrils are rich in β-sheet structure and the β-strands run perpendicular to the fibril axis. In this conformation, the β-strands are hydrogen-bonded into β-sheets lying parallel to the fibril axis (Figure 1). This particular conformation appears to be rare in nature and is more typical of denatured proteins [22]. It has been shown that some insect silks exhibit the cross-β conformation, but their β-strands usually run parallel to the fibril axis [22]. A comparison is shown in figure 1. Perpendicular β-strands are generally reserved to amyloid fibrils. Protofibrils have also been found to be rich in β-sheet structure [13, 25]. This is a brief review of our collective knowledge of amyloid

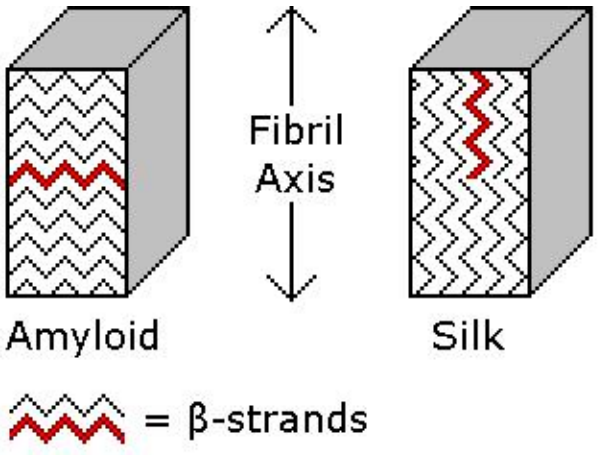


Figure 1. The cross-β conformation. In amyloid fibrils, β-sheets lie parallel to the fibril axis. These are composed of β-strands running perpendicular to the fibril axis. In comparison, insect silks with cross-β structure possess β-strands running parallel to the fibril axis [22]. The β-strands are shown forming β-sheets on the front faces of the fibrils in the diagram. One strand is bold and highlighted in red on each fibril.

fibrils. As previously mentioned, these fibrils are found in many human diseases.

Other Amyloid Diseases

The amyloidogenic protein in each amyloid disease is unique. Furthermore, the means by which each becomes amyloidogenic can differ. The role of the fibrils in each disease, when it is known, can also differ from one disease to the next. A few examples of diseases other than AD marked by the presence of amyloid fibrils are familial amyloid polyneuropathy (FAP), secondary amyloidosis, and type II diabetes. These represent a small cross-section of diseases in which amyloid fibrils are found. Briefly looking at each should provide some insight into the diverse nature of amyloid diseases.

The culprit protein in FAP is transthyretin (TTR), which is normally responsible for transporting retinol-binding protein in addition to thyroxine. Certain mutations in the TTR protein destabilize it such that the normally soluble protein can misfold and become prone to aggregation [26, 27]. The fibrils of TTR can accumulate in many different tissues, but often end up in the heart where the deposits can lead to congestive heart failure. More stable variants of TTR can also

aggregate into amyloid fibrils in the heart, but in these cases the impact is less severe and the age of onset is later in life [26]. Many other diseases can be tied to mutations in fibril-forming proteins [27]. These include familial early-onset AD, Creutzfeldt-Jakob disease, and several others.

Secondary amyloidosis is a condition that occasionally arises in response to extended or severe inflammation. In this disease, the amyloidogenic protein is amyloid A (AA), a proteolytic product of the circulatory precursor serum amyloid A (SAA) [26]. Fibrils of AA are deposited mainly in the spleen, kidneys, and liver where they can cause organ failure. In secondary amyloidosis, severe inflammation and tissue damage lead to ramping of SAA production up to 1000 fold of basal levels. It is not known exactly what drives the conversion of SAA to AA leading to the deposition of AA fibrils. However, it has been suggested that the disease state results from an inability to clear the excess protein [26]. Another amyloid condition marked by protein overproduction is light chain amyloidosis [26].

An example of amyloid as a secondary component of a disease occurs in type II diabetes. The central problem in this disease is

insulin underproduction and insulin resistance leading to dangerously elevated blood glucose levels. The amyloidogenic protein is islet amyloid polypeptide (IAPP), which is normally released into the bloodstream concurrently with insulin to regulate blood glucose levels [26, 28]. In type II diabetes, IAPP can aggregate into amyloid fibrils that are deposited in the pancreas where they can lead to the destruction of insulin-producing β-cells. These fibrils can then exacerbate the pathology of this disease by further hampering insulin production.

It is clear that amyloid fibrils are pervasive in many human diseases. They are not always the defining characteristic of a given disease, such as in type II diabetes, but their impact is nonetheless significant and destructive. Moreover, the constituent proteins in each are varied both in their amino acid sequences and in the causes of their amyloidogenicity. Amyloid fibrils have been under scientific scrutiny for some time and continue to be studied. In the history of amyloid research, many important findings have been made to establish a body of knowledge about these fibrils. Little detailed information about a common amyloid fibril structure is available. However, much more is known about the proteins and peptides that

misfold to form those fibrils. The peptide responsible for AD amyloid fibrils, Aβ, has been thoroughly studied. The fibrils found in AD are composed primarily of misfolded and aggregated Aβ peptide. We have learned a bit more specifically about these fibrils. Before discussing them, it is first helpful to have a basic understanding of the Aβ peptide.

The Aβ Peptide

The Aβ peptide is a cleavage product from the APP, which is a large transmembrane protein found on the surfaces of cells in many different tissues. The exact functions of APP have not yet been established. Furthermore, it has been shown that deletion of the APP gene in mice does not cause early death or a serious disease state [29]. It is possible that this could be due to the existence of several mammalian homologs to this gene [29]. In any case, APP is evolutionarily conserved and expressed in all mammals. This suggests it serves an important role [29]. There are numerous isoforms of APP that arise from alternative splicing of the APP gene. Some such as the 751 and 770 amino acid isoforms are found in numerous cell types while others such as the 695 amino acid isoform are found predominantly in neuronal cells. There is also added variation due to

several post-translational modification of APP [9, 29]. APP metabolism is still further complicated by variable proteolytic cleavage of the extracellular domain. Though the whole of APP metabolism is quite complicated, we are focused only on the products of proteolytic cleavage.

APP can be cleaved at specific sites by the α-, β-, and γ-secretases (Figure 2). First, either α-secretase cleaves 12 residues out from the membrane-spanning domain or β-secretase cleaves 28 residues out. This releases the large soluble α- or β-APP_s domains, respectively. Only when β-secretase cleavage has occured can γ-secretase cleavage result in the Aβ peptide. γ-secretase cleaves about 12 to 14 residues into the membrane-spanning domain, releasing the Aβ peptide [9]. These alternate cleavage patterns are shown in figure 2. The peptide can range in length from 39 to 43 residues [30]. The 43 residue sequence is shown in figure 3. The 40-residue variant is that most commonly found in amyloid fibrils. A number of studies have been conducted on these particular amyloid fibrils.

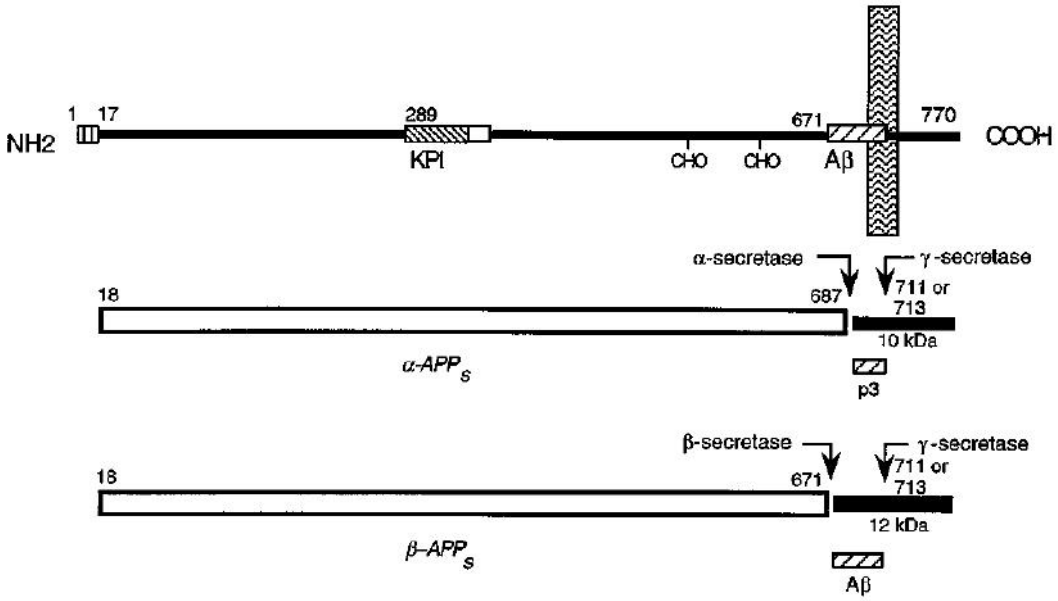


Figure 2. APP metabolism. In this example, a 770 residue isoform is used. Cleavage by β-secretase at position 671 followed by γ-secretase at position 711 to 713 yields the Aβ peptide [9]. (Adapted from Selkoe, D.J., *Amyloid beta-protein and the genetics of Alzheimer's disease.* J Biol Chem, 1996. **271**(31): p. 18295-8.)

DAEFRHDSGY	EVHHQKLVFF	AEDVGSNKGA	IIGLMVGGVV	IAT
10	20	30	40	

Figure 3. The Aβ(1-43) amino acid sequence. In the 40-residue variant, the amyloid core extends roughly from the vicinity of residue 15 to that of residue 36. The remaining amino- and carboxy-terminal residues are solution accessible and are not involved in protected β-sheet structure [31-34].

Aβ Amyloid

Limited proteolysis and hydrogen-deuterium (HD) exchange studies on the 40-residue isoform of Aβ in amyloid fibrils have shown the presence of a stable core [31-33]. The remainder of the peptide is exposed to digestion and HD (hydrogen-deuterium) exchange. Only about half of the residues of the Aβ peptide are involved in protected β-sheet structure in this core. The remaining residues at the amino- and carboxy-terminal ends of the peptide are not involved and are accessible to solvent. These regions span the first 13 to 16 residues at the amino terminus and the last 4 residues at the carboxy terminus [32, 34]. Aβ protofibrils also possess a protected core, though the degree of protection is less [13]. This suggests that protofibril structure may be similar to that of fibrils. The presence of a stable core in amyloid fibrils is further supported by stability studies on fibrils of single proline mutants of Aβ [34].

Scanning proline mutagenesis was used in conducting these experiments [34]. This technique entails generating single proline mutants at each position in the Aβ sequence and growing fibrils from the mutants to be analyzed [34, 35]. These mutants can be very informative since the rigid nature of proline and the fixed angle bend it

imparts to the peptide can have a significant impact on a given protein structure. Prolines are expected to have little impact on unstructured regions and less impact on turn regions when compared to that on β-sheets [34]. In fact, prolines are not usually found in amino acid sequences involved in β-sheet structure where they appear to be highly disfavored [34, 36, 37]. Prolines are more amenable to unstructured regions and turns that are capable of incorporating the rigid amino acid without being distorted. For these reasons, prolines are expected to destabilize fibrils when inserted into positions involved in β-sheet structure [34].

Fibrils from mutant peptides with proline in the amino- and carboxy-terminal regions share, for the most part, stabilities similar to those of wild-type fibrils. Fibrils from mutants in the core sequence are destabilized to varying degrees [34]. It is the amyloid core that is involved in fibril formation and the protected nature of it once incorporated into fibrils highlights the stability of amyloid fibrils. In addition to the residues involved in fibril formation, more is known about Aβ amyloid fibrils. This information has been applied to build a model of amyloid fibril structure. Our model describes the structure of Aβ protofilaments, the constituents of Aβ amyloid fibrils. It is based

on the aforementioned data, particularly the scanning proline mutagenesis and fibril stability results [34]. The model is shown in figure 4. It predicts a tightly packed amyloid core with the unstructured, solvent accessible amino- and carboxy-terminal regions projecting out from it. It is not certain that these regions are unstructured, but their high degree of solvent accessibility suggests they are not involved in the tightly packed and protected β-sheet structure of the amyloid core [31-33]. With that said, the core is the focus of the model.

The model is organized as a parallel β-helix, a structure consisting of β-strands coiling down its length and forming β-sheets between parallel β-strands [34]. In the model, the Aβ rungs are stacked in register down its length [34]. Each Aβ subunit within contains three β-strands separated by two turns forming roughly a triangle (Figure 4). The turns are in the vicinity of residues 22 to 23 and 29 to 30 resulting in three β-strands that are 5 to 7 residues in length: 15-21, 24-28, and 31-36. The core β-sheet structure ends in the region of residues 15 to 16 and 36 to 37. From these regions, the solvent accessible amino- and carboxy-termini extend out from the core. This model aims to describe the structure of Aβ amyloid fibrils,

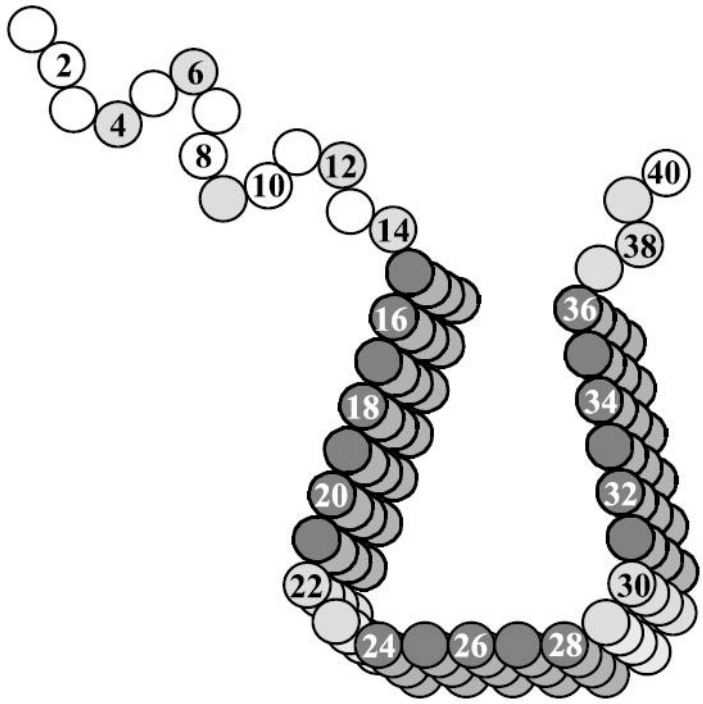


Figure 4. Aβ amyloid protofilament model. Aβ monomers are stacked down the length of the filament with residues 1-14 and 37-40 extending in disorder out from the amyloid core. Residues 15-21, 24-28, and 31-36 comprise β-strands. Residues 22-23 and 29-30 comprise turn regions [34]. (Adapted from Williams, A.D., et al., *Mapping abeta amyloid fibril secondary structure using scanning proline mutagenesis.* J Mol Biol, 2004. **335**(3): p. 833-42.)

though it is not set in stone. As further research is conducted, the model will continue to grow and evolve. The research presented here represents an effort to further our understanding of amyloid fibril structure. Towards that goal, ELISA techniques have been used to study the binding of anti-amyloid antibodies to amyloid fibrils.

Anti-amyloid Antibodies

There are several anti-amyloid antibodies available in our lab [40]. They are all of the IgM class, a pentameric species with ten antigen-binding sites and a molecular weight of around 900 kDa [38]. IgM antibodies are the products of the primary immune response. They are the first antibody species produced in response to a given antigen. Production of antibodies of other classes, including IgG, requires a class switch event involving gene rearrangements to take place [38]. IgG antibodies are the products of the secondary immune response after the class switch event. The IgM molecule is composed of five IgG-like subunits [38]. A diagram of the IgM molecule is shown in figure 5e. The subunits resemble IgG molecules in structure (Figure 5a). Each subunit possesses one μ heavy chain and one light chain held together by disulfide bonds. The heavy chain contains four constant domains, C_H1 through C_H4, and one variable domain, V_H

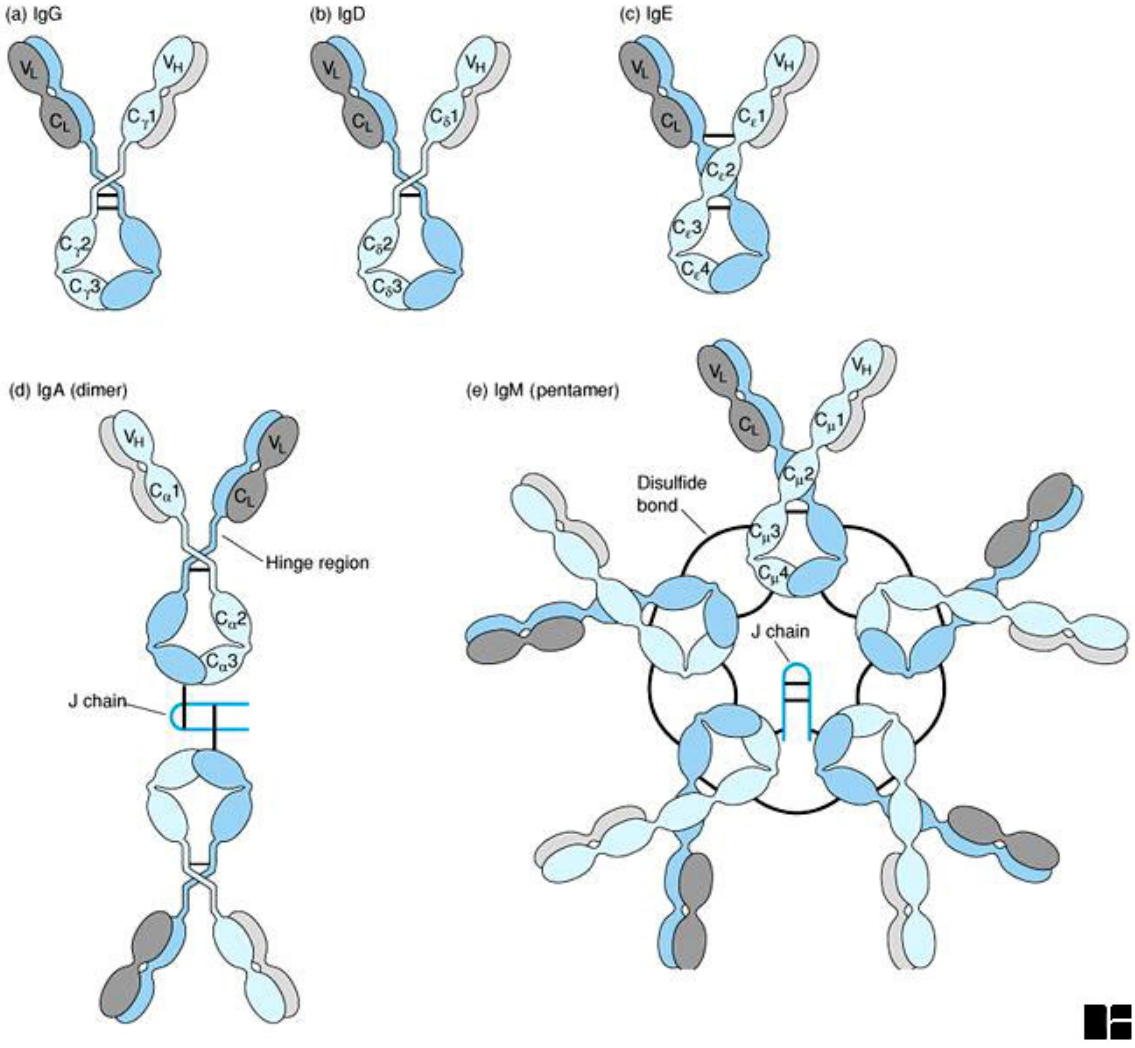


Figure 5. Major immunoglobulin classes. IgM class antibodies (e) are pentameric species when compared to IgG class antibodies (a). They possess ten binding sites compared to two for IgG molecules [38]. (Adapted from Kuby, J., *Immunology*. 3rd Edition ed. 1997.)

(Figure 5e). The light chain contains one constant domain, C_L, and one variable domain, V_L (Figure 5e). The IgG-like subunits are held together by disulfide bonds and additionally by a small polypeptide called the J chain between two of the subunits (Figure 5e). Each of the ten antigen-binding sites is comprised of six complementarity determining regions (CDRs) looping out from the two variable domains, three from the heavy chain and three from the light chain [39]. These loops are responsible for antigen binding and amino acid differences between them provide for binding diversity. In IgM molecules, the multiple binding sites can bind cooperatively to an antigen provided there are a sufficient number of target sites on the antigen. Because each binding site contributes to the overall affinity, its individual affinity need not be as strong. This is the avidity effect. In the case of amyloid fibrils, the apparently regular, repeating structure could potentially accommodate multivalent binding [40]. The avidity effect may be important to amyloid binding. This may explain why, to date, we have only obtained IgM antibodies.

Two well-studied anti-amyloid antibodies are WO1 and WO2, isolated by Dr. Brian O'Nuallain [40]. These antibodies possess κ light chains. They have been shown to possess germ-line sequences by

sequence analysis (Kimberly Salone, unpublished data). That is, the WO1 and WO2 sequences are made up of genes already encoded in the genome and contain variable regions that have not been altered by somatic mutation. The antibodies were isolated from mice immunized with Aβ amyloid fibrils. Monoclonal antibodies were selected so that they bind only amyloid fibrils and not Aβ monomer. This was done by carrying out binding to immobilized Aβ amyloid fibrils in the presence of soluble Aβ monomer. The antibodies were isolated from high-density mouse myeloma cultures. These antibodies also bind amyloid fibrils other than Aβ including amyloids from immunoglobulin light chain, transthyretin, and β2-microglobulin. This binding of different targets by the antibodies is very unusual and supports the notion of a common structural motif among all amyloid fibrils. Furthermore, the apparent structural specificity makes these antibodies very useful in studying amyloid structure. WO1 has recently been shown to bind Aβ protofibrils as well (Dr. Merav Geva, unpublished data). This result coupled with the other characteristics shared between amyloid fibrils and protofibrils indicates that these two species may be structurally related. A study of amyloid fibril structure may provide some insight into protofibril structure as well.

There are limits in the use of the anti-amyloid antibodies. A major limitation is that all of these anti-amyloid antibodies are of the IgM class. Since these are large, flexible, multivalent species, they are poorly suited for many structural studies. For instance, no IgM molecules have yet been crystallized. Due to such limitations, another goal of this thesis work has been to generate novel anti-amyloid antibodies more suitable for these studies. To this end, phage display techniques have been applied.

Phage Display Principles

For our study, phage display was used to generate amyloid-specific Fab antibodies more amenable to structural work. Phage display is a powerful technique that can be used for the affinity selection of specific proteins or peptides out of a massive library. Such a library can exceed sixty billion unique peptides or antibody forms allowing for sampling of a broad range of potential binders to a given target. Furthermore, the selection process is much faster than traditional hybridoma screening and can be completed in a relatively short period of time [41]. Phage display involves two major steps. The first step is the expression of a library of proteins or peptides as a fusion protein with one of the phage coat proteins. This results in a

phage library whose constituents each have mutant proteins or peptides expressed on its coat. The number of copies depends on the phage display system used. The second is the affinity selection of the phage library for a given target. Phage expressing proteins or peptides with high affinity for the substrate can be separated from those with low or no affinity simply by binding the phage to the target and washing away unbound phage. In order to better understand exactly how this process works, one must first understand the M13 bacteriophage that is used in phage display experiments.

The M13 bacteriophage is a filamentous phage that infects *E. coli* by interacting with the F pili found on F+ cells through its five tail fibers. It is used in phage display for several reasons. The structure and life cycle of M13 are well understood [42]. It is easy to work with and manipulate as is the host, *E. coli*. It does not kill the cells after infection, but only slows their growth, allowing production of large amounts of phage by simply culturing infected cells. The phage particles are extremely hardy, resistant to low and high pH as well as other denaturants. Several of the phage coat proteins will tolerate the addition of sequences of peptides or small proteins without disruption of their structures or that of the phage particle [41]. This is key to the

phage display technique. When DNA is added to the phage genome making it longer, the phage particle simply incorporates more of the major coat protein to encompass the added DNA inside the phage filament [41]. The M13 phage is a robust and versatile tool that can easily be manipulated for use in phage display experiments. A discussion of the phage structure and life cycle will shed more light on these advantages and on the inner workings of the phage display technique.

The M13 phage particle consists of a protein coat encapsulating a circular single-stranded DNA (ssDNA) genome. The genome encodes the genes for eleven proteins, five of which comprise the phage coat and five of which are nonstructural proteins involved in viral replication. Gp8 is the 5kDa major coat protein with about 2700 copies per wild-type phage particle (Figure 6, top). It serves to encapsulate the phage genome. Five copies each of gp3 and gp6 are found at one end of the particle and five each of gp7 and gp9 at the other. Gp3, the tail fiber protein, and gp6 are involved in the infection process. Gp7 and gp9 recognize a packaging signal in the phage genome and are necessary for formation of the mature phage particle [42]. Any of these proteins can be modified with the addition of a

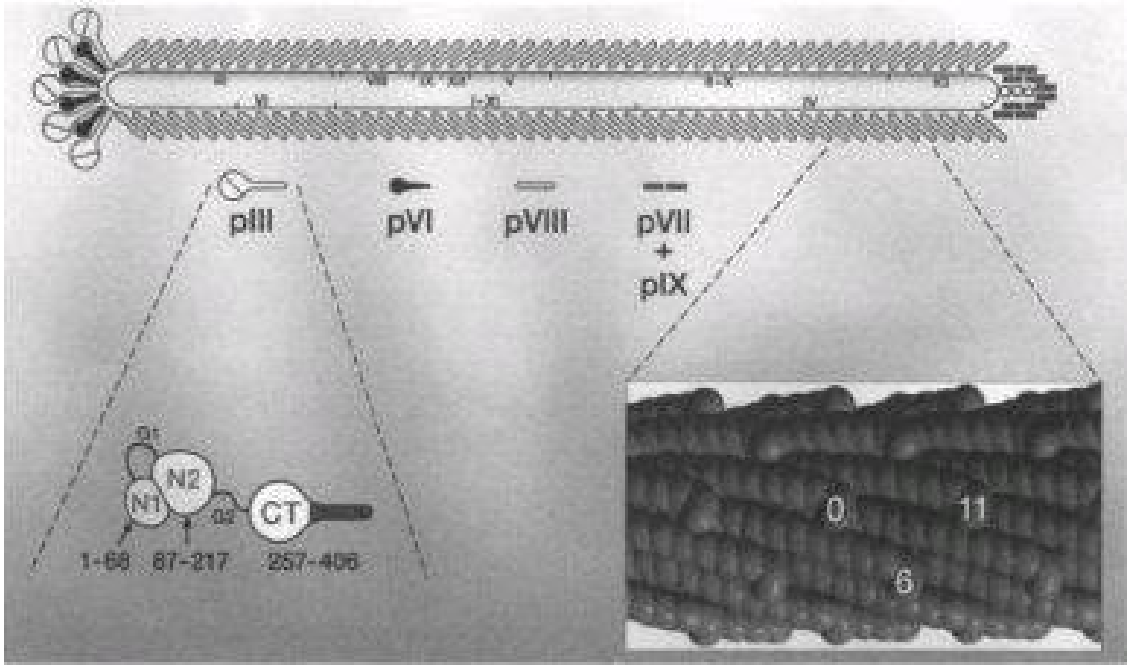


Figure 6. A diagram of the M13 bacteriophage. The phage protein coat encapsulating the phage genome is shown at the top. In the bottom left is a subdomain breakdown of the gp3 coat protein, also called pIII. Gp3 consists of three domains separated by flexible glycine-rich linkers: the amino terminal domain (N1), the middle domain (N2), and the carboxy-terminal domain (CT) [41]. (Adapted from Barbas, C.F., 3rd, et al., *Phage Display: A Laboratory Manual*. 2002.)

sequence to be displayed, but each coat protein has limitations as to how it can be modified [41]. Gp3 is the most commonly modified coat protein in phage display experiments and presents the fewest complications. Gp3 was modified for this work.

Gp3 consists of three domains separated by flexible glycine-rich linkers: the amino terminal domain (N1), the middle domain (N2), and the carboxy-terminal domain (CT) (Figure 6, bottom). N1 and N2 are involved in the process of viral infection while CT is involved in phage coat structure [42]. Any of the three can be deleted or modified for phage display experiments, however CT is typically not modified due to the potential for disruption of phage coat structure [41]. N1 was replaced with the mutants for this work. The domain replacement effectively eliminates the ability of the transgenic gp3 to be involved in the infection of a bacterial host. If all five copies of gp3 were modified, the phage would be incapable of infecting the bacterial host. This is a problem when it comes to proliferation of the selected mutant phage. It is dealt with by the use of phagemid vectors and helper phage.

Phagemid vectors are phage genomes propagated in the form of plasmids that contain a number of modifications. They possess only the transgenic phage coat protein gene and none of the other ten genes (Figure 7, top left). Phagemid vectors, therefore, cannot direct the production of phage particles on their own. They possess the M13 origin of replication and a functional phage-packaging signal just as wild-type phage. They also have a bacterial plasmid origin of replication and an antibiotic resistance marker. This plasmid structure allows phagemid amplification in *E. coli* cells and selection for transfected cells via an antibiotic. When phagemid vectors are transformed into *E. coli* cells, they are replicated as plasmids and do not induce the production of phage particles [41]. Helper phage must be introduced to help production of phage particles.

Helper phage are essentially wild-type phage capable of normal infection all but for a few important differences. They have drastically reduced proliferation potential due to an altered phage-packaging signal that is poorly recognized during phage assembly. Helper phage particles can still be produced, albeit at a much slower rate and titer than phage with wild-type packaging signals. When *E. coli* carrying phagemid vectors are infected with helper phage, they express

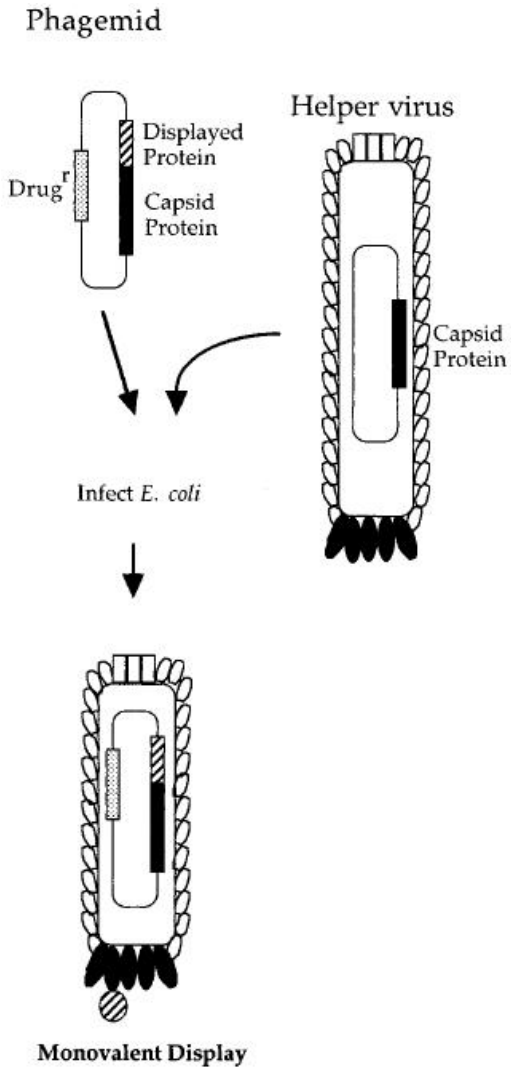


Figure 7. A diagram of phagemid display. *E. coli* cells infected with the phagemid are coinfected with helper phage. The phagemid only provides the one capsid protein gene, which is a fusion with a displayed protein gene. The helper phage genome provides all the other genes necessary to produce phage particles. It also provides the nonmutant form of the gene present in the phagemid. These result in chimeric phage particles, with proteins encoded by both the phagemid and helper phage genome [41]. (Adapted from Hoess, R.H., *Protein design and phage display.* Chem Rev, 2001. **101**(10): p. 3205-18.)

proteins from both types. Since the helper phage carry a different antibiotic resistance marker than the phagemid vectors, kanamycin in the case of the VCSM13 helper phage, *E. coli* cells can be selected for possession of both markers. This prevents the uninfected cells from out-competing the slower growing helper phage infected cells. The helper phage genome guides the production of all the necessary phage proteins while the phagemid genomes produce the transgenic tail fiber proteins. This results in the production of chimeric phage particles (Figure 7, bottom). Either a phagemid vector or a helper phage genome will be packaged into each phage particle. Since the helper phage genome has a substantially reduced capacity to be packaged into phage particles, the vast majority of the particles will contain phagemid vectors. Moreover, each will bear a combination of transgenic and wild-type copies of the altered coat protein. There are five copies of gp3 per phage particle, part of which will be transgenic and the rest wild-type. The number of copies of each can be controlled somewhat by adjusting the ratio of infecting helper phage to phagemid vectors present in the cells. The ratio can be skewed tremendously towards helper phage so most of the phage particles contain either one copy or no copies of the transgenic gp3. The particles with no copies of the transgenic gp3 are of no value, but they

can be selected against so they are likewise not a burden. However, the particles with one copy will present the transgenic gp3 while retaining infectivity since they have four copies of wild-type gp3 [41]. Having discussed how the M13 bacteriophage and its variants, the phagemid vector and helper phage, function in a phage display system, it is next important to discuss how a library of phagemid vectors is generated.

A cDNA library of mutants must be generated before phage display experiments can be carried out. This can be done with some form of random mutagenesis on a starting cDNA sequence. Error prone PCR is one method that can be used. This technique is simply a PCR reaction of the sequence using conditions that result in random base substitutions. It relies on the use of different concentrations of manganese and skewed dNTP concentrations in the PCR reaction to increase the frequency of these mutations. The specific PCR conditions used will be discussed later. Once the population of mutant cDNA sequences is acquired, it must be cloned into the M13 phage genome as part of one of the phage coat protein genes. This process will be discussed in detail later.

The phage particles produced through phagemid display present the mutant proteins or peptides on their coats. They can be selected for the ability of the displayed mutant to interact with a specific substrate. Furthermore, since the phage particles contain the DNA sequences of the mutants, the binding ability of each phage can be coupled to the mutant DNA sequence it possesses. Therein lies the power of phage display. Because the binding ability is associated with the DNA sequence, mutant genes coding for strong or weak binders can easily be isolated, amplified, and characterized. This can be done entirely without any special knowledge of the target or the means by which the mutants may bind it. Phage display does not depend on a knowledge of the intricacies of binding. It simply samples through a huge library of possibilities to find those that have the desired properties. This is a boon to studies involving poorly characterized or difficult to study substrates and it allows phage display to cover broad swathes of sequence space quickly and cheaply.

Chapter II
Methods

There is little detailed information available about a common amyloid fibril structure. We are left with the only concrete information being the macroscopic structural cues. There is somewhat more known about Aβ amyloid fibrils, but a detailed molecular structure remains elusive. A working model of Aβ amyloid has been developed [34], but further investigation is required to test that model. The work described herein aims to probe deeper into amyloid fibril structure by studying the binding properties of anti-amyloid antibodies.

Section 1. Anti-amyloid Antibodies

Determining Antibody Binding Properties

ELISA techniques were used for determining antibody binding affinity to amyloid fibrils. An ELISA experiment involves coating the wells of a polystyrene assay plate with a target antigen and determining if or how strongly a particular antibody binds to the antigen. This is done by first incubating the coated plate with the antibody in question, the primary antibody. The plate is next incubated with a secondary antibody that binds to the primary antibody. The secondary antibody is a conjugate that provides for a

means of detection. Biotinylated secondary antibodies were used in this protocol. These will bind streptavidin-conjugated molecules. Streptavidin-Europium was used as the labeling agent for detection of anti-amyloid antibodies binding to substrates. Time-resolved fluorescence was used for detecting the Europium. This technique relies on the very long lag time between the excitation and fluorescence of Europium. By the time Europium fluoresces, background fluorescence from most all other compounds has decayed. Europium also exhibits a large Stokes shift with the excitation and emission wavelengths of Europium at 340 and 615 nm, respectively. These qualities make Europium a very sensitive and specific vehicle for detection. The ELISA techniques used in these experiments have been well established [40]. A diagram of the ELISA protocol is shown in figure 8.

In brief, 96-well high-binding polystyrene ELISA plates with flat-bottom wells (Corning/Costar) were coated using 50 to 100 ng of Aβ amyloid fibrils or other aggregates per well. The fibrils were suspended in 50 µL of 1xPBS (Fisher, Appendix I) in each well. A working suspension of 1 µg/mL to 2 µg/mL of the fibrils was prepared for coating the plates. Two plate columns were coated for each

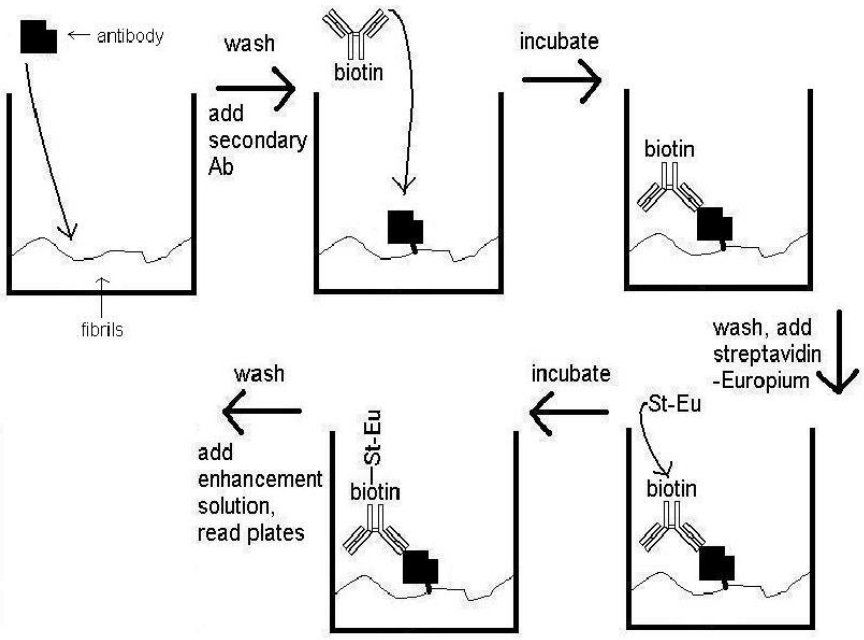


Figure 8. A diagram of the ELISA protocol. This figure shows one ELISA plate well. Plates coated with amyloid fibrils are incubated with a primary antibody, a biotinylated secondary antibody, and then streptavidin-Europium. An enhancement solution is added to the wells and the plate is read.

dilution series (Figure 9). The plates were incubated overnight at 37°C uncovered to allow the solutions to dry in the wells.

The plates were washed 2 times with ELISA wash buffer (Appendix I) to remove dried salts and unbound fibrils. To block the plates, each well was filled with 250 µL of ELISA blocking solution (Appendix I). The plates were covered with plate sealers (Costar) and incubated at 37°C for 1 hour. The plates were emptied and 100 µL of ELISA blocking solution was pipeted into each well. A 400 to 800 nM solution of the antibody to be tested was prepared in ELISA blocking solution. 100 µL of the antibody preparation was transferred into well A1, making 200 µL in total in the well, and pipeted up and down 4 times to mix (Figure 9). This process was continued down column 1, then from well H1 to well A2, and down thru well F2. For each step, 100 µL of the mixture was transferred to the next well in the series and mixed as before. The remaining 100 µL at the end of each dilution series was discarded. The last 2 wells of each dilution series were left with only ELISA blocking solution in them. This process generates a dilution series decreasing by a factor of 2 per well, with the last 2 wells providing background readings since they contain no primary antibody. Readings from the last two wells are subtracted from the others to

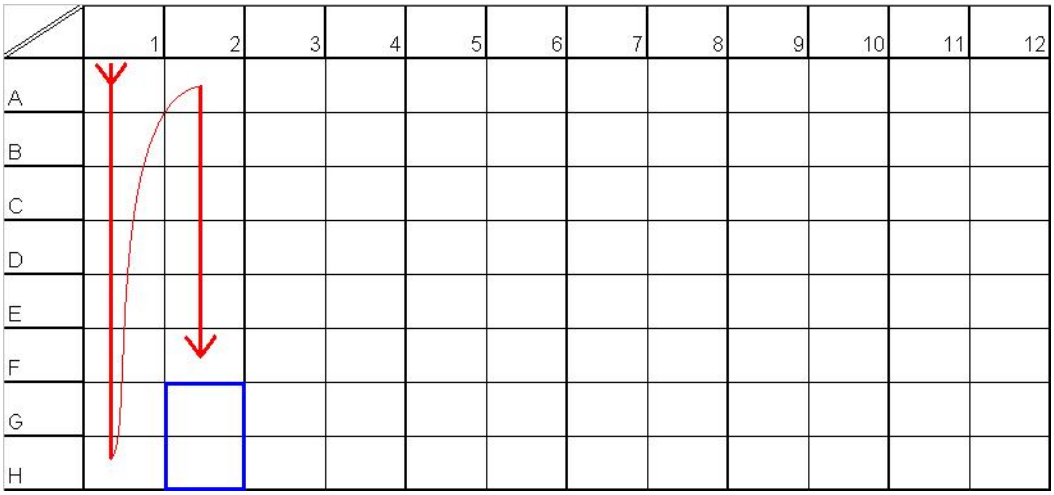


Figure 9. ELISA plate layout. Dilution series are set up down pairs of columns. An example dilution series in columns 1 and 2 would begin with the highest concentration in well A1. Each well down the column would have one half the concentration of the previous well. The series would continue from well H1 to well A2 and down through well F2. The last 2 wells would be left without the substrate to provide background readings.

remove background binding of the secondary antibody and streptavidin-Europium from the affinity calculation. The process was repeated for each dilution series. The plates were covered with plate sealers and incubated at 37°C for 1 hour. When buffer effects on binding were to be analyzed, the appropriate buffers were used in place of ELISA blocking solution for the primary antibody-binding step (Table 1). For the remainder of the protocol, ELISA blocking solution was used in all cases.

The plates were washed 2 times with ELISA wash buffer. A 1:5000 dilution of the secondary antibody, biotinylated goat anti-mouse IgM (μ-chain specific, Sigma), was prepared in ELISA blocking solution. 100 μL was pipeted into each well. The plates were covered with plate sealers and incubated at 37°C for 40 minutes. The plates were washed 2 times with ELISA wash buffer. A 1:1000 dilution of Delfia Europium-labeling streptavidin (Perkin Elmer) was prepared in ELISA blocking solution. 100 μL was pipeted into each well. The plates were covered with plate sealers and incubated at room temperature in the dark for 1 hour. The plates were washed 3 times with ELISA wash buffer. 100 μL of Delfia enhancement solution

Table 1. Buffers for salt and pH effects experiments. All buffer compounds except citric acid were ordered from Calbiochem. The first 3 buffers in the table were used for testing the effects of the amount of salt. The first 5 buffers excluding the third were used for testing the effects of different cations and anions. HEPES is a buffer of very low ionic strength, so it should not interfere greatly with comparing the different salts. Na_2HPO_4 has roughly double the ionic strength of the other 2 salts so it was used at half the concentration for a balanced comparison. The last 8 buffers were used for testing pH effects.

Buffer compound	Salt	pH
5 mM HEPES	-	7.5
5 mM HEPES	150 mM NaCl	7.5
5 mM HEPES	600 mM NaCl	7.5
5 mM HEPES	150 mM KCl	7.5
5 mM HEPES	75 mM Na_2HPO_4	7.5
5 mM citric acid	150 mM NaCl	3.0
5 mM citric acid	150 mM NaCl	5.8
5 mM PIPES	150 mM NaCl	5.8
5 mM PIPES	150 mM NaCl	7.4
5 mM Bicine	150 mM NaCl	7.4
5 mM Bicine	150 mM NaCl	8.5
5 mM CHES	150 mM NaCl	8.5
5 mM CHES	150 mM NaCl	10.0

(Perkin Elmer) was pipeted into each well. The enhancement solution chelates Europium from the complexes and into solution for detection. A Wallac Victor^2 1420 Multilabel Counter was used for detection. Each reading was taken for 400 μs after a 400 μs delay (Perkin Elmer).

The binding data were analyzed using Microsoft Excel and plotted as sigmoid curves in Kaleidagraph. The fluorescence counts for each assay were all divided by 4,800 counts/fmol to obtain the femtomoles of Europium in each well. These values were plotted against $-\log_{10}$(antibody concentration) at each point to obtain sigmoid curves (Figure 10). Two key features of these curves are the magnitude and the midpoint of the sigmoid curve (Figure 10). The magnitude is indicative of the number of available antigen binding sites while the midpoint tells the affinity of the antibody for the antigen.

After preparing the binding data as described, it was plotted in Kaleidagraph against $\log_{10}$(antibody concentration). Sigmoid curve fits were obtained using equation 1 in Kaleidagraph. The binding affinity from each curve was obtained from the inverse log of the x value at the midpoint (10^*m1*) after fitting the sigmoid curve in Kaleidagraph

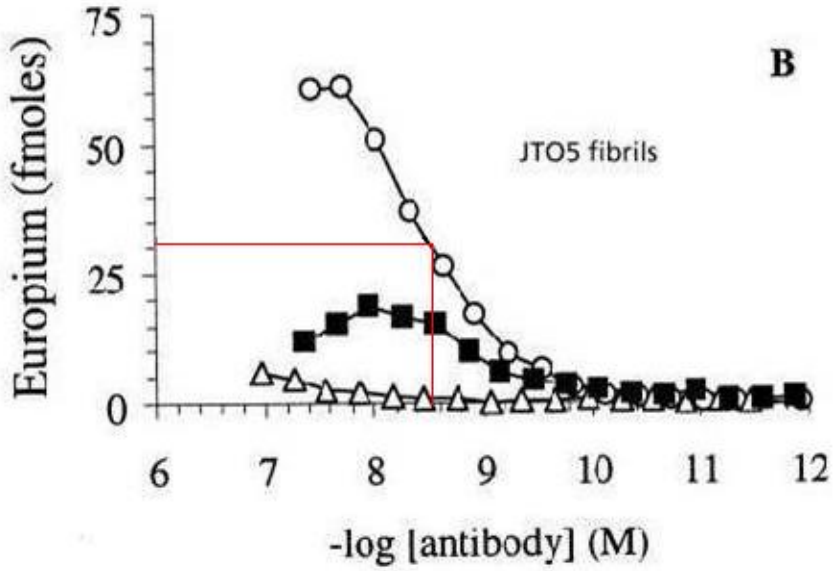


Figure 10. An example of ELISA data. These curves show the binding of WO1 to Aβ amyloid (open circles), fibrils of antibody light chain (JTO5, closed squares), and a control IgM (open triangles) [40]. The midpoint of the Aβ amyloid sigmoid is denoted by the red lines. The binding affinity is obtained by getting the inverse log (10^x) of the x value at that point. (Adapted from O'Nuallain, B. and R. Wetzel, *Conformational Abs recognizing a generic amyloid fibril epitope.* Proc Natl Acad Sci U S A, 2002. **99**(3): p. 1485-90.)

(Equation 1). The binding affinity is the antibody concentration at which one half maximal binding is reached. This value is reported as a molar concentration (M).

$$y = m3 / (1 + e^{((m1 - m0) / m2)}).$$ **Equation 1.**

This equation was entered into Kaleidagraph. The starting values were: *m1 = 1, m2 = 1, and m3 = 20.* After the best fit sigmoid was calculated in Kaleidagraph, values were returned for *m1*, *m2*, and *m3*. The midpoint x value of the sigmoid was reported in *m1*, the slope of the tangent line to the midpoint was reported in *m2*, and the magnitude of the sigmoid was reported in *m3*. For determining antibody binding affinity, *m1* was used. All 3 values were used for concentration determination calculations.

Determining Antibody Concentration

ELISA techniques were used for determining antibody concentration. The protocol shares many similarities with that for determining binding affinity, but there are several important differences. The purpose was to determine concentration rather than binding activity, so the ELISA plate was coated with a capture antibody rather than amyloid fibrils. The antibodies whose concentrations are to be tested are diluted significantly and all to the same level as a standard antibody of known concentration. The capture antibody will bind these antibodies to the plate with very high affinity. From this stage on, the protocol was the same as that for determining binding

activity. After the protocol is completed, the concentrations of the unknowns are calculated relative to the known standard.

For this protocol, 96-well high-binding polystyrene ELISA plates with flat-bottom wells (Corning/Costar) were used. They were coated using a 1:1000 dilution of a capture antibody, goat anti-mouse IgM (μ-chain specific, Sigma). 50 μL was pipeted into each well. Two columns were coated for each antibody to be assayed along with an additional 2 columns for a control antibody. The plates were covered with plate sealers and incubated at 37°C for 1 hour. They were washed 2 times with ELISA wash buffer. To block the plates, each well was filled with 250 μL of ELISA blocking solution. They were covered with plate sealers and incubated at 37°C for 1 hour.

The plates were emptied and 100 μL of ELISA blocking solution was pipeted into each well. 1:100 dilutions of the antibodies to be tested were prepared in ELISA blocking solution. Likewise, a 1:100 dilution of the standard antibody was prepared. If any of the resulting data sets did not produce a complete sigmoid curve, the initial dilution was adjusted when repeating the experiment. Mouse IgM (Calbiochem) was used as the standard since the unknowns were

mouse IgM antibodies. It is imperative that the concentration of the standard antibody be known since it is later used in calculating the concentrations of the antibodies of interest. 100 µL of the antibody preparation was transferred into well A1, making 200 µL in total in the well, and pipeted up and down 4 times to mix (Figure 9). This process was continued down column 1, then from well H1 to well A2, and down thru well F2. For each step, 100 µL of the mixture was transferred to the next well in the series and mixed as before. The remaining 100 µL at the end of each dilution series was discarded. The last 2 wells of each dilution series were left with only ELISA blocking solution in them. This process generates a dilution series starting at a 1:200 dilution and decreasing by a factor of 2 per well with the last 2 wells providing background readings since they contain no primary antibody. The process was repeated for each antibody including the standard antibody. The plates were covered with plate sealers and incubated at 37°C for 1 hour. The remainder of the protocol is already described under the heading *"Determining Antibody Binding Properties"* starting at the secondary antibody incubation step.

The resulting data were analyzed using Microsoft Excel and plotted as sigmoid curves using Kaleidagraph. For each concentration

determination experiment, a sigmoid curve fit for the standard antibody was obtained using equation 1 in Kaleidagraph. The *m1*, *m2*, and *m3* values were collected from the sigmoid fit results. Before proceeding further, the other antibody data had to be checked for consistency. To do so, sigmoid fits were obtained for each of the other sets of antibody data. The antibody concentrations from the standard antibody were substituted for these curves since their concentrations were still unknown at this stage. The purpose of these sigmoid fits was to make sure the magnitudes of all the curves are comparable to the standard curve. Therefore, the only the relevant value from these curves is the magnitude, *m3*. Generally, they are very close within the same experiment. If they are not, then aberrant curves should be scaled to have the same magnitude as the standard curve. This simply requires multiplying each y value of the unknown by the ratio of the standard curve magnitude to the aberrant curve magnitude. If this scaling is not performed, the calculated concentration will be wrong.

To calculate the concentration of an unknown, a y value was selected from the middle linear segment of the sigmoid curve data. y values as near the midpoint of the curve as possible were selected

(Figure 10, red lines). The y value along with the initial antibody dilution factor, the dilution factor at the selected data point, and the sigmoid fit data from Kaleidagraph were all entered into equation 2. This equation yields the concentration of the unknown antibody. The calculation was repeated with multiple y values from the linear segment. This served to verify the concentration results and obtain greater accuracy.

$$Concentration = d*2\text{^}w*10\text{^}(-m2*ln((m3-y)/y)+m1)$$ **Equation 2.**

The reported concentration is molar (M). *d* is the initial dilution factor of the unknown antibody, 100 in this protocol. *w* is the well number in the middle linear segment of the sigmoid curve selected for concentration determination. It is not the number from the ELISA plate, but rather the number of the dilution step in the series. For example, *w* would be 9 for well A2 in figure 9. *y* is the activity, y value measured in fmoles of Europium, in the selected well. *ln* is natural log. *m1*, *m2*, and *m3* are the values obtained from the sigmoid fit to equation 1in Kaleidagraph.

Antibody Fragmentation

Reduced IgM (rIgM) fragments of WO2 were generated for use in antibody fragment binding assays. The rIgM fragment is similar to a reduced IgG in that it consists of one heavy and one light chain only (Figure 5). It is a monovalent fragment of the IgM molecule. That is, it possesses only one binding domain. A reduction and alkylation

protocol was used to separate the fragments at disulfide bonds and subsequently alkylate the cysteines preventing reassociation (Pierce).

Before fragmentation, the WO2 sample was purified with an IgM purification column, HiTrap IgM Purification HP (Amersham Pharmacia Biotech), using the provided protocol. The following reduction and alkylation protocol was adapted from the Immunopure IgM Fragmentation Kit (Pierce). 500 µL of a 1 to 2 mg/mL WO2 sample was transferred into a 1.5 mL microcentrifuge tube along with 36 µL of 42 mg/mL 2-mercaptoethanolamine, and 500 µL of 50 mM Tris pH 8.0. The final concentration of 2-mercaptoethanolamine should be 1.5 mg/mL. This concentration is intended to reduce the WO2 to rIgM fragments without further reduction to separate heavy and light chains. The reaction was incubated for 30 minutes in a 37°C water bath. At the end of this time, 65 µL of 123 mg/mL iodoacetic acid was added to a final concentration of 8 mg/mL. The reaction was incubated for 15 minutes at room temperature in the dark. Iodoacetic acid alkylates sulfhydryl groups on cysteines, preventing them from reforming disulfide bonds. When this reaction was complete, the sample was injected into a 3 mL capacity dialysis cassette of 3 kDa MW cutoff (Pierce). It was dialyzed overnight at 4°C against 1xPBS

with 0.02% sodium azide added as a preservative. Fragmentation was verified by running a nonreducing PAGE gel of the sample.

Section 2. Phage Display

The pComb3X Phagemid Vector

The pComb3X phage display vector was used for the phage display work described herein. It was obtained from the Barbas laboratory [42]. This vector is approximately 3.4kb in length, excluding the *SfiI*-flanked Fab DNA segment. This segment is approximately 1.5kb in length [42]. This vector has numerous properties desirable for phage display experiments [42]. A breakdown of the characteristics of this vector is shown in figure 11. The vector imparts ampicillin / carbenicillin resistance to *E. coli* cells possessing it. This allows for simple selection of infected cells. The gene encoding the fusion protein in the plasmid possesses a few important additions. The ompA and pelB signal peptides direct the secretion of the light and heavy chains, respectively, into the bacterial periplasm. This becomes useful when expression of soluble Fab protein is desired. There is a hexahistidine tag (H6) useful for nickel-affinity purification of the Fab protein. There is a hemagglutinin (HA) tag which allows for detection of the Fab using anti-HA antibodies. There is an amber codon useful

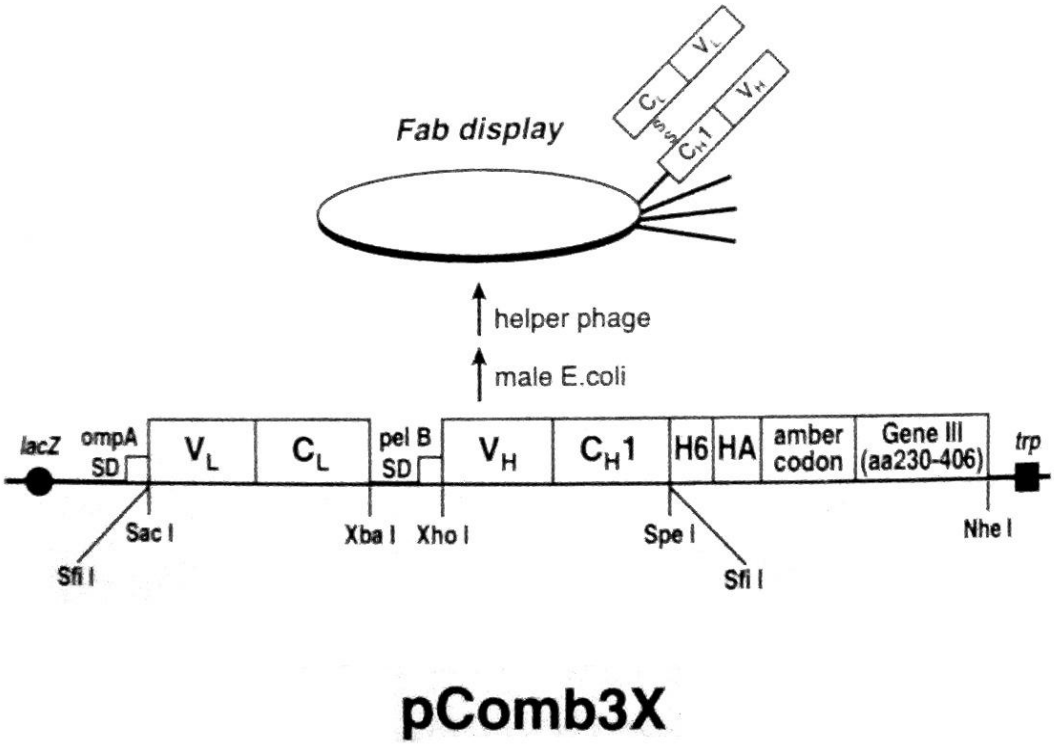


Figure 11. The pComb3X phagemid display vector. This vector is approximately 3.4kb in length, excluding the *SfiI*-flanked Fab DNA segment [42]. This segment is approximately 1.5kb in length. The diagram shows the region immediately flanking the antibody genes. *lacZ* is the promoter. Shine-Dalgarno (SD) sequences, which help to bring the mRNA initiation codon to the ribosome, precede each gene. *SfiI*, *SacI*, *XbaI*, *XhoI*, *SpeI*, and *NheI* are restriction sites. ompA and pelB are leader sequences that encode signal peptides directing protein secretion into the periplasm. V_L and C_L are the variable and constant domains of the antibody light chain, respectively. V_H and C_H1 are the variable and constant domains of the antibody heavy chain, respectively. H6 is a hexahistidine tag. HA is a hemagglutinin tag. The amber codon is a stop codon that is suppressed in certain cell strains. *trp* is the transcription terminator. (Adapted from Barbas, C.F., 3rd, et al., *Phage Display: A Laboratory Manual*. 2002.)

for controlling expression of the fusion protein. This codon allows for this control because of the way different bacterial strains interpret it. In suppressor strains, this codon is interpreted as an amino acid and results in expression of the full-length fusion of the Fab heavy chain and phage gp3 fragments. In nonsuppressor strains, it is interpreted as a stop codon. This results in expression of the heavy chain without the phage gp3 fragment (Figure 11). Both the heavy and light chains are exported to the periplasm. The oxidizing environment there facilitates the association of the two chains via disulfide bonding (Figure 11). This allows for soluble expression of Fab protein.

PCR Random Mutagenesis

The goal of the phage display experiments was to generate a library of antibody fragments and select for those with amyloid-binding properties. PCR random mutagenesis was used to generate the starting library. Before beginning this procedure, a stock of the starting phagemid clone was prepared since only a very small amount was available. The starting clone was pComb3XTT provided by the Barbas laboratory [42]. Electrocompetent *E. coli* cells (XL1-Blue, Stratagene) were transformed with the pComb3XTT vector. Before transformation, the received pComb3XTT vector preparation and an

electroporation cuvette (Gene Pulser Cuvette, BIO-RAD) was placed on ice for 10 minutes. Just before transformation, a tube of 100 µL of XL1-Blue cells was thawed on ice. 0.5 µL of the received pComb3XTT vector preparation was added to the tube of thawed cells and mixed by pipeting up and down. The tube was incubated on ice for 1 minute. A 200 µL pipet tip with the end snipped off was used to transfer the cells to the electroporation cuvette. The cuvette was transferred to a BIO-RAD Gene Pulser and electroporation was carried out at 2.5 kV, 25 µF, and 200 Ω. A time constant of 4.0 to 4.5 is expected. Anything outside this range indicates likely failed electroporation, possibly due to presence of too much salt. The cuvette was flushed immediately after electroporation with 1 mL followed by 2 flushes with 2 mL of room temperature SOC medium. These flushes were combined into a 50 mL polypropylene tube. This culture was shaken at 225 rpm for 1 hour at 37°C in a New Brunswick Scientific C25 Incubator Shaker.

10 mL of SB medium, 3 µL of 100 mg/mL carbenicillin, and 30 uL of 5 mg/mL tetracycline was added to the culture. Carbenicillin selects for cells carrying the phagemid. The 15 mL culture was shaken at 225 rpm for 1 hour at 37°C. 4.5 µL of 100 mg/mL carbenicillin was added and the culture was shaken for another hour. The culture was

transferred to a 1 L Erlenmeyer flask. 185 mL of prewarmed (37°C) SB medium, 92.5 µL of 100 mg/mL carbenicillin, and 370 µL of 5 mg/mL tetracycline was added. The 200 mL culture was shaken overnight at 225 rpm and 37°C. The next day, the culture was split into 5 roughly 40 mL lots in 50 mL polypropylene tubes. Glycerol stocks were prepared from all but 1 tube by adding glycerol to approximately 15% in each tube. That is about 7 mL of glycerol added to each tube and mixed thoroughly by pipeting up and down. These glycerol stocks were stored at -80°C. With an ample supply of pComb3XTT infected cells in storage, the remaining tube was used for a phagemid DNA preparation following the maxiprep (Qiagen) protocol. The pComb3XTT phagemid preparation was used in PCR random mutagenesis [43].

The pComb3XTT clone encodes a human Fab antibody specific to tetanus toxoid, an approximately 150 kDa MW bacterial protein [43]. The Fab fragment of an IgG (Figure 5a) possesses the light chain variable (V_L) and constant (C_L) domains. It also possesses the heavy chain variable domain (V_H) and constant domain 1 (C_H1). Since the goal was to get anti-amyloid antibodies, the heavy and light chain genes were mutagenized to generate a library of mutants. PCR

primers were designed for amplifying the Fab DNA. The sense primer, PC3SENSE, is just before V_L and the reverse primer, PC3REVERSE, is just after C_H1 (Figure 11, Table 2). Error-prone PCR was used to generate mutated Fab DNA from the phagemid clone. This technique involves the addition of manganese to the reaction. This causes dNTP missubstitutions. Several sets of conditions based on a published protocol [44] were tested before useable yields could be obtained.

The following reaction mix provided the best yields: 100 pmol sense primer, 100 pmol reverse primer, 10 µL 10xPCR buffer (Promega), 28 µL $MgCl_2$ (7 mM final from 25 mM stock), 0.2 mM dATP, 0.2 mM dGTP, 1 mM dCTP, 1 mM dTTP, 0.25 mM $MnCl_2$ (200 mM stock, autoclaved), 5 Units Taq (Promega), volume to 100 µL with nuclease-free water (Promega). The following cycling conditions were used: 5 minute preheat at 95°C, 50 cycles of 15 seconds at 94°C, 30 seconds at 45°C, and 90 seconds at 72°C. Normally, 20 to 30 cycles are executed, but 50 cycles were used to increase yields. The 5 minute preheating step was used to ensure that the DNA strands were fully melted.

Table 2. PCR primers. PC3SENSE and PC3REVERSE were used for amplifying the Fab DNA, including both heavy and light chain sequences, from the pComb3X vector. They were also used in the mutagenic PCR of this DNA sequence. OMPSEQ and PELSEQ were used for sequencing reactions of the light and heavy chain sequences, respectively.

Primer Name	Length	Sequence (5′ -> 3′)
PC3SENSE	41	GAGGAGGAGGAGGAGGAGTGGCACTGGCTGGTTTCGCTACC
PC3REVERSE	39	GAGGAGGAGGAGGAGGAGAGAAGCGTAGTCCGGAACGTC
OMPSEQ	22	AAGACAGCTATCGCGATTGCAG
PELSEQ	21	ACCTATTGCCTACGGCAGCCG

The mutagenic PCR products were gel purified via the PCR purification protocol (Qiagen). Both the purified pComb3X phagemid vector and purified mutagenic PCR products were digested with the restriction endonuclease, *SfiI* (Roche). Digestion was carried out by combining approximately 20 µg of the phagemid or 10 µg of the mutagenic PCR products with 360 Units of *SfiI* and 20 µL of 10x buffer M. DNA concentrations were calculated by taking absorbance readings at 260 nm using a Molecular Devices Spectramax Plus spectrometer. For each sample, a blank reading was first taken by filling a quartz cuvette with deionized water. The cuvette was emptied and the DNA sample was diluted 1:50 into deionized water and transferred into the same quartz cuvette to be read. The concentration was calculated using equation 3. The total amount of DNA in a given sample was calculated by multiplying this concentration by the total volume of the sample. The digestion reaction volumes were adjusted to 200 µL with nuclease-free water and the reaction was incubated for 5 hours at 50°C. The mutagenic PCR products and the phagemid vector with the Fab insert cut out were gel purified using the spin miniprep protocol.

$$DNA\ concentration = A_{260} * d * 50\ \mu g/mL$$ **Equation 3.**

A_{260} is the absorbance reading of the sample at 260 nm. d is the dilution factor of the DNA sample into deionized water, 50 as described above. $50\ \mu g/mL$ is a constant used to relate the absorbance at 260 nm to the amount of DNA in the sample.

The purified products were ligated with T4 DNA ligase (Roche) to generate a phagemid library. Ligation was carried out by combining approximately 1.4 µg of cut pComb3X, 1.4 µg of cut mutagenic PCR products, 40 µL of 5x ligase buffer (Roche), and 10 µL of T4 DNA ligase. The reaction volume was adjusted to 200 µL with nuclease-free water and the reaction was incubated overnight at room temperature. Successful ligation was verified by running the ligation reaction products on a 1% agarose gel alongside the cut products and the uncut phagemid. This library was ethanol precipitated and washed for concentration, purification, and storage. At a later stage in the work, 6 clones were selected to be sent off for sequencing to verify successful mutagenesis. The OMPSEQ primer was used for these sequencing reactions (Table 2). The resulting electropherograms were examined for errors over 350 bases from each clone. The number of mutations relative to the unmutated clone were counted and divided into the total number of bases counted to get the mutation rate. Roughly a 1.5% rate of base mutation was found. Furthermore, BLAST searches on these sequences verified them to be human antibody κ light chain.

Amplification of Helper Phage

Before undertaking the phage display experiments, helper phage needed to be prepared. These must be ordered in a small amount and amplified significantly to provide enough for the phage display experiments. VCSM13 helper phage (Stratagene), derived from the M13 K07 mutant, were ordered and amplified to an appropriate titer for use in the phage display experiments by using the protocol adapted from [42].

To being the procedure, 2 mL of SB medium was inoculated with 2 µL of *E. coli* cells (XL1-Blue, Stratagene). 4 µL of 5 mg/mL tetracycline was added and the culture was shaken at 225 rpm for 1 hour at 37°C. Tetracycline selects for F+ male *E. coli* cells. During the incubation, 3 dilutions of the ordered VCSM13 helper phage were made up in SB medium: 10^{-6}, 10^{-7}, and 10^{-8}. 1 µL of each dilution was added to a separate 50 µL lot of this culture and incubated at room temperature for 15 minutes. In the mean time, 3 LB+tetracycline agar plates were prewarmed to 37°C. The 3 lots of infected cells were each diluted into 1 mL of SB medium and plated on a separate LB+tetracycline agar plate. These plates were incubated overnight at 37°C. Sometimes the lowest dilution plate may have no colonies or

the highest dilution plate may have a lawn from which individual colonies cannot be picked. This is the reason 3 phage dilutions are used. It ensures there is at least one plate from which isolated VCSM13 phage plaques can be picked.

The next day, 10 mL of prewarmed (37°C) SB medium was inoculated with 10 µL of XL1-Blue cells. 20 µL of 5 mg/mL tetracycline was added and the culture was shaken at 225 rpm for 1 hour at 37°C. A single VCSM13 plaque was transferred from one of the plates to the culture using a sterile pipet tip. The culture was shaken at 225 rpm for 2 hours at 37°C. It was transferred into to a 1 L Erlenmeyer flask with 240 mL of prewarmed (37°C) SB medium. 500 µL of 5 mg/mL tetracycline and 350 µL of 50 mg/mL kanamycin was added. Kanamycin selects for cells infected with VCSM13 phage since this phage genome imparts kanamycin resistance. The 250 mL culture was shaken overnight at 225 rpm and 37°C.

The next day, the culture was split into 6 50 mL polypropylene tubes and spun at 2,500g for 15 minutes using the Beckman Avanti J-25I centrifuge and the JA-20 rotor. The supernatants were transferred to fresh 50 mL tubes and incubated in a water bath at 70°C for 20

minutes. They were spun again at 2,500g for 15 minutes in the same centrifuge and rotor. The supernatants were transferred to fresh 50 mL tubes and stored at 4°C until needed.

After the VCSM13 helper phage preparation was completed, the phage titer was determined. The protocol adapted from [42] was used to check for a sufficient phage titer. 2 mL of SB medium was inoculated with 2 µL of XL1-Blue cells. 4 µL of 5 mg/mL tetracycline was added and the culture was shaken at 225 rpm for 1 hour at 37°C. During the incubation, 3 dilutions of the VCSM13 helper phage preparation were made up in SB medium: 10^{-7}, 10^{-8}, and 10^{-9}. 1 µL of each phage dilution was added to a separate 50 µL lot of this culture and incubated at room temperature for 15 minutes. The infected cells were diluted into 1 mL of SB medium and plated onto 3 separate LB+tetracycline agar plates. These were incubated overnight at 37°C.

The next day, the number of plaques on each plate was counted. The 10^{-7} plate may have an uncountable lawn or the 10^{-9} plate may have few or no colonies. At least 1 or 2 plates should have an adequate number of colonies to count. The phage titer was determined by entering the count and the phage dilution factor for

each plate into equation 4. The titer should be approximately 10^{12} to 10^{13} (plaque-forming units/mL) pfu/mL. The titer slowly decreases over time, but the VCSM13 phage preparation is stable for months at 4°C.

$$\textit{Phage input titer} = (n * d * 50\ \mu L) / 1\ \mu L \quad \textbf{Equation 4.}$$

n is the number of colonies counted on the plate. *d* is the dilution factor of the phage preparation: 10^7, 10^8, or 10^9. *50 µL* is the volume of the cell culture infected. *1 µL* is the volume of the phage preparation dilution used for infection. The units are pfu/mL [42].

Phage Selection

The first round of phage selection, also called panning, began with library ligation and transformation. The protocol for this process was adapted from [42]. To begin with, 1.4 µg of *SfiI*-cut pComb3X was combined with 650 ng of *SfiI*-cut mutagenic PCR product into a 1.5 mL microcentrifuge tube. 10 µL of T4 DNA ligase (Invitrogen) and 40 µL of 5x ligase buffer was added and the sample volume was adjusted to 200 µL with nuclease-free water. This ligation reaction was incubated overnight at room temperature to allow for complete ligation. Successful ligation was verified by running the ligation reaction products on a 1% agarose gel.

The ligation products were precipitated by adding 1 µL of glycogen, 20 µL (0.1 volumes) of 3 M sodium acetate pH 5.2, and 440 µL (2.2 volumes) of ethanol. The reaction was mixed by inverting the tube several times. The reaction was incubated overnight at 4°C. The ligation products were spun down in a tabletop microcentrifuge (Eppendorf Centrifuge 5417R) at 20,000 rpm and 4°C for 15 minutes. The supernatant was discarded and the pellet was washed twice with 70% ethanol. The tube containing the pellet was drained, tapped dry onto a paper towel, and left to sit for 15 minutes in a fume hood to evaporate the remaining ethanol. The dried pellet was dissolved in 30 µL of nuclease-free water by heating to 37°C and vortexing to assist dissolution. This is the ligated library sample. It is imperative that this sample is well washed and well dried. Remaining salt or ethanol could interfere with transformation.

Before transformation, the ligated library sample and 2 electroporation cuvettes were placed on ice for 10 minutes. Just before transformation, a tube of 100 µL of XL1-Blue cells was thawed slowly on ice. Though 2 transformations were ultimately done, only one tube of cells was thawed at a time. This was done to prevent thawed cells sitting too long before transformation. The longer they

sit, the lower the transformation efficiency. Only after completely finishing the first transformation process, was the second tube of cells thawed.

7 µL of the ligated library sample was added to the tube of thawed *E. coli* cells and mixed by pipeting up and down. The remaining ligated library sample was stored at -80°C after completing both transformations. The cells were incubated on ice for 1 minute after adding the library sample. A 200 µL pipet tip with the end snipped off was used to transfer the cells to the electroporation cuvette. The cuvette was transferred to the BIO-RAD Gene Pulser and electroporation was carried out at 2.5 kV, 25 µF, and 200 Ω. A time constant of 4.0 to 4.5 is expected. The cuvette was flushed immediately after electroporation with 1 mL followed by 2 flushes with 2 mL of room temperature SOC medium. These flushes were combined into a 50 mL polypropylene tube. This culture was shaken at 225 rpm for 1 hour at 37°C.

10 mL of SB medium, 3 µL of 100 mg/mL carbenicillin, and 30 uL of 5 mg/mL tetracycline was added to the culture. 2 µL was removed from the culture and diluted into 200 µL of SB medium. Onto

2 separate LB agar+carbenicillin plates, 10 µL and 100 µL of this 1:100 dilution was plated and the plates were incubated overnight at 37°C. These plates were used for determining phage titer (Equation 5). *The next day, the number of colonies on each plate was counted. The phage titer was determined by entering the counts, the plating volumes, 10 µL or 100 µL, and the culture volumes, 15 mL, into equation 5.* The 15 mL culture was shaken at 225 rpm for 1 hour at 37°C. 4.5 µL of 100 mg/mL carbenicillin was added and the culture was shaken for another hour.

$$\text{Phage output titer} = (n * 100 * V_c) / p \quad \textbf{Equation 5.}$$

n is the number of colonies counted on the plate. 100 is the dilution factor of the infected culture: 200 µL / 2 µL. V_c is the volume of the cell culture infected: 15 mL or 8 mL. *p* is the plating volume: 0.01 mL or 0.1 mL. The units are plaque-forming units/mL or pfu/mL [42].

The culture was transferred to a 1 L Erlenmeyer flask and 2 mL of VCSM13 helper phage was added. 183 mL of prewarmed (37°C) SB medium, 92.5 µL of 100 mg/mL carbenicillin, and 370 µL of 5 mg/mL tetracycline were added. The 200 mL culture was shaken at 225 rpm for 2 hours at 37°C. 280 µL of 50 mg/mL kanamycin was added and the culture was shaken overnight at 225 rpm and 37°C. Kanamycin selects for helper phage infected cells. This prevents the faster-

growing uninfected cells from out-competing and overtaking the phage-producing infected cells.

The 200 mL culture was transferred to a 500 mL polypropylene centrifuge bottle and spun at 3,000g for 15 minutes at 4°C using the Beckman Avanti J-25I centrifuge and the JLA-10.5 rotor. The resulting supernatant was transferred to a clean 500 mL centrifuge bottle and 32 mL of 25% PEG-8000 / 15% NaCl was added. This was pipeted up and down to mix and kept on ice for 30 minutes. During this waiting period, the cell pellet was resuspended in 1 mL of SB medium, transferred to a 2 mL microcentrifuge tube, and stored at -80°C. The pellet can later be used in a phagemid DNA preparation. The supernatant with 25% PEG-8000 / 15% NaCl added was spun at 15,000g in the same centrifuge and rotor as earlier for 15 minutes at 4°C. The pellet is the phage pellet. The supernatant was discarded and the bottle was drained by sitting it lip-down on paper towels for 10 minutes. The bottle was gently tapped to the paper towels to remove the last few drops and the lid was wiped dry.

The phage pellet was thoroughly resuspended in 2 mL of 1% BSA in 1xPBS. This suspension was transferred to a 2 mL

microcentrifuge tube and spun in a tabletop microcentrifuge at 20,000 rpm and 4°C for 5 minutes. The resulting clarified supernatant was transferred to a clean 2 mL microcentrifuge tube. The pellet, consisting mainly of cell debris, was discarded. Sodium azide was added to the preparation to 0.02% as a preservative so the supernatant could be stored at 4°C. This preparation is the phage library, which was used immediately (the same day) for panning. It can be stored and used at a later date, but it must be reamplified before panning. This is necessary, because the activity of the presented Fab may drop over time in storage since it is not as rugged as the rest of the phage particle.

Immediately after library ligation and transformation was completed, the first round of panning was started. This process was employed for 3 rounds, though more rounds could be used if needed. The protocol was adapted from [42]. To begin with, 2 wells of a 96-well high-binding polystyrene ELISA plate with flat-bottom wells (Corning/Costar) were coated with 200 ng of Aβ amyloid fibrils suspended in 50 µL of 1xPBS. The plate was incubated overnight at 37°C uncovered. The coated wells were rinsed 2 times with ELISA wash buffer. 250 µL of 3% BSA was added to each well. The plate

was covered with a plate sealer (Costar) and incubated for 1 hour at 37°C. During the incubation, a starter culture was prepared. 2 mL of SB medium and 4 µL of 5 mg/mL tetracycline was added to a 15 mL polypropylene tube and inoculated with 2 µL of XL1-Blue cells. An identical culture was prepared and both were shaken at 225 rpm for 2 to 2.5 hours at 37°C. The OD of each should reach about 1. This culture was used at a later stage in the protocol.

The blocking solution was shaken out of the plate and 50 µL of the phage library preparation was added to both wells. The plate was sealed and incubated for 1 hour at 37°C. The phage solution was shaken out of the plate and both wells were washed 5 times each with ELISA wash buffer in the first round of panning. In the second and third rounds of panning, they were washed 10 times each. The thorough washing should remove most of the unbound phage from the wells. The remaining wash buffer was shaken out and 50 µL of freshly prepared 10 mg/mL trypsin (Sigma) in 1xPBS was added to each well. There is a trypsin-sensitive flexible linker between the heavy chain and gp3 fragment in the pComb3X construct. This allows trypsin to cleave bound phage particles from the plate, freeing them into solution [42]. The plate was sealed and incubated for 30 minutes at 37°C. The

contents of each well were pipeted up and down 10 times to thoroughly resuspend cleaved phage particles. The contents of both wells were transferred to one of the 2 mL cultures prepared earlier. The infected culture was incubated at room temperature for 15 minutes.

6 mL of prewarmed (37°C) SB medium, 1.6 µL of 100 mg/mL carbenicillin, and 12 µL of 5 mg/mL tetracycline were added to a 50 mL polypropylene tube. The phage-infected 2 mL culture was transferred to this tube. 2 µL was taken from this culture and diluted into 200 µL of SB medium. Onto 2 separate LB agar+carbenicillin plates, 10 µL and 100 µL of this 1:100 dilution was plated and incubated overnight at 37°C. These plates were used for determining phage output titer (Equation 5). The 8 mL culture was shaken at 225 rpm for 1 hour at 37°C. 2.4 µL of 100 mg/mL carbenicillin was added and the culture was shaken for another hour. In the mean time, 10^{-8} and 10^{-9} dilutions of the phage preparation were prepared in 1% BSA in 1xPBS. 50 µL lots of XL1-Blue cells were infected with 1 µL of each phage dilution. These were incubated at room temperature for 15 minutes. Onto 2 separate LB agar+carbenicillin plates, each lot of infected cells was plated. These plates were used for determining

phage input titer (Equation 4). All 4 plates, input and output titer, were incubated overnight at 37°C. *The next day, the number of colonies on each plate was counted. The input titers were determined by entering the counts and phage dilution factors into equation 4. The output titers were determined by entering the counts, the plating volumes, and the culture volumes, 8 mL, into equation 5.*

The 8 mL culture was transferred to a 1 L Erlenmeyer flask along with 2 mL of VCSM13 helper phage. 90 mL of prewarmed (37°C) SB medium, 46 µL of 100 mg/mL carbenicillin, and 184 µL of 5 mg/mL tetracycline was added. The 100 mL culture was shaken at 225 rpm for 2 hours at 37°C. 140 µL of 50 mg/mL kanamycin was added and the culture was shaken overnight at 225 rpm and 37°C. An ELISA plate was coated as described earlier and incubated overnight. This plate is for use in the next round of panning, so it was not prepared during the final round of panning.

The 100 mL culture was transferred to a 500 mL polypropylene centrifuge bottle and spun at 3,000g for 15 minutes at 4°C using the Beckman Avanti J-25I centrifuge and the JLA-10.5 rotor. The supernatant was transferred to a clean 500 mL centrifuge bottle and

16 mL of 25% PEG-8000 / 15% NaCl was added. This was pipeted up and down to mix and kept on ice for 30 minutes. In the mean time, the cell pellet was resuspended in 1 mL of SB medium, transferred to a 2 mL microcentrifuge tube, and stored at -80°C. Also, the ELISA plate wells coated overnight were washed and blocked as described earlier. The supernatant with 25% PEG-8000 / 15% NaCl added was spun at 15,000g in the same centrifuge and rotor for 15 minutes at 4°C. The pellet is the phage pellet. The supernatant was discarded and the bottle was drained by sitting it lip-down on paper towels for 10 minutes. The bottle was gently tapped to the paper towels to remove the last few drops and the lid was wiped dry.

The phage pellet was thoroughly resuspended in 2 mL of 1% BSA in 1xPBS. This suspension was transferred to a 2 mL microcentrifuge tube and spun in a tabletop microcentrifuge at 20,000 rpm and 4°C for 5 minutes. The resulting clarified supernatant was transferred to a clean 2 mL microcentrifuge tube. The pellet, consisting mainly of cell debris, was discarded. Sodium azide was added to the preparation to 0.02% as a preservative so the supernatant could be stored at 4°C. This preparation is the phage library, which was used immediately for the next round of panning.

That is, the protocol was started over from the beginning right away, except on the last round of panning.

Phage ELISA

During the panning process, the progression was monitored to ensure that the library was being enriched in amyloid-binding phage. Phage ELISA experiments were run on the phage libraries at each step to test the affinity of the library at a given stage for amyloid. The phage ELISA protocol shares some similarities to the ELISA protocol already described except for a few key differences. In place of a primary antibody, a phage library was used. For a secondary antibody, an anti-M13 phage antibody was used. Therefore, this protocol tests the ability of the library as a whole to bind amyloid fibrils. It was also used to test individual clones.

For each phage ELISA, columns 1 and 2 of a 96-well high-binding polystyrene ELISA plate with flat-bottom wells were coated with 200 ng of Aβ amyloid fibrils suspended in 50 µL of 1xPBS. The plate was incubated overnight at 37°C uncovered. The next day, the plate was washed 2 times with ELISA wash buffer. To block the plate, each well was filled with 250 µL of ELISA blocking solution. The plate

was covered with a plate sealer and incubated at 37°C for 1 hour. 100 µL of ELISA blocking solution was pipeted into each well of columns 1 and 2. 100 µL of the fresh phage preparation was transferred into well A1, making 200 µL in total in the well, and pipeted up and down 4 times to mix (Figure 9). This process was continued down column 1, from well H1 to well A2, and down thru well F2. The plate was covered with a plate sealer and incubated at 37°C for 1 hour. The last 2 wells are for taking background readings since they contain no phage.

The plates were washed 2 times with ELISA wash buffer. A 1:5000 dilution of the secondary antibody, biotinylated anti-M13 phage (Exalpha), was prepared in ELISA blocking solution. 100 µL of this preparation was pipeted into each well. The plate was covered with a plate sealer and incubated at 37°C for 40 minutes. The plate was washed 2 times with ELISA wash buffer. A 1:1000 dilution of Delfia Europium-labeling streptavidin (Perkin Elmer) was prepared in ELISA blocking solution. 100 µL was pipeted into each well. The plate was covered with a plate sealer and incubated at room temperature in the dark for 1 hour. The plate was washed 3 times with ELISA wash buffer. 100 µL of Delfia enhancement solution (Perkin Elmer) was

pipeted into each well and a Wallac Victor^2 1420 Multilabel Counter was used for detection. The binding data were analyzed much the same as in the other ELISA experiments. However, no concentration values were available. Binding results were plotted against log(dilution factor of phage) and the curves were examined qualitatively. No calculations were done based on these data.

After the panning process was completed and the library was enriched in fibril-binding phage, clones were selected for further analysis. The protocol for picking clones begins with preparing a starter culture. 2 mL of SB medium and 4 µL of 5 mg/mL tetracycline were added to a 15 mL polypropylene tube and inoculated with 2 µL of XL1-Blue cells. An identical culture was prepared for each round of panning conducted and for the nonpanned library (4 cultures total for 3 rounds of panning and the nonpanned library). These cultures were shaken at 225 rpm for 2 to 2.5 hours at 37°C. The OD of each should reach about 1. 50 µL of each phage preparation, one from each round of panning, was added to a separate culture and incubated at room temperature for 15 minutes. Onto LB agar+carbenicillin plates, 10 µL of each culture was plated. These plates were incubated overnight at

37°C. Less or more culture may be plated if 10 µL results in too many or too few colonies.

The next day, 2 mL of SB medium, 4 µL of 5 mg/mL tetracycline, and 1 µL of 100 mg/mL carbenicillin were added to several 15 mL polypropylene tubes. Enough tubes were prepared for the desired number of clones. Isolated colonies were picked from each plate with sterile pipet tips and cultures were inoculated with a single clone into each tube. 8 clones were picked on the first run of this protocol and 16 on the next. The cultures were shaken at 225 rpm for 2 to 2.5 hours at 37°C. The plates were stored by sealing with parafilm and keeping at 4°C. 6 mL of prewarmed (37°C) SB medium, 3 µL of 100 mg/mL carbenicillin, and 12 µL of 5 mg/mL tetracycline was added to a 50 mL polypropylene tube for each clone. The phage-infected 2 mL cultures were added to these tubes. The 8 mL cultures were shaken overnight at 225 rpm and 37°C. The following day, glycerol stocks were prepared from these cultures by adding glycerol to approximately 15% in each culture tube. That is about 1 to 1.2 mL of glycerol per tube. These glycerol stocks were mixed thoroughly by pipeting up and down and stored at -80°C.

After selecting clones, the affinity of each was tested to determine if it possessed the desired binding properties. This entailed producing small-scale phage preparations of the clones and testing their binding properties by phage ELISA. The protocol for small scale phage preparations was adapted from [42]. For each clone to be tested, 10 mL of SB medium, 20 µL of 5 mg/mL tetracycline, and 5 µL of 100 mg/mL carbenicillin was added to several 50 mL polypropylene tubes. Each was inoculated with a glycerol stock scraping from a different clone. The cultures were shaken at 225 rpm for 6 hours at 37°C. 100 µL of VCSM13 helper phage was added to each culture. The cultures were shaken for an additional 2 hours at 225 rpm and 37°C. 14 µL of 50 mg/mL kanamycin was added to each culture and the cultures were shaken overnight at 225 rpm and 37°C.

The next day, 1.2 mL of each supernatant was transferred into a fresh 2 mL microcentrifuge tube. These tubes were spun at 3,500 rpm in a tabletop microcentrifuge for 15 minutes. The supernatants were transferred to fresh 2 mL microcentrifuge tubes and the cell pellets were frozen since they can later be used in phagemid preparations. To the 1.2 mL supernatants, 300 µL of 25% PEG-8000 / 15% NaCl was added. The supernatants with 25% PEG-8000 / 15% NaCl added were

mixed by inverting the tubes several times. They were incubated on ice for 30 minutes. The tubes were spun at 20,000 rpm and 4°C for 15 minutes. For each tube, the supernatant was drawn out with a pipet, taking care not to disturb the pellet. All tubes were spun 20 seconds longer and the remaining supernatant was drawn out. Each tube was carefully tapped upside down on a paper towel to remove the last of the PEG. All the tubes were allowed to dry for 10 minutes in a fume hood. Each phage pellet was resuspended in 100 µL of 1% BSA in 1xPBS. These clonal phage preparations were used right away in phage ELISAs as previously described. The only difference was that 100 µL of a clonal phage preparation was used in place of 100 µL of a phage library preparation. The binding curves were plotted and examined in the same manner as the phage library ELISA experiments.

Production of Soluble Fab

Soluble Fab production was explored in selected clones as well as the original unmutated clone. Each phagemid clone was isolated and transformed into *E.coli* cells of a nonsuppressor strain. Cultures were grown up and induced to produce soluble Fab protein and whole cell extracts from these cultures were tested for the presence of Fab

protein. After growing up induced cultures, an acetone extraction protocol (Dr. Ronald Wetzel) was used to remove lipids and get a total protein extract. Western blots of the protein extracts were run.

For each clone, a cell pellet prepared earlier was used in a plasmid preparation to isolate and purify the phagemid DNA. Pellets saved from the clonal phage ELISA experiments were used. These were subjected to the spin miniprep protocol (Qiagen). Electrocompetent *E. coli* cells of a nonsuppressor strain (TOP10, Invitrogen) were transformed with each phagemid clone following the protocol already described under the heading *"PCR Random Mutagenesis"*. The only difference was the use of the TOP10 strain of *E. coli* in place of the XL1-Blue strain. After electroporation, 10 mL of SB medium, 3 µL of 100 mg/mL carbenicillin, and 30 uL of 5 mg/mL tetracycline was added to the 5 mL of SOC medium flushes. The 15 mL culture was shaken at 225 rpm for 1 hour at 37°C. 4.5 µL of 100 mg/mL carbenicillin was added and the culture was shaken overnight at 225 rpm and 37°C. The next day, glycerol stocks were prepared from the cultures by adding glycerol to approximately 15% in each tube and mixing thoroughly by pipeting up and down. These glycerol stocks were stored at -80°C. The remaining material from the plasmid

preparation of each clone was sent off for sequencing. Including the unmutated clone, five clones were sequenced in total. The PELSEQ and OMPSEQ primers were used for these sequencing reactions (Table 2). BLAST searches on the resulting sequences verified them to be human antibody heavy chain Fd fragment and κ light chain, respectively.

For testing soluble Fab production, fresh cultures were prepared using the glycerol stocks as inoculants. For each clone, 5 mL of SB medium, and 2.5 µL of 100 mg/mL carbenicillin were added to several 50 mL polypropylene tubes. Since the heavy and light chain genes are under the *lacZ* promoter in the pComb3X vector, IPTG can induce their expression. Each tube was inoculated with a glycerol stock scraping from a different TOP10 culture clone. The cultures were shaken for 6 hours at 225 rpm and 37°C. 50 µL of 0.1 M IPTG was added to each culture and the cultures were shaken overnight at 225 rpm and 37°C.

The following day, 1 mL of each culture was transferred to a 2 mL microcentrifuge tube. The tubes were spun at 5,000 rpm in a tabletop microcentrifuge for 5 minutes. The supernatants were discarded and the cell pellets were frozen at -80°C. The pellets were

thawed and each was resuspended in 80 µL of cell suspension buffer. 8 µL of 20% SDS and 8 µL of 1M βME was added. Each cell suspension was pipeted up and down and vortexed vigorously to mix. They were heated to 90°C for 2 minutes and then cooled. 1 mL of acetone was added to each tube and mixed by vortexing. The tubes were incubated on ice for 10 minutes. They were spun at 5,000 rpm in a tabletop microcentrifuge for 1 minute. The supernatants were discarded and the pellets were left in a fume hood for 15 minutes to dry. The pellets were resuspended in 300 µL of [7.5 parts 1xPBS, 2.25 parts NuPage 4x loading dye (Invitrogen), 0.25 parts 1M βME] by pipeting up and down and vortexing vigorously. They were heated to 90°C for 2 minutes and then cooled. The tubes were spun at 5,000 rpm in a tabletop microcentrifuge for 1 minute. A protease inhibitor, Fluka Pefabloc SC (Fisher), was added to 1mM final concentration to prevent protein degradation. 25 µL of each sample was loaded into a NuPage polyacrylamide gel lane (Invitrogen) for analysis. The SeeBlue Plus 2 MW standard (Invitrogen) was loaded into one lane of the gel. The gel was run through a SDS-PAGE experiment at 150 V for 70 minutes using a BIO-RAD PowerPac 200 following the NuPage protocol (Invitrogen). 1x MOPS SDS running buffer (Invitrogen) was used in the run with NuPage antioxidant (Invitrogen) added. Gels prepared in

this fashion were used in western blot experiments to determine if there is any Fab protein present.

For each western blot, a western transfer was run onto a PVDF membrane (BIO-RAD). The NuPage protocol (Invitrogen) was followed for the transfer. After the transfer, the PVDF membrane was used in a western blot. The membrane was blocked by incubating in a 5% BSA solution for 1 hour. The membrane was washed 3 times with ELISA wash buffer by shaking the membrane in the buffer for 5 minutes each wash. The membrane was incubated in a 1:2500 dilution of the primary antibody in ELISA blocking solution for 1 hour. For blots against the HA tag of the fusion protein, a monoclonal anti-HA biotin conjugate antibody (Sigma) was used. In another replicate of the same experiment, a monoclonal anti-HA HRP conjugate antibody (Roche) was used. For blots against the antibody chains, a polyclonal goat anti-human IgG, heavy and light chain, HRP conjugate (Pierce) was used. Since the gel running conditions were reducing, it was necessary to use chain-specific antibodies rather than anti-Fab antibodies. A polyclonal mixture was used in case some of the antibody mutant clones have mutations in the epitope recognized by a particular monoclonal antibody. In this experiment, a purified human

IgG was run on the same gel as the positive control. After the primary antibody incubation, the membrane was washed 3 times as before. When the primary antibody was a biotin conjugate, ExtrAvidin Peroxidase (Sigma) was used as a secondary diluted to 1:5000 in ELISA blocking solution. The membrane was incubated in this solution for 1 hour. It was washed 3 times as before. After a membrane was labeled with an HRP conjugate, it was treated with a peroxidase substrate to stain the labeled bands. A CN/DAB substrate (Pierce) was used following the provided protocol. The membrane was incubated in this substrate and monitored until bands developed.

Chapter III
Antibody Binding Results and Discussion

Several experiments were conducted using the anti-amyloid antibodies available in our lab. Among these were experiments studying the binding characteristics of these antibodies to Aβ amyloid fibrils. These included salt and pH effect experiments to examine anti-amyloid antibody binding properties. These also included binding studies using fragments of these IgM antibodies to determine the importance of avidity effects to binding. The majority of the work focused primarily on exploring anti-amyloid antibody binding to different amyloid fibrils, specifically fibrils of proline and alanine mutants of Aβ. These experiments sought to explore the impact of single-residue changes and potential fibril structural differences on antibody binding.

Salt and pH Effects on WO1 Binding to Aβ Fibrils

This set of experiments was designed to gain some insight into the nature of WO1 binding to Aβ amyloid. They ask the question of whether electrostatic or hydrophobic interactions are predominant in WO1 binding. Electrostatic interactions are sensitive to changes in buffer ionic strength and pH conditions, whereas hydrophobic

interactions are not significantly impacted. This is important as a reliance on electrostatic interactions supports a specific mode of binding. A dependence on hydrophobic interactions, on the other hand, more likely suggests nonspecific binding. Binding of the WO1 antibody to Aβ fibrils was tested under various salt and pH conditions (Table 1). All solutions used in the salt effect experiments were buffered with 5 mM HEPES. Due to the low ionic strength of this buffer compound, it should not greatly impact the overall ionic strength of the buffer. In addition, these solutions were buffered to pH 7.5, near physiological pH conditions. All solutions used in the pH effect experiments contained 150 mM NaCl to provide approximate physiological ionic strength conditions.

Four different salts were tested at comparable ionic strengths to determine if the particular salt present in the buffer has a significant impact on antibody binding. The four chosen were 1xPBS, NaCl, KCl, and $NaPO_4$ (Table 1). 1xPBS is the standard buffer used in the binding experiments. The other three salts were chosen to compare two different anions and cations. The affinity varied from about 2 nM in 1xPBS to about 10 nM in 75 mM $NaPO_4$, less than an order of magnitude difference between the two extremes (Figure 12). Though

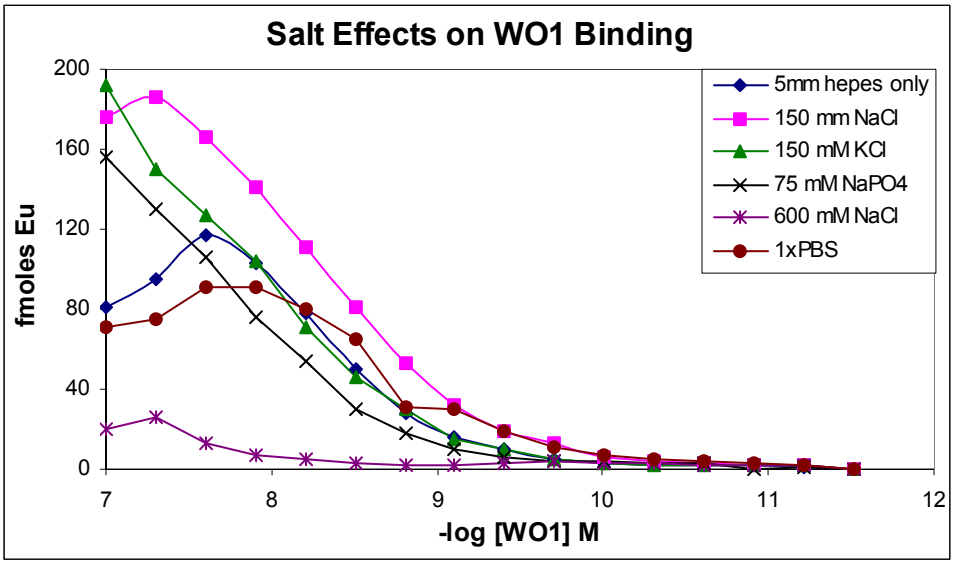


Figure 12. Salt effect on WO1 binding. Binding under various salt conditions was calculated from sigmoid midpoints: 5 mM HEPES only was 4 nM, 150 mM NaCl was 4 nM, 150 mM KCl was 8 nM, 75 mM $NaPO_4$ was 10 nM, 600 mM NaCl was 20 nM, and 1xPBS was 2 nM.

there was some variation, binding was relatively comparable in the presence of the different salts.

Binding was tested under three different ionic strength conditions: 0 mM NaCl, 150 mM NaCl, and 600 mM NaCl (Table 1). Binding was strongest in the near physiological ionic strength buffer, 150 mM NaCl, at an affinity of 4 nM (Figure 12). In a low ionic strength buffer, 5 mM HEPES only, binding is similar. In a high ionic strength buffer, 600 mM NaCl, binding dropped sharply. This manifested in a reduction of both the magnitude and the affinity of binding. The significantly reduced binding in high salt suggests that electrostatic interactions are relatively important to binding and hydrophobic interactions are relatively unimportant. That is not to say that binding is solely controlled by electrostatic interactions, but it does suggest that they are relatively important to binding.

WO1 binding was tested in a range of pH conditions (Table 1). The data produced a continuum of binding affinities with the strongest binding at near physiological conditions, pH 7.4 (Figures 13a & b). There was, however, a discontinuity at pH 5.8 between the PIPES and citrate buffers (Figure 13b). We are not sure exactly why this

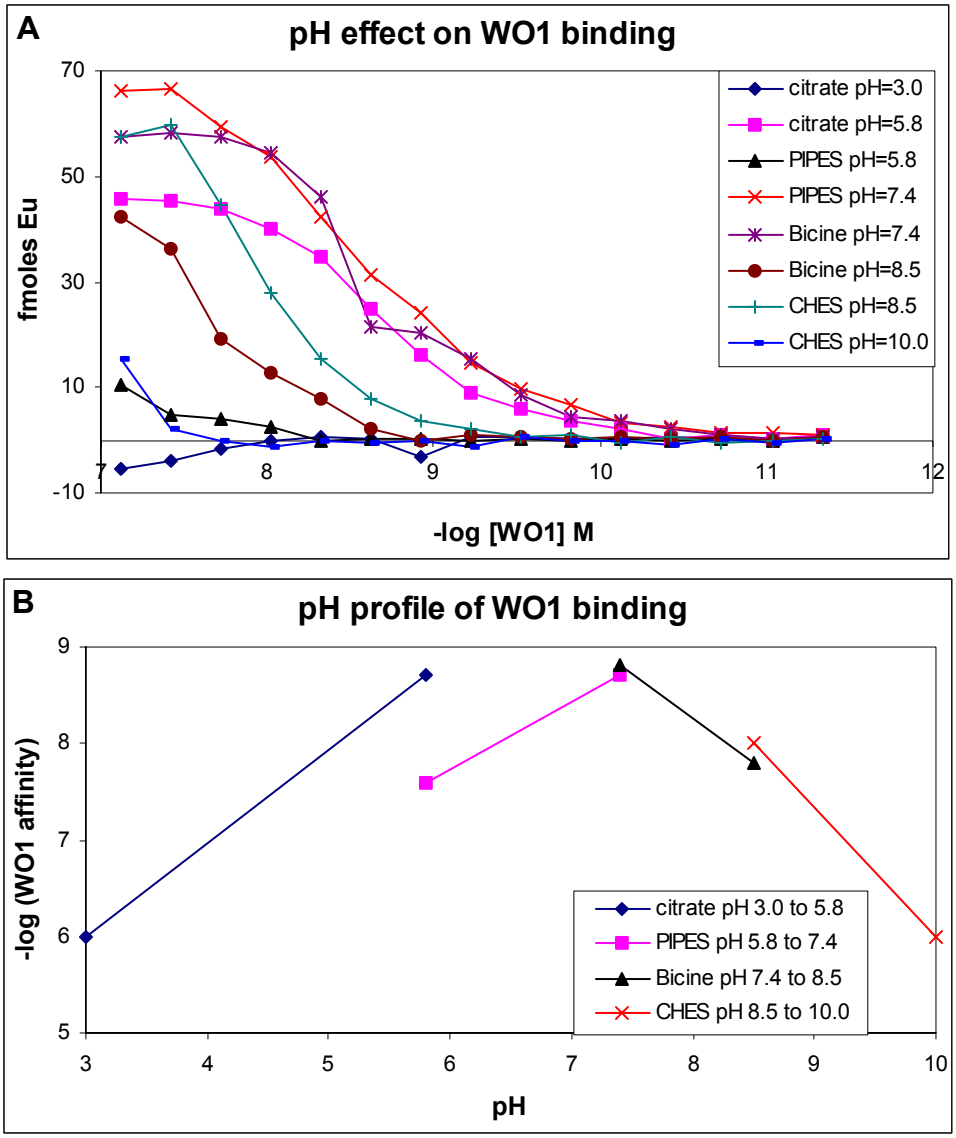


Figure 13. pH effect on WO1 binding. The curves in graph A show binding under various pH conditions. Binding affinities were calculated from the sigmoid midpoints: citrate pH 3.0 showed essentially no binding, pH 5.8 was 2 nM, PIPES pH 5.8 was more than 20 nM, pH 7.4 was 2 nM, Bicine pH 7.4 was 1.5 nM, pH 8.5 was 16 nM, CHES pH 8.5 was 10 nM, pH 10.0 was very low binding (could not be calculated, but no better than 50 nM). Graph B is a plot of -log(affinity) across the pH range of 3.0 to 10.0. Affinities for the pH 3.0 and 10.0 data points could not be calculated since they were so low. The value 6 was substituted for each of these.

inconsistency appeared, but it may be due to buffer effects besides the pH. Even with the gap present, a clear trend arose with binding dropping off sharply at higher and lower pH conditions. This indicated that WO1 is pH-optimized for Aβ amyloid binding. If hydrophobic interactions were predominant in binding, this would likely not be the case. This reinforces the salt effect results suggesting that binding depends at least in part on electrostatic interactions.

Binding of rIgM WO2 Fragments to Aβ Fibrils

This study was conducted to determine if antibody fragments of lower valency than IgM can still bind Aβ fibrils. Since IgM molecules possess ten antigen binding domains (Figure 5), there is likely some avidity effect involved in their binding to amyloid fibrils. That is, several binding domains contribute to the binding affinity in a cooperative manner. This study explores the importance of that effect in the binding of the WO2 IgM molecule to Aβ amyloid. WO2 possesses very similar binding properties to WO1.

The fragment generated was rIgM, a monovalent fragment of the IgM molecule. The advantage of working with this particular fragment is that the same secondary antibody, biotinylated goat anti-mouse IgM

(μ-chain specific), can be used as with the whole IgM molecules in ELISA experiments. The same binding and concentration determination experiments were run on these fragments as on the whole IgM antibodies. The only difference was in calculating concentrations. The molecular weight of the fragment was treated as approximately 90 kDa instead of 900 kDa, so the effective concentration was increased by a factor of ten.

WO2 rIgM binds less strongly to Aβ fibrils than WO2 IgM, possibly due to the reduction in valency (Figure 14a). However, control rIgM generated from mouse IgM (Calbiochem) binds more strongly than control IgM (Figure 14b). In fact, it binds with similar affinity to WO2 rIgM. This is a surprising result. Perhaps exposure of constant regions enhances nonspecific binding of the rIgM fragment. Due to the weaker binding of WO2 rIgM and the stronger binding of control rIgM, WO2 fragments do not bind significantly more strongly than control IgM fragments. Avidity effects appear to be important in WO2 binding to Aβ amyloid fibrils.

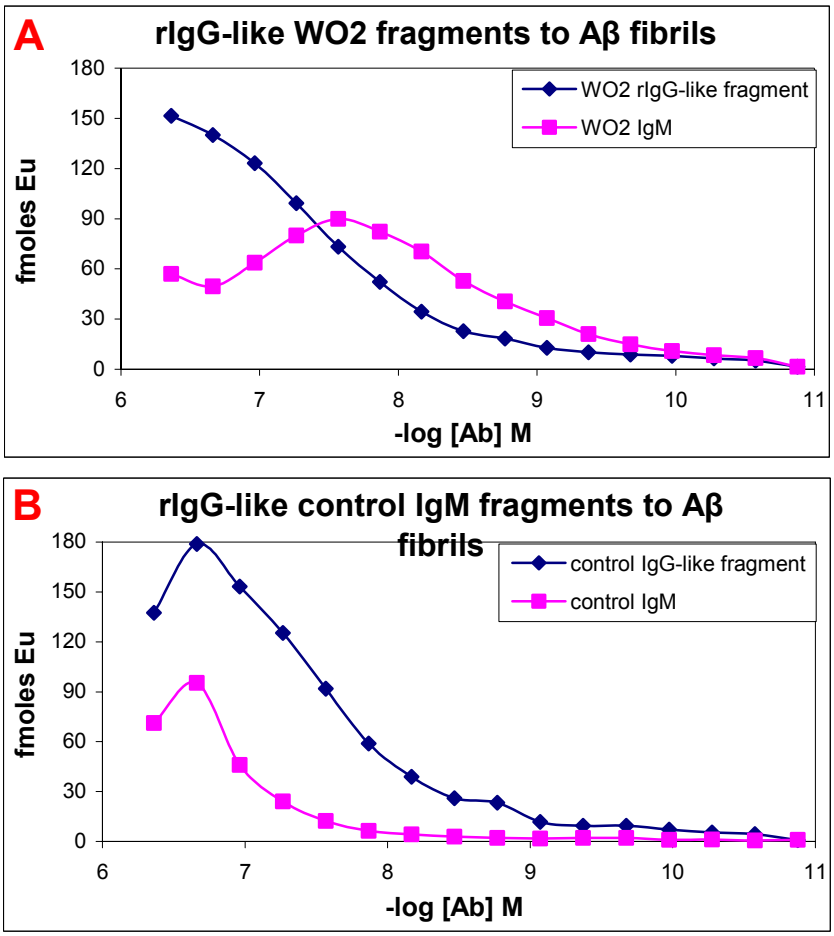


Figure 14. Binding of WO2 rIgM fragments to Aβ fibrils. Graph A shows that the WO2 rIgM fragment bound much less strongly than the WO2 IgM: 32 nM versus 2.5 nM. Graph B shows that the control rIgM fragment bound more strongly than the control IgM: 25 nM versus 130 nM. The fragments ultimately bound with very similar affinity: 32 and 25 nM.

PGA1 Binding to Aβ Amyloid versus Polyglutamine Aggregates

Among the battery of antibodies available in our lab are several raised against polyglutamine aggregates. In characterizing these, we found one to be of particular interest because of its ability to bind Aβ amyloid more strongly than polyglutamine aggregates. This antibody, PGA1, bound Aβ aggregates much more strongly than it did polyglutamine aggregates. PGA1 is a monoclonal IgM isolated from mouse myeloma cultures (Dr. Brian O'Nuallain, unpublished data). It was generated from a mouse immunized with amyloid-like polyglutamine aggregates [45]. Approximate PGA1 affinities were: 20 nM to Aβ fibrils, 70 nM to Q30 aggregates, and 70 nM to Q50 aggregates. PGA1 bound to Aβ fibrils at least three times better than to either polyglutamine aggregate tested (Figure 15). In addition, the magnitude of the binding affinity at saturation was significantly higher for Aβ fibrils. These are surprising results considering that PGA1 was raised against polyglutamine aggregates. The antibody bound aggregates of entirely different protein constituents more strongly than the immunogenic aggregates. This highlights the amyloid structure-specific rather than amino acid sequence-specific nature of these antibodies.

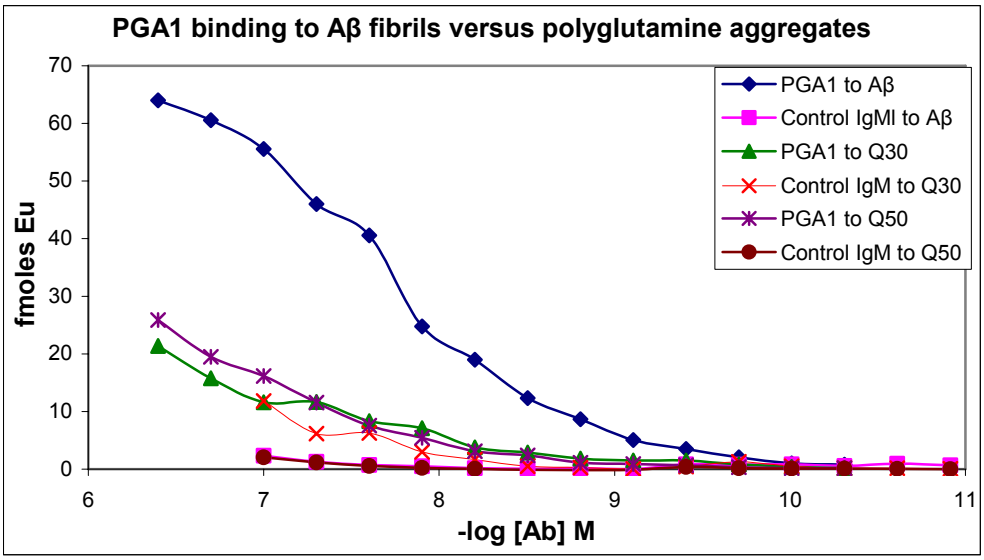


Figure 15. PGA1 binding to Aβ fibrils versus polyglutamine aggregates. Approximate PGA1 affinities: to Aβ fibrils was 20 nM, to Q30 aggregates was 70 nM, to Q50 aggregates was 70 nM.

WO1 and PGA1 Binding to Fibrils of Aβ Proline Mutants

Learning the effects of mutating different residues could tell more about where and how the anti-amyloid antibodies bind to Aβ fibrils. Towards this end, WO1 and PGA1 binding to a number of fibrils of Aβ mutants was analyzed. The first set tested was made up of proline mutant Aβ fibrils. These were the products of a proline scanning mutagenesis project [34]. Fibrils of these mutants were provided by Angela Williams. Though prolines are known to destabilize β-sheet structure, a defining characteristic of amyloids, fibrils managed to grow for all the proline mutants tested. However, the mutant fibrils may be structurally different from wild-type as reflected in varied fibril stabilities and HD exchange protection [34]. EMs of these fibrils were obtained and thioflavin T (ThT) binding was measured to show that the samples are indeed fibrils and not amorphous aggregates [34]. In addition, HD exchange studies suggest that the proline mutant fibrils are structurally similar to wild-type Aβ fibrils [34]. Of course, the fibrils are probably not structurally identical to wild-type. The purpose of these experiments was to determine if the proline mutant Aβ fibrils are still recognized as amyloid by the anti-amyloid antibodies. These experiments also explored differences in binding to each proline mutant fibril.

WO1 binding to a number of proline mutant fibrils of Aβ was tested. Binding was tested in triplicate where possible. Due to the lack of involvement of the amino terminus (~15 residues) in fibril structure [31-33], many mutants from that region were not tested. Only a representative few mutants from the amino terminus were selected. Mutants at residues 18, 19, 20, and 31 were also not tested. These fibrils were not available at the time of this experiment. A double proline mutant (23, 30) and a quadruple proline mutant (9, 23, 30, 37) were tested. These both possess proline mutations in each of the turn regions in the model (Figure 4). The quadruple mutant possesses two additional mutations, one N-terminal and the other C-terminal of the amyloid core in the model. The affinity of WO1 for most of the mutant fibrils was comparable to that for wild-type Aβ fibrils (Figures 16 & 17). In figure 16, the affinity is represented as a function of the free energy difference approximation ($\Delta\Delta G_{app}$) between WO1 binding to wild-type fibrils and proline mutant fibrils. These calculations are not entirely legitimate since the binding curve midpoints on which they are based do not represent true dissociation constant (Kd) values. However, they are useful approximations for looking at the data. The affinity was not drastically lower for any of

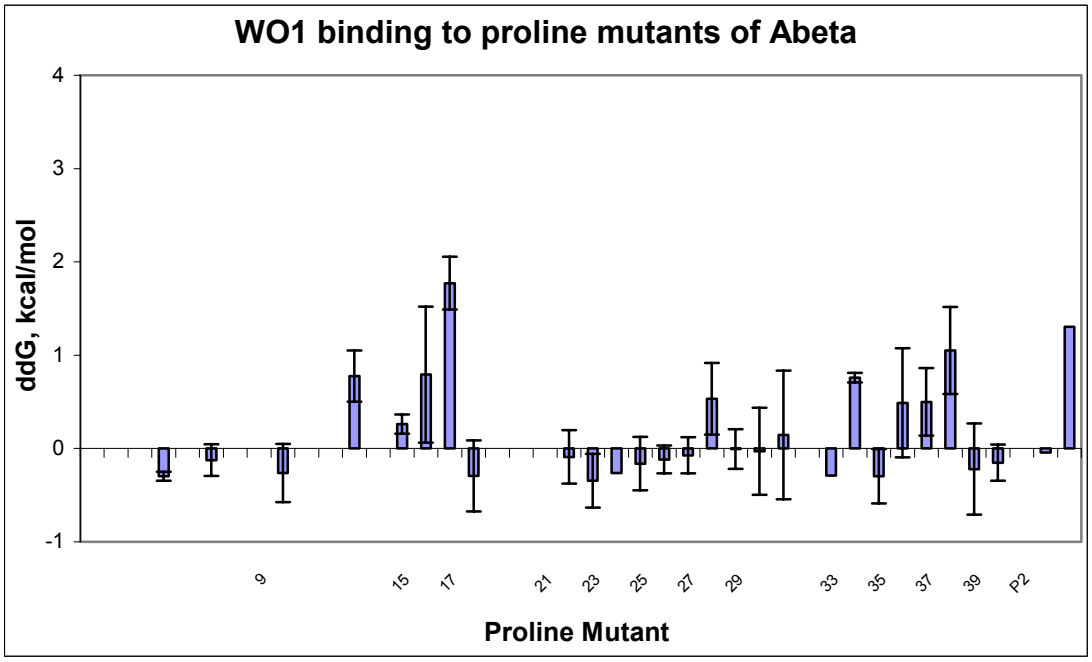


Figure 16. Summary of WO1 binding to proline mutants of Aβ. The six sets of sigmoid curves on the following pages show the binding affinity obtained for WO1 binding to fibrils of each mutant. These represent one set of data, but it was obtained in triplicate with a few exceptions: single replicates for D23P and I32P, duplicates for F4P, N27P, G29P, 2P and 4P, and 5 replicates for K16P. 2P and 4P are the double (23, 30) and quadruple (9, 23, 30, 37) proline mutants, respectively. From the curves, the binding affinity of WO1 for each mutant fibril was calculated. The free energy difference approximation ($\Delta\Delta G_{app}$) for WO1 binding to each mutant relative to WT fibrils was calculated using the equation: $\Delta\Delta G_{app}$ = R*T*ln(WT affinity / mutant affinity). R = 1.987 kcal/(°K * mol) and T = 310.14 °K. These values were plotted on the bar graph with the error bars showing the standard deviation between replicates. In this figure, a higher, positive $\Delta\Delta G_{app}$ indicates that WO1 binds more strongly to the particular proline mutant than to WT.

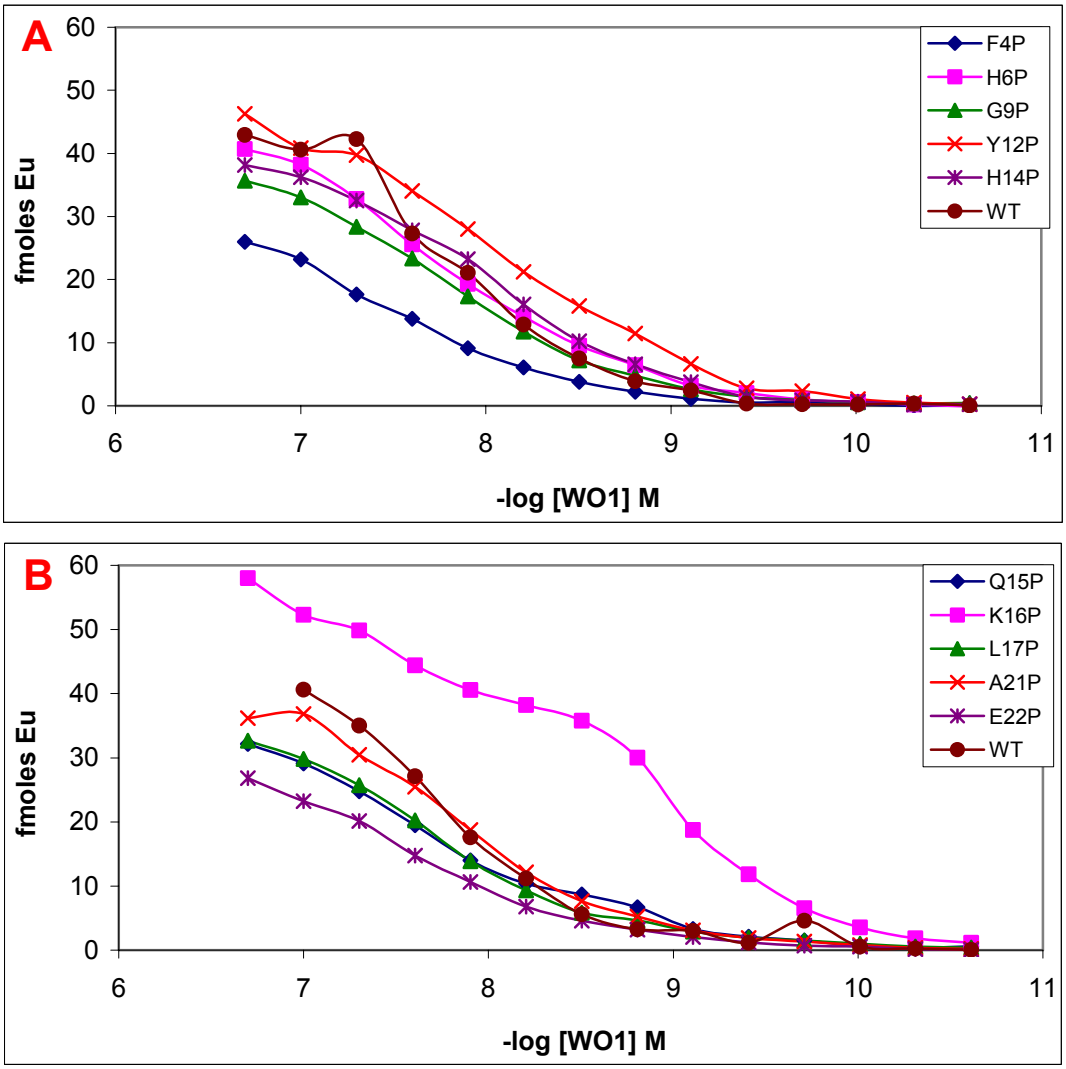


Figure 17. WO1 binding to proline mutants of Aβ. These graphs show one set of ELISA binding data for WO1 binding to proline mutants of Aβ. Kaleidagraph was used to calculate the affinity of WO1 for each mutant by obtaining a sigmoid fit of each curve and extracting the midpoint. For those curves that did not reach an obvious plateau, the highest data point was duplicated at x = 6 to approximate a plateau suitable for a sigmoid curve fit.

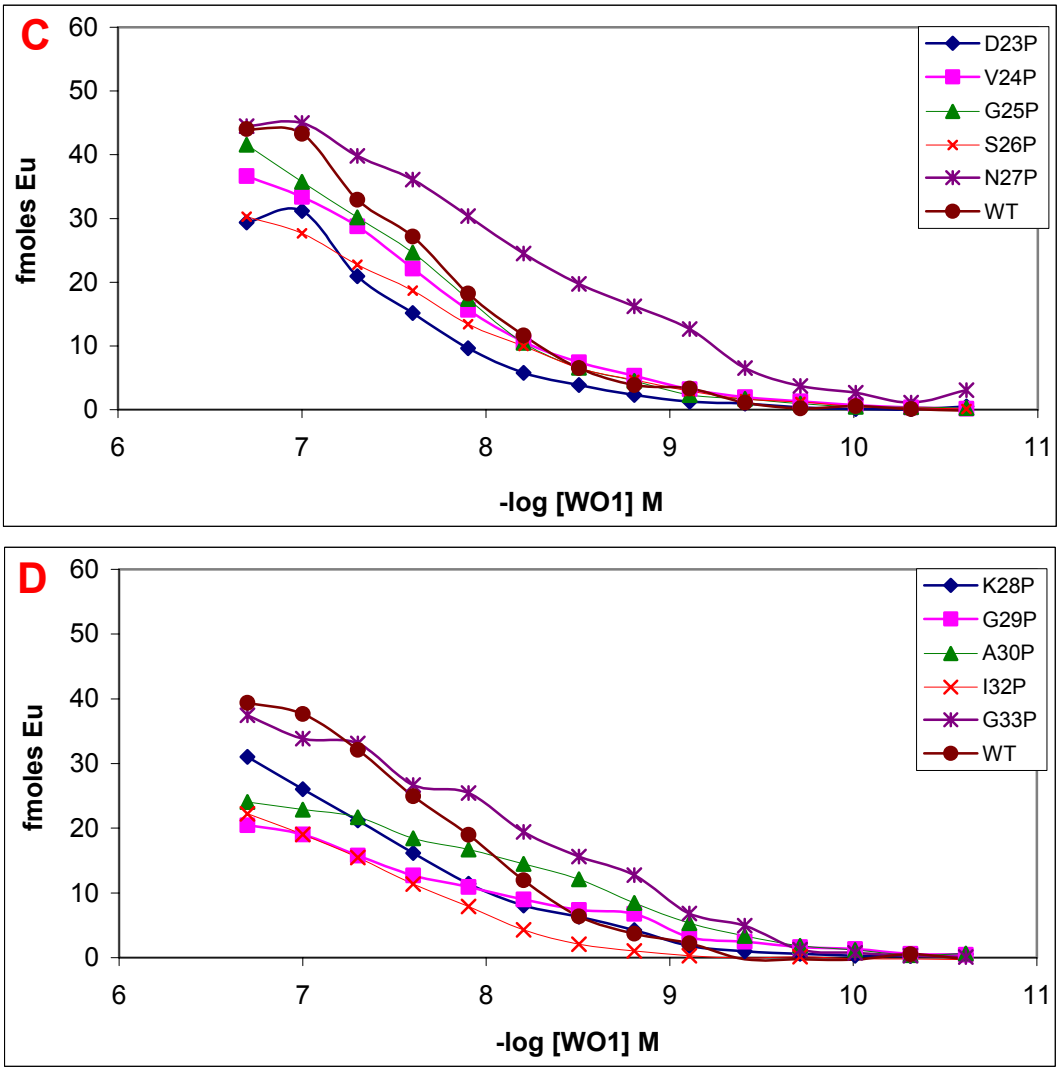


Figure 17. Continued.

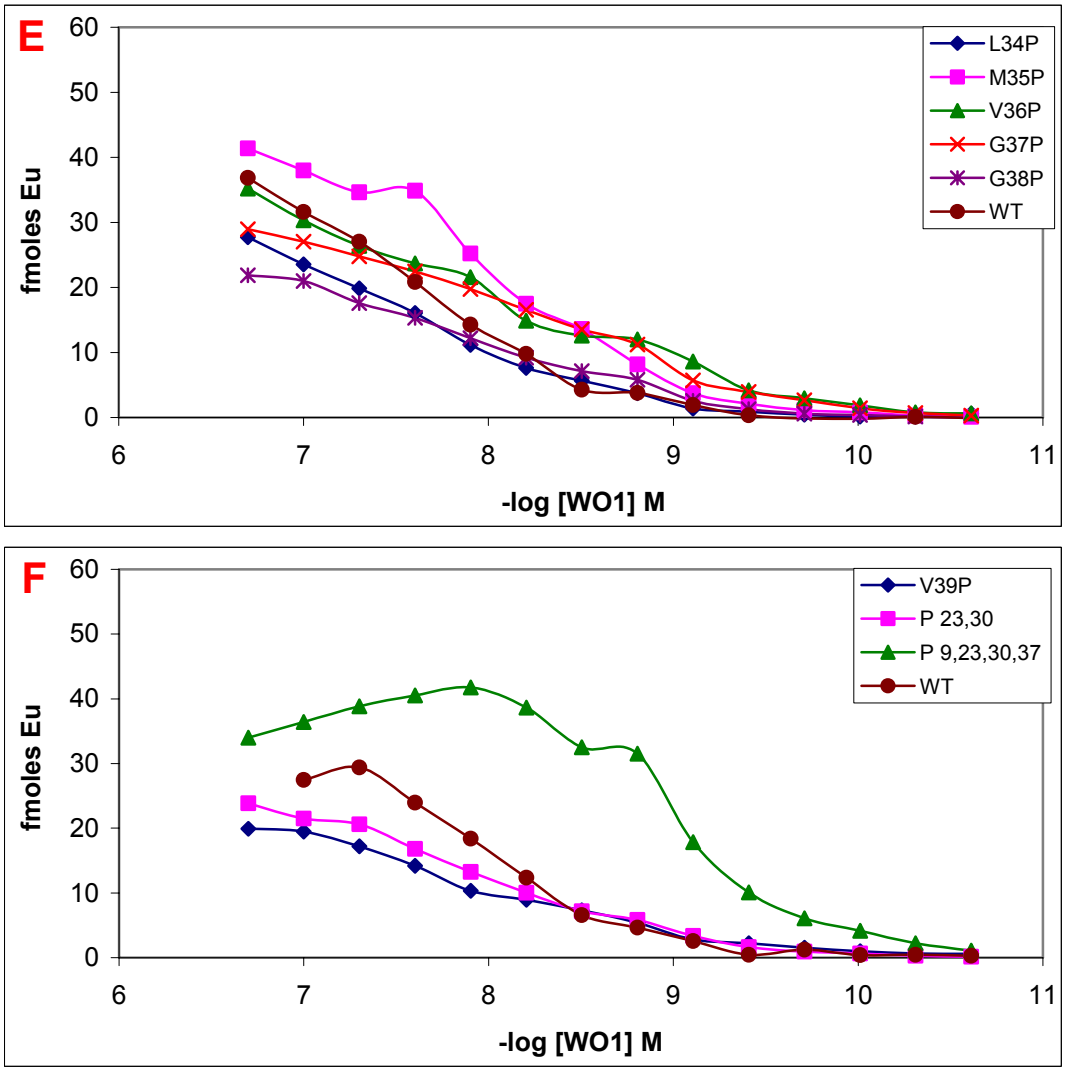


Figure 17. Continued.

the mutant fibrils, but the affinity for several was significantly higher than that for wild-type fibrils. In many cases, such as the mutants at residues 4, 6, 9, and 14, the difference was relatively small with $\Delta\Delta G_{app}$ values less than about 0.5 kcal/mol. Several mutant fibrils, such as those at residues 12, 15, 33, and 37, showed significantly better binding with $\Delta\Delta G_{app}$ values around 0.7 to 1 kcal/mol. One mutant stood up above all the rest. The K16P mutant fibrils were bound much more strongly with a $\Delta\Delta G_{app}$ value around 1.8 kcal/mol. This amounts to about twenty times stronger binding compared to wild-type fibrils. The peak representing this mutant stands out prominently in figure 16.

Since WO1 managed to bind most of the proline mutant fibrils comparably or better to wild-type (Figures 16 & 17), it appears that the structural differences between the different mutant fibrils did not remove the amyloid characteristics of the fibrils as seen by WO1. Of particular note, WO1 bound the K16P mutant fibrils of Aβ much more strongly than wild-type. In our model of Aβ protofilament structure, residue 16 lies towards the end of a β-sheet (Figure 18a). It is near the interface between the unstructured amino-terminus and the amyloidogenic core of the Aβ peptide. The dramatic difference in WO1

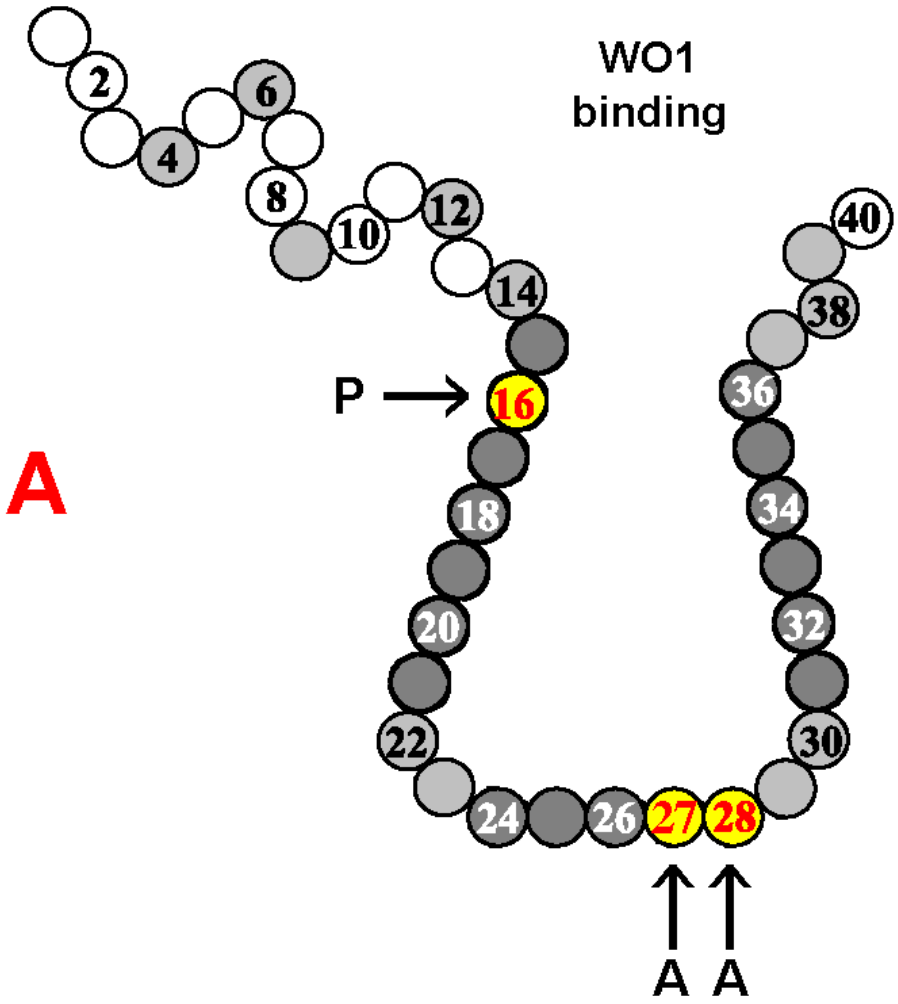


Figure 18. Aβ protofilament cross-section: WO1 and PGA1 binding to mutant fibrils. Based on the binding data, the most significant residues are highlighted in yellow and pointed out with arrows. This figure considers proline (P), alanine (A), cysteine (C), and carboxymethylthio-modified cysteine (^{CMT}C) mutant data. There are other residues with significant binding enhancement in some cases, but only the most significant are shown here. Note that residues 16 and 36 each lie between the amyloid core and the amino- or carboxy-terminus, respectively. Also note that residues 27, 28, 30, and 31 all flank the second turn within the amyloid core.

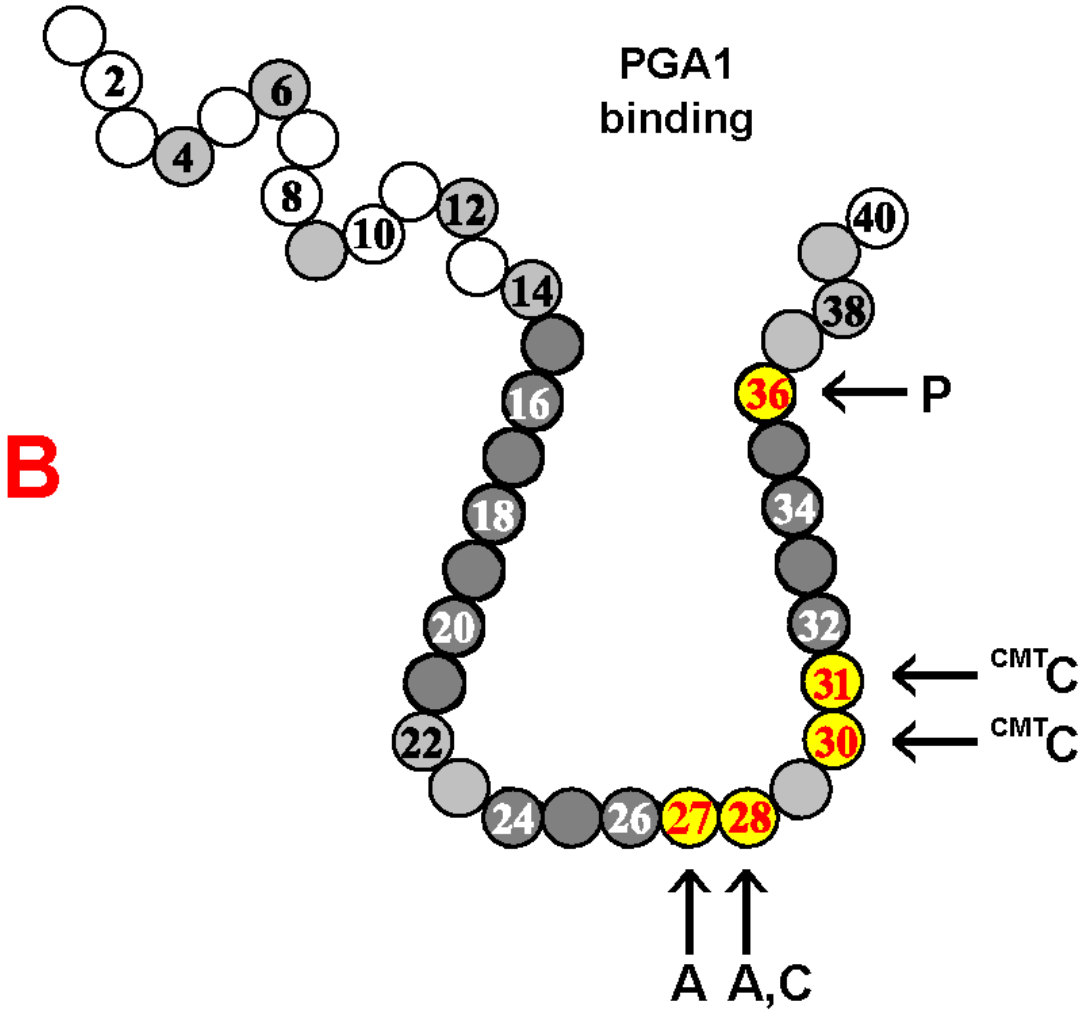


Figure 18. Continued.

affinity for K16P over all the other single proline mutant fibrils and wild-type Aβ suggests that this residue is at an important junction to WO1 binding. There are many possible explanations for why this may be the case. One possible explanation is that the rigid proline, while destabilizing fibril structure globally, may serve to solidify a structural epitope recognized by WO1. Another explanation is that the destabilization may simply make the antibody epitope more accessible to WO1. The second explanation could involve "frayed" fibril ends. As was earlier mentioned, fibrils are composed of multiple protofilaments wound about one another [23]. It could be the case that fibril destabilization could weaken the association of these protofilaments at the fibril ends. These frayed ends could make the WO1 binding site more accessible. This will be discussed in more detail later.

WO1 binding to double and quadruple proline mutant fibrils was also tested [31-33]. These results are shown in figures 16 and 17f. WO1 binding to the double proline (residues 23 and 30) mutant fibrils was similar to wild-type. WO1 binding to the quadruple proline (residues 9, 23, 30, and 37) mutant fibrils was surprisingly good. With four prolines in the sequence, one would have predicted that fibrils would not grow or would be very unstable. Given that the fibrils did

grow, one might expect a greatly altered fibril structure. However, the binding data suggests that the fibrils maintained amyloid character as seen by WO1. The enhanced affinity of WO1 for these fibrils may be primarily due to the proline at residue 37 since the single proline mutants at the other three residues (9, 23, and 30) all seem to have little impact on binding (Figure 16). In building our model of the amyloid structure, we have interpreted this result to indicate that positions 9 and 37 are N-terminal and C-terminal, respectively, to the β-sheet portion of the amyloid, and positions 23 and 30 are in turn regions between β-sheet elements (Figure 18). Prolines are more likely to be tolerated in turn and disordered segments, and at these positions might thus not be destabilizing to fibril structure.

Since PGA1 possesses strong binding to Aβ amyloid (Figure 15), its binding was also tested against the array of available proline mutant Aβ fibrils. PGA1 binding was tested in duplicate. Just as with WO1, the goal was to see the effects of proline mutations on antibody binding. Furthermore, this allowed for a comparison of the binding profiles of WO1 and PGA1 to the proline mutant fibrils. For the most part, the PGA1 binding profile resembles that of WO1 except for a few major differences (Figure 19). The enhanced binding for K16P, at

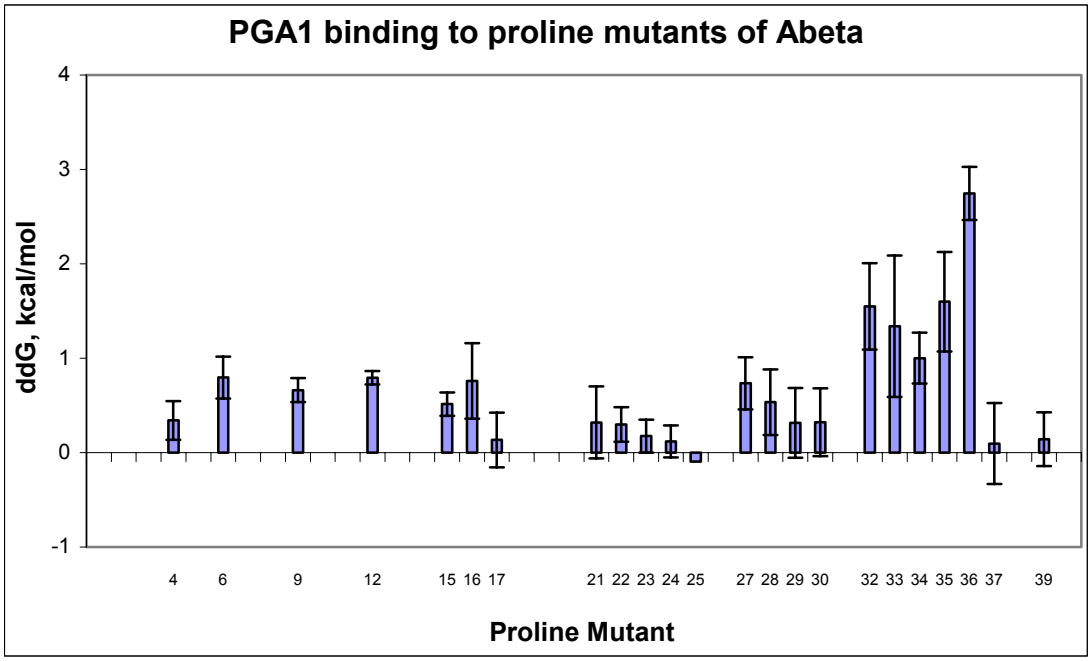


Figure 19. Summary of PGA1 binding to proline mutants of Aβ. Data is in duplicate except: 4 replicates for V36P and a single replicate for G25P. From the binding curves (not shown), the binding affinity of PGA1 for each mutant fibril was calculated. The free energy difference approximation ($\Delta\Delta G_{app}$) for PGA1 binding to each mutant relative to WT fibrils was calculated using the equation shown in figure 16. These values were plotted on the bar graph with the error bars showing the standard deviation between replicates. In this figure, a higher, positive $\Delta\Delta G_{app}$ indicates that PGA1 binds more strongly to the particular proline mutant than to WT.

about 0.8 kcal/mol, is not nearly as pronounced as was found for WO1. There is an island of enhanced binding from mutants I32P to V36P. PGA1 binding to V36P was particularly good with a $\Delta\Delta G_{app}$ value around 3.7 kcal/mol. This amounts to about one hundred times stronger binding compared to wild-type fibrils. This suggests that residue 36 has a strong influence on the PGA1 binding site, not unlike the relationship between residue 16 and WO1 binding. In our model, residue 36 lies towards the end of a β-sheet near the interface between the unstructured carboxy-terminus and the amyloidogenic core of the Aβ peptide (Figure 18b). It is within a region of the peptide reminiscent of the locale of residue 16. Therefore, the enhanced binding of PGA1 may be due to similar effects as were discussed for WO1 binding. This suggests that the PGA1 and WO1 binding sites may be related. However, the marked differences in binding to the proline mutants K16P and V36P emphasizes that the binding sites are not identical. The other clear difference is the greater magnitude of binding enhancement to the mutants in the range of residues 32 to 37 (Figures 16 & 19). Though both WO1 and PGA1 bind to Aβ fibrils, the different binding patterns they exhibit to proline mutants suggests they do not target the exact same binding site.

WO1 and PGA1 Binding to Fibrils of Aβ Alanine Mutants

A project currently in progress involves alanine scanning mutagenesis of the Aβ peptide sequence. Fibrils of these mutants are grown up and analyzed with the same techniques used for the proline mutants (Angela Williams, unpublished data). Alanine mutants should not have drastically altered fibril structures when compared to proline mutants. This means the resulting binding data should be more informative as to local effects of different residues on antibody binding. Not all of the alanine mutant fibrils were assayed since not all were available at the time of testing.

Binding was tested in duplicate for all available mutant fibrils. Like the proline mutant results, WO1 binding to most of the alanine mutant fibrils was comparable to wild-type. There were, nonetheless, a few exceptions (Figure 20). The N27A mutant fibrils were bound much more strongly with a $\Delta\Delta G_{app}$ value around 2.1 kcal/mol. This amounts to about thirty times stronger binding compared to wild-type fibrils. In the model, this residue lies within a β-sheet (Figure 18a). Asparagine is a polar amino acid, but it carries no formal charge under physiological pH conditions. The drastically improved binding to this alanine mutant is surprising. It is possible that the smaller alanine

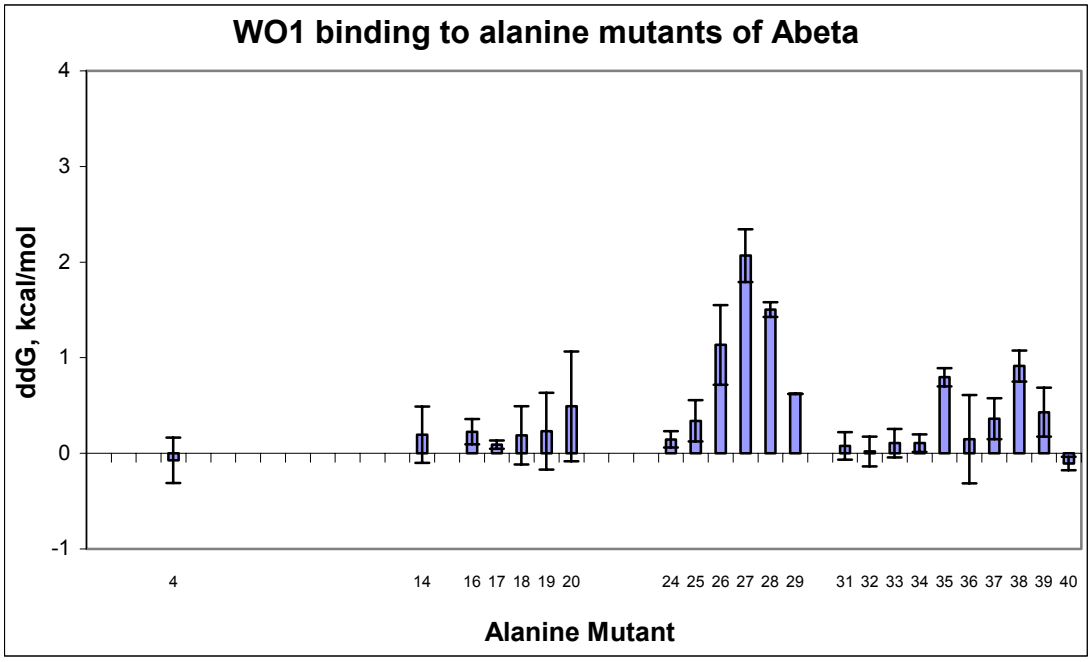


Figure 20. Summary of WO1 binding to alanine mutants of Aβ. Data is in duplicate except: 3 replicates for K16A and L34A. From the binding curves (not shown), the binding affinity of WO1 for each mutant fibril was calculated. The free energy difference approximation ($\Delta\Delta G_{app}$) for WO1 binding to each mutant relative to WT fibrils was calculated using the equation shown in figure 16. These values were plotted on the bar graph with the error bars showing the standard deviation between replicates. In this figure, a higher, positive $\Delta\Delta G_{app}$ indicates that WO1 binds more strongly to the particular alanine mutant than to WT.

may be more favorable in this position to the packing of the amyloid core. This may, in turn, stabilize the epitope recognized by WO1. The large difference in binding affinity suggests that residue 27 is very important in WO1 binding to Aβ amyloid.

The K28A mutant fibrils were bound much more strongly with a $\Delta\Delta G_{app}$ value around 1.5 kcal/mol. This amounts to about ten times stronger binding compared to wild-type fibrils. The alanine is hydrophobic and is much smaller than the positively-charged lysine. The enhanced binding to these fibrils may stem from a net reduction in positive charge of the fibrils. The less positive charge may be more favorable to anti-amyloid antibody binding. However, considering the results at residue 27, the charge difference may be less important. Since residue 28 is directly beside residue 27, it may be affected in a similar manner though to a lesser degree than residue 27. The alanine may be better suited to packing simply because of the smaller size of the side group.

The PGA1 binding results followed a similar pattern to the WO1 results (Figure 21). The N27A mutant fibrils were bound even more strongly with a $\Delta\Delta G_{app}$ value around 2.8 kcal/mol. This amounts to

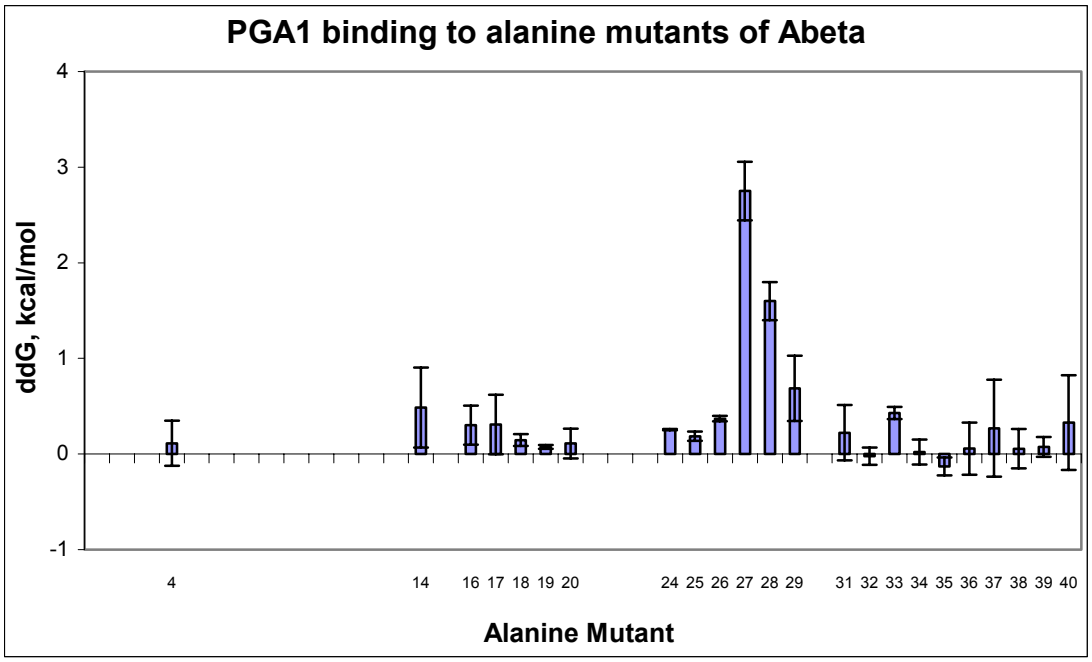


Figure 21. Summary of PGA1 binding to alanine mutants of Aβ. Data is in duplicate. From the binding curves (not shown), the binding affinity of PGA1 for each mutant fibril was calculated. The free energy difference approximation ($\Delta\Delta G_{app}$) for PGA1 binding to each mutant relative to WT fibrils was calculated using the equation shown in figure 16. These values were plotted on the bar graph with the error bars showing the standard deviation between replicates. In this figure, a higher, positive $\Delta\Delta G_{app}$ indicates that PGA1 binds more strongly to the particular alanine mutant than to WT.

about ninety times stronger binding compared to wild-type fibrils (Figure 18b). This is three times the ratio demonstrated by WO1. The K28A mutant fibrils were bound comparably at a $\Delta\Delta G_{app}$ value of around 1.6 kcal/mol. This suggests that residues 27 and 28 carry a similar importance to both WO1 and PGA1 binding, but residue 27 appears to be even more critical in PGA1 binding.

PGA1 Binding to Cysteine and Modified Cysteine Mutants of Aβ

Among the mutant Aβ amyloid fibrils available in our lab are a series of single cysteine mutants. In addition to these fibrils are two sets that have been modified at the cysteine residue. These exploit the fact that the wild-type Aβ sequence contains no cysteines (Figure 3). One set was modified with the addition of an acetic acid group by reaction of the cysteine with iodoacetic acid (IAA). These are carboxymethylthio-modified (CMT) fibrils. The other set was modified with the addition of a methyl group by reaction of the cysteine with methyl iodide (MeI). These are methylthio-modified (MT) fibrils. All three sets of fibrils are products of the work of Dr. Shankaramma Shivaprasad. The CMT-modification provides a negatively charged group at the residue while the MT-modification provides a hydrophobic group. Since these modifications should not alter fibril structure to the

degree that proline does, testing antibody binding to these fibrils should be more telling as to the impact of local changes on antibody binding. These experiments were run to get more insight into the involvement of individual residues in antibody binding. They act as a supplement to the alanine mutant data. None of the three sets of fibrils are complete, so only a few selected mutants were tested (Table 3). PGA1 was the anti-amyloid antibody used in this work. Accordingly, the cysteine mutant binding results were interpreted in relation to the other PGA1 binding results.

Binding was tested to all three modified cysteine mutant fibrils at residue 36 (valine in wild-type) due to its prominence in the proline mutant data. There did not seem to be much difference in binding to any of these fibrils or wild-type, suggesting that local changes at this residue are less important (Table 3). Binding was tested to all three modified cysteine mutant fibrils at residue 28 and to unmodified cysteine mutant fibrils at residue 16 because these residues are lysines in wild-type Aβ (Figure 3). The modified mutant fibrils for residue 16 were not available. Since lysine is a positively charged residue at physiological pH, these experiments were intended to observe the effect of removing or reversing this charge on PGA1

Table 3. PGA1 binding to cysteine mutant fibrils. This table shows the affinity of PGA1 for each mutant and for WT fibrils (run on the same plate on the same day). These data are in single replicates. From the binding curves (not shown), the binding affinity of PGA1 for each mutant fibril was calculated. The free energy difference approximation ($\Delta\Delta G_{app}$) for PGA1 binding to each mutant relative to WT fibrils was calculated using the equation shown in figure 16. These values are shown in the next to last column. Fibril stability is shown in the last column. Fibril stability is expressed as a free energy difference ($\Delta\Delta G$) of fibril formation between the mutant and WT fibrils [34]. These values were calculated from the critical concentrations, the molar concentration of soluble peptide present at equilibrium, of the fibrils [34]. A positive $\Delta\Delta G$ value indicates that the mutant is less stable than WT. The two most dramatic differences are bold and highlighted in red.

	Residue	Mutant Affinity (nM)	WT Affinity (nM)	Binding $\Delta\Delta G_{app}$ (kcal/mol)	Stability $\Delta\Delta G$ (kcal/mol)
Cysteine mutant	K**16**C	16	12	-0.18	0.42
	K**28**C	3.6	20	1.06	0.89
	I**31**C	20	41	0.44	1.47
	I**32**C	25	20	-0.14	2.18
	V**36**C	9.6	12	0.14	1.73
CMT-modified cysteine mutant	K**28**C	22	20	-0.06	1.56
	A30C	***0.44***	***41***	***2.79***	***1.67***
	I31C	***3.5***	***41***	***1.52***	***1.75***
	M**35**C	5.6	12	0.47	2.37
	V**36**C	17	12	-0.21	2.66
MT-modified cysteine mutant	D**23**C	32	20	-0.29	-0.23
	K**28**C	8.7	20	0.51	0.29
	A**30**C	20	41	0.44	0.34
	I**31**C	18	41	0.51	1.46
	V**36**C	12	12	0.00	1.84

binding. These fibrils gave much the same PGA1 binding results as wild-type aside from a moderate binding improvement for the unmodified cysteine mutant at residue 28 (Table 3). Removal of the positive charge at residue 28 appears to have a positive impact on PGA1 binding as seen for the K28C and K28C-MT fibrils. However, a charge reversal due to CMT-modification eliminates the enhanced binding (Table 3). The most interesting results from this work came from PGA1 binding to the CMT-modified fibrils at residues 30 and 31 (alanine and isoleucine in wild-type). PGA1 binding to CMT-modified A30C and I31C was quite good with $\Delta\Delta G_{app}$ values around 2.8 kcal/mol and 1.5 kcal/mol, respectively. These represent roughly ninety- and ten-fold improved PGA1 binding affinity (Table 3, Figure 18b). Replacement of these hydrophobic groups with a negatively charged group seems to be beneficial to binding. In comparison, replacement with the hydrophobic methyl group yielded little change in binding affinity as seen in the binding results to the MT-modified fibrils (Table 3). From these data, it appears that PGA1 binding to Aβ fibrils is not very sensitive to charge differences at residues 16 and 36. PGA1 binding appears to be sensitive to charge differences at residues 28, 30, and 31.

Correlation Analysis

Several characteristics of anti-amyloid antibody binding to fibrils were investigated through the aforementioned experiments. The salt effects results suggest that electrostatic interactions are relatively important to WO1 binding and hydrophobic interactions are relatively unimportant. The pH results suggest that the interaction between WO1 and fibrils is pH-optimized. This further supports the salt effect results since electrostatic interactions are more sensitive to pH than hydrophobic interactions. The WO1 and PGA1 binding results to the many different mutant fibrils looked more closely into amyloid fibril structure. None of the sets of mutants were complete, but there were several noteworthy findings within the available binding results. WO1 binding to K16P fibrils and PGA1 binding to V36P fibrils was greatly enhanced. Both WO1 and PGA1 binding to N27A and K28A fibrils were significantly enhanced. PGA1 binding to A30C-CMT and I31C-CMT fibrils was considerably enhanced while binding to K28C was somewhat enhanced. These are the highlights of the results, but much more information was made clear through comparisons of the binding data to other available data.

An issue mentioned in the results was that WO1 and PGA1 bound comparably or better to most of the mutant fibrils compared to wild-type fibrils. This was somewhat unexpected since one would presume the antibodies would bind significantly less strongly to at least some of the mutant fibrils. A possible explanation for this bias could relate to fibril stability. Most of the proline [34] and alanine (Angela Williams, unpublished data) mutant fibrils were destabilized compared to wild-type fibrils. It could be that the antibodies are better able to bind destabilized fibrils. This relationship could be considered in terms of the fibril superstructure. Mutations causing fibril destabilization could weaken the association of the protofilaments. This could result in these protofilaments coming unwound at fibril ends like the frayed ends of a rope. Frayed fibril ends could make the antibody binding sites more accessible. The fibril stability data were compared to the antibody binding data to look for any potential correlation (Figure 22, Table 4). Antibody binding data were plotted versus fibril stability and best fit lines were determined (Figure 22). Many different comparisons were made, but no correlation was found between any set of binding data and fibril stability (Table 4). It is possible that fibril stability plays a role in antibody binding, but it does not appear to be the dominant factor. A closer look at the data shows some overlap

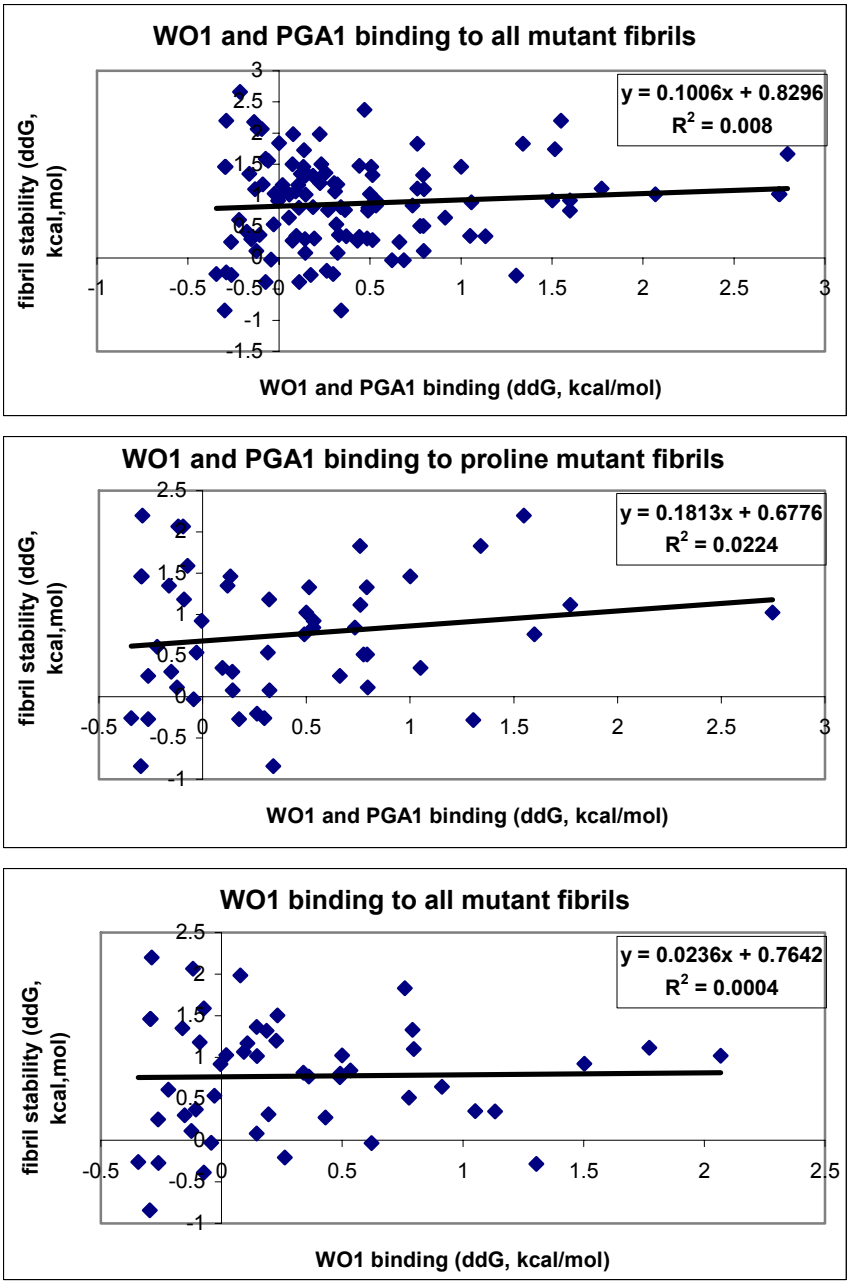


Figure 22. Comparison plots of antibody binding to fibril stability. These plots are examples of the comparisons done for antibody binding versus fibril stability. A best fit line was plotted for each set of data and a correlation coefficient (R^2) found. The first plot shown involves both WO1 and PGA1 binding to all the available mutants including proline, alanine, and cysteine mutants. The other two plots make more specific comparisons of subsets of the data.

Table 4. Comparison table of antibody binding to fibril stability. The first column lists all the different sets of antibody binding data compared to different sets of fibril stability data. The second and third columns show the slope and correlation coefficient (R^2) from the best fit done for each set of data. The highest R^2 value was only 0.14. None of the comparisons showed any significant correlation.

Fibril stability comparison	Slope	R^2
WO1/PGA1 to all mutants	0.1	0.008
WO1/PGA1 to all core mutants (15-36)	0.015	0.0003
WO1/PGA1 to pro mutants	0.18	0.022
WO1/PGA1 to ala mutants	-0.033	0.0013
WO1/PGA1 to core pro mutants (15-36)	0.029	0.0009
WO1/PGA1 to core ala mutants (15-36)	-0.18	0.067
WO1 to pro/ala mutants	0.024	0.0004
PGA1 to pro/ala mutants	0.14	0.019
WO1 to core pro/ala mutants (15-36)	-0.095	0.0087
PGA1 to core pro/ala mutants (15-36)	0.069	0.0073
WO1 to pro mutants	0.031	0.0005
PGA to pro mutants	0.32	0.071
WO1 to ala mutants	-0.052	0.0027
PGA1 to ala mutants	-0.02	0.0006
WO1 to core pro mutants (15-36)	0.095	0.0054
PGA to core pro mutants (15-36)	0.21	0.045
WO1 to core ala mutants (15-36)	-0.28	0.14
PGA1 to core ala mutants (15-36)	-0.083	0.018

Between them (Figure 23). For the proline mutant fibrils, the data overlap at residues 15, 16, 27, and generally 33 to 36 (Figures 23a & b). For the alanine mutant fibrils, the data overlap at residues 27 and 28 (Figures 23c & d). These data include the mutant fibrils to which the antibodies bound particularly well. This suggests that fibril stability may have some impact on binding.

Another issue mentioned in the results is the importance of the overall charge of the fibril or of certain residues within the Aβ sequence. Considering all the mutant fibril binding data, it appears that less positively charged or more negatively charged fibrils are often bound better by the WO1 and PGA1 antibodies. This is evidenced by anti-amyloid antibody binding to the K16P, K28A, K28C, A30C-CMT, and I31C-CMT mutant Aβ fibrils. This is not always the case such as for PGA1 binding to K16P, K16C, and K28C-CMT mutant fibrils and for WO1 binding to K16A fibrils. Nonetheless, the charge of these residues appears to have a strong impact on anti-amyloid antibody binding. A comparison of the antibody binding data to hydrophobicity change data was employed to further investigate these results [46]. The binding data were compared to the change in hydrophobicity due to the replacement of a wild-type residue with

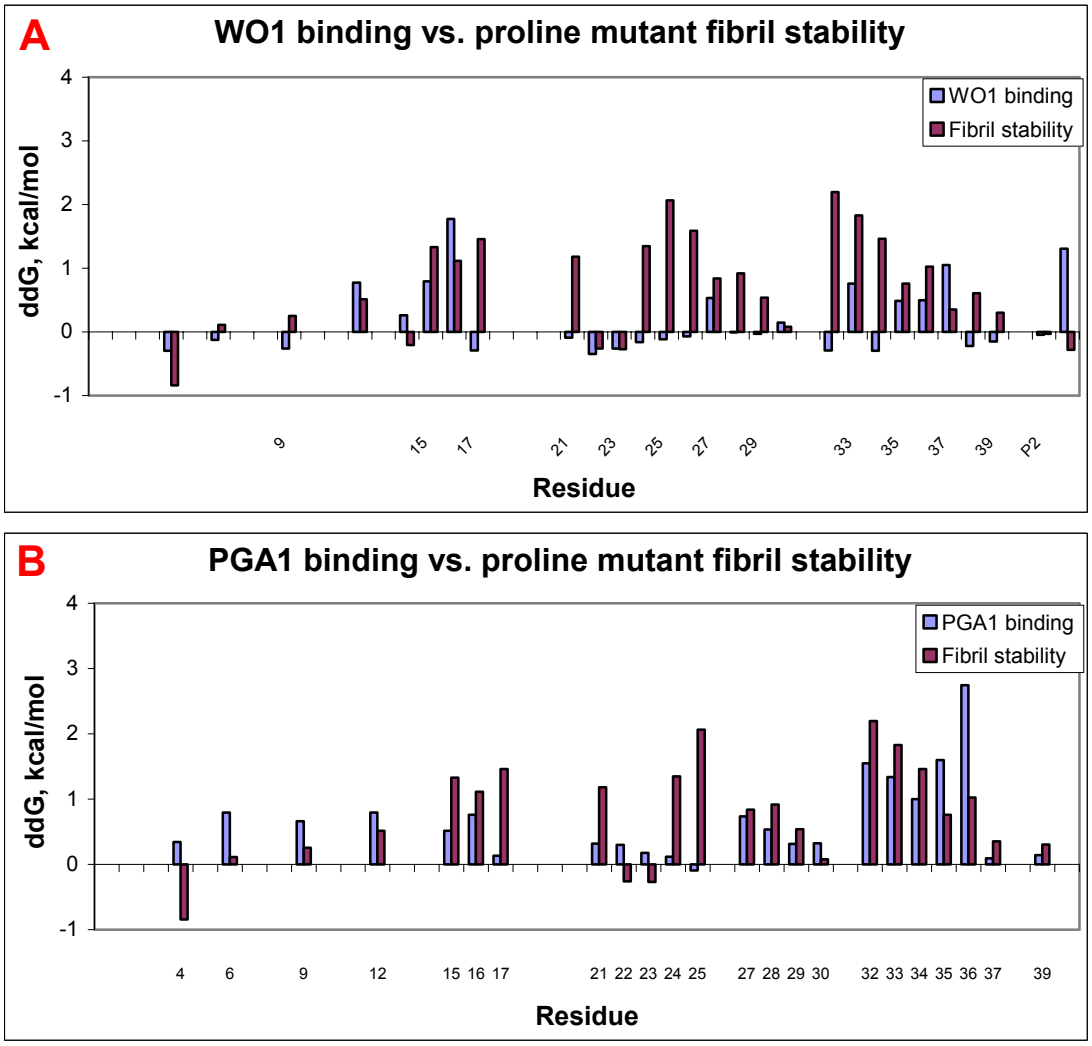


Figure 23. WO1 and PGA1 binding to proline and alanine mutant fibrils versus fibril stability. The binding data were plotted alongside proline and alanine mutant fibril stability data. A positive fibril stability value indicates that the mutant is destabilized compared to WT fibrils. A positive $\Delta\Delta G_{app}$ value for antibody binding indicates the antibody bound more strongly to the mutant fibrils than to WT fibrils.

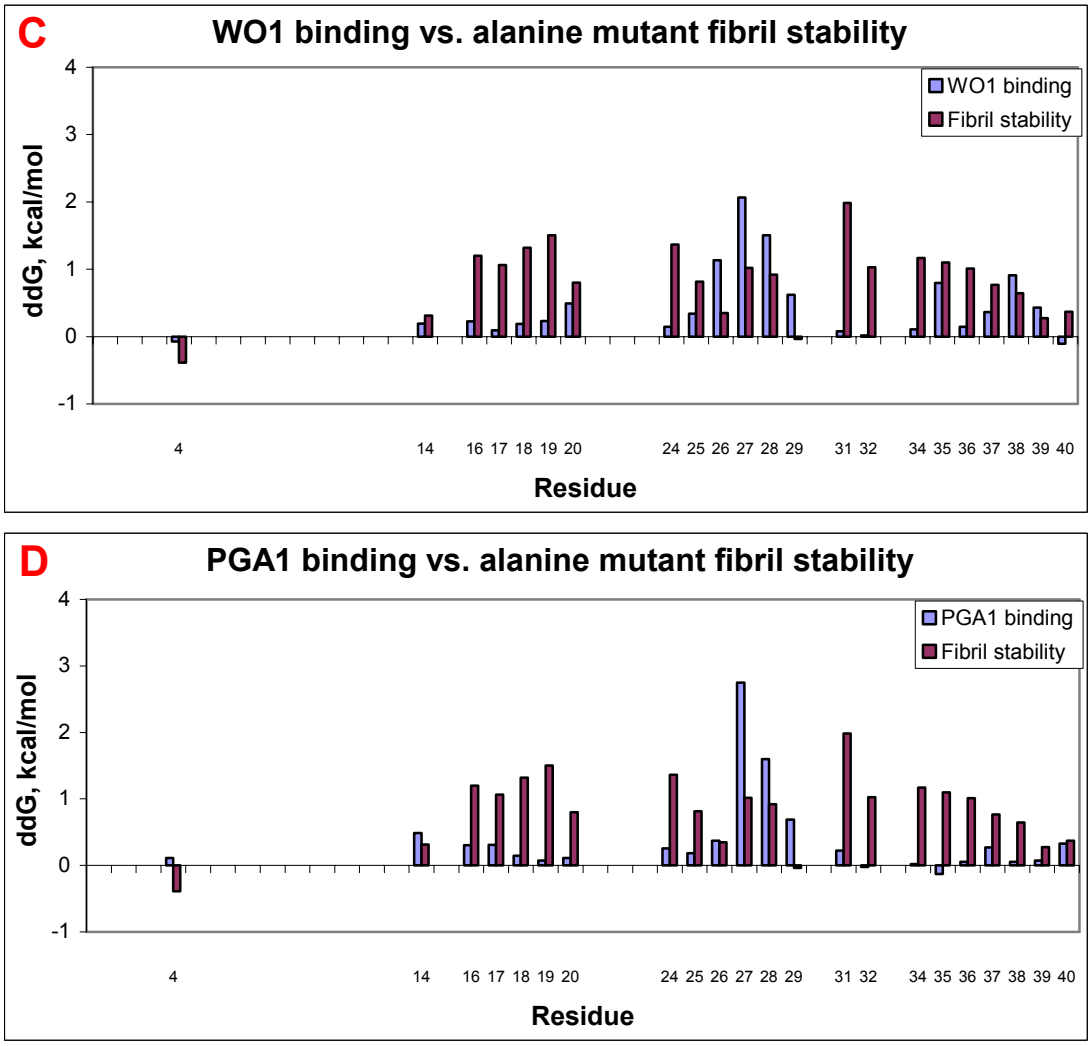


Figure 23. Continued.

either proline or alanine. The hydrophobicity change data are based on water/octanol partitioning of individual amino acids [46], so they only approximate the change in the Aβ peptide. The hydrophobicity change data were compared to the antibody binding data to look for any potential correlation (Figure 24, Table 5). Antibody binding data were plotted versus hydrophobicity change and best fit lines were determined (Figure 24). Many different comparisons were made, but no correlation was found for any of them (Table 5). This suggests that WO1 and PGA1 binding do not correlate simply with the bulk hydrophobicity or hydrophilicity of amyloid fibrils. However, there does appear to be some correlation at certain residues. WO1 binding data to the proline mutant fibrils coincides with the hydrophobicity change data significantly at residues 16, 33, and 37 (Figure 25a). Residue 16 was expected to stand out due to the positive charge and highly hydrophilic nature of lysine. There was no correlation at residue 28, the other lysine to proline mutation. Perhaps substituting a rigid proline at position 28 alters the fibril structure unfavorably for WO1 binding. Residues 33 and 37 are both glycines in wild-type Aβ. Glycine is a somewhat hydrophilic, uncharged residue. WO1 may bind more strongly to these mutants because of the increased hydrophobicity or it may do so because of the significant structural

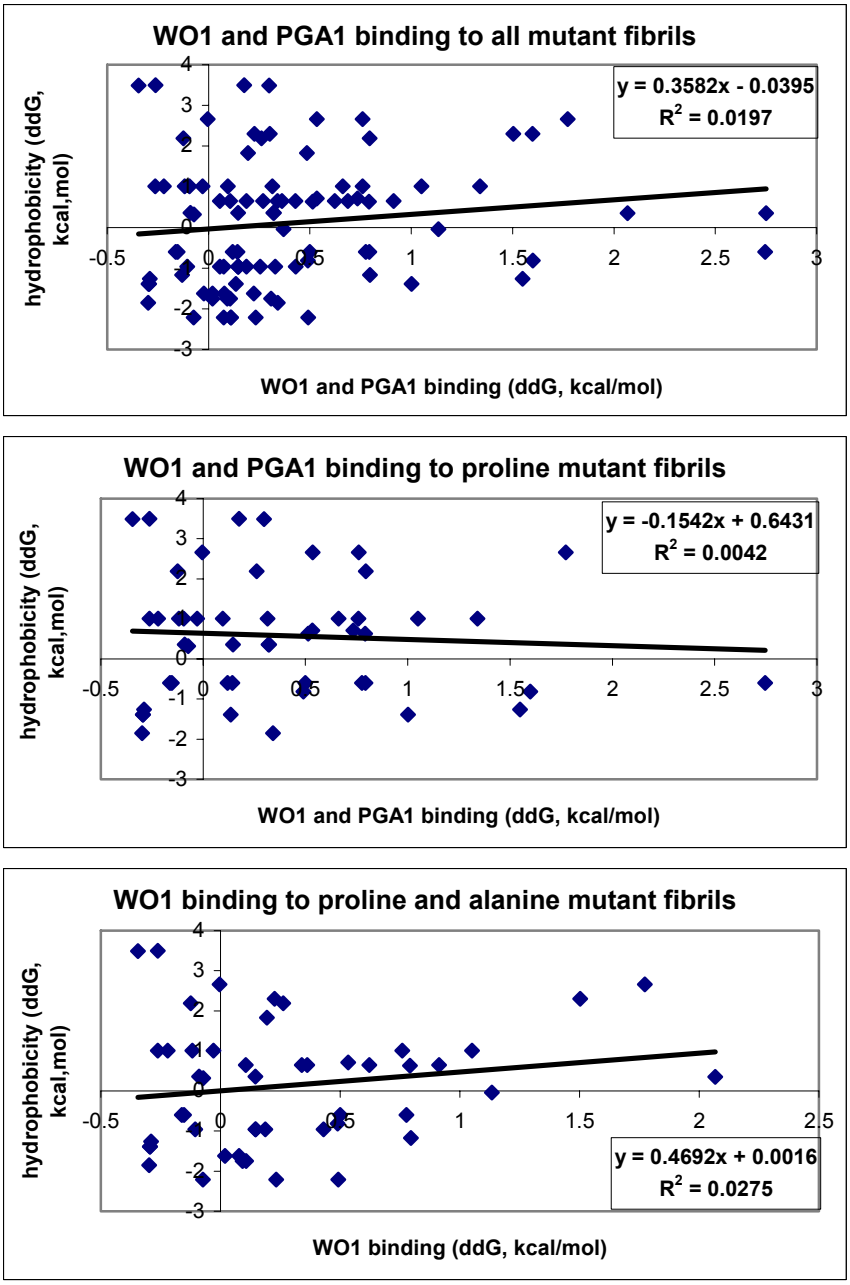


Figure 24. Comparison plots of antibody binding to hydrophobicity change. These plots are examples of the comparisons done for antibody binding versus hydrophobicity change. A best fit line was plotted for each set of data and a correlation coefficient (R^2) found. The first plot shown involves both WO1 and PGA1 binding to all the available proline and alanine mutant fibrils. The other two plots make more specific comparisons of subsets of the data.

Table 5. Comparison table of antibody binding to hydrophobicity change. The first column lists all the different sets of antibody binding data compared to different sets of hydrophobicity change data. The second and third columns show the slope and correlation coefficient (R^2) from the best fit done for each set of data. The highest R^2 value was only 0.25. None of the comparisons showed any significant correlation.

Hydrophobicity comparison	Slope	R^2
WO1/PGA1 to pro/ala mutants	0.36	0.02
WO1/PGA1 to core pro/ala mutants (15-36)	0.32	0.017
WO1/PGA1 to pro mutants	-0.15	0.0042
WO1/PGA1 to ala mutants	1.05	0.18
WO1/PGA1 to core pro mutants (15-36)	-0.26	0.013
WO1/PGA1 to core ala mutants (15-36)	1.04	0.22
WO1 to pro/ala mutants	0.47	0.028
PGA1 to pro/ala mutants	0.32	0.017
WO1 to core pro/ala mutants (15-36)	0.48	0.03
PGA1 to core pro/ala mutants (15-36)	0.23	0.011
WO1 to pro mutants	0.46	0.026
PGA to pro mutants	-0.62	0.067
WO1 to ala mutants	1.11	0.17
PGA1 to ala mutants	1.01	0.2
WO1 to core pro mutants (15-36)	0.53	0.034
PGA to core pro mutants (15-36)	-0.84	0.14
WO1 to core ala mutants (15-36)	1.1	0.2
PGA1 to core ala mutants (15-36)	1.01	0.25

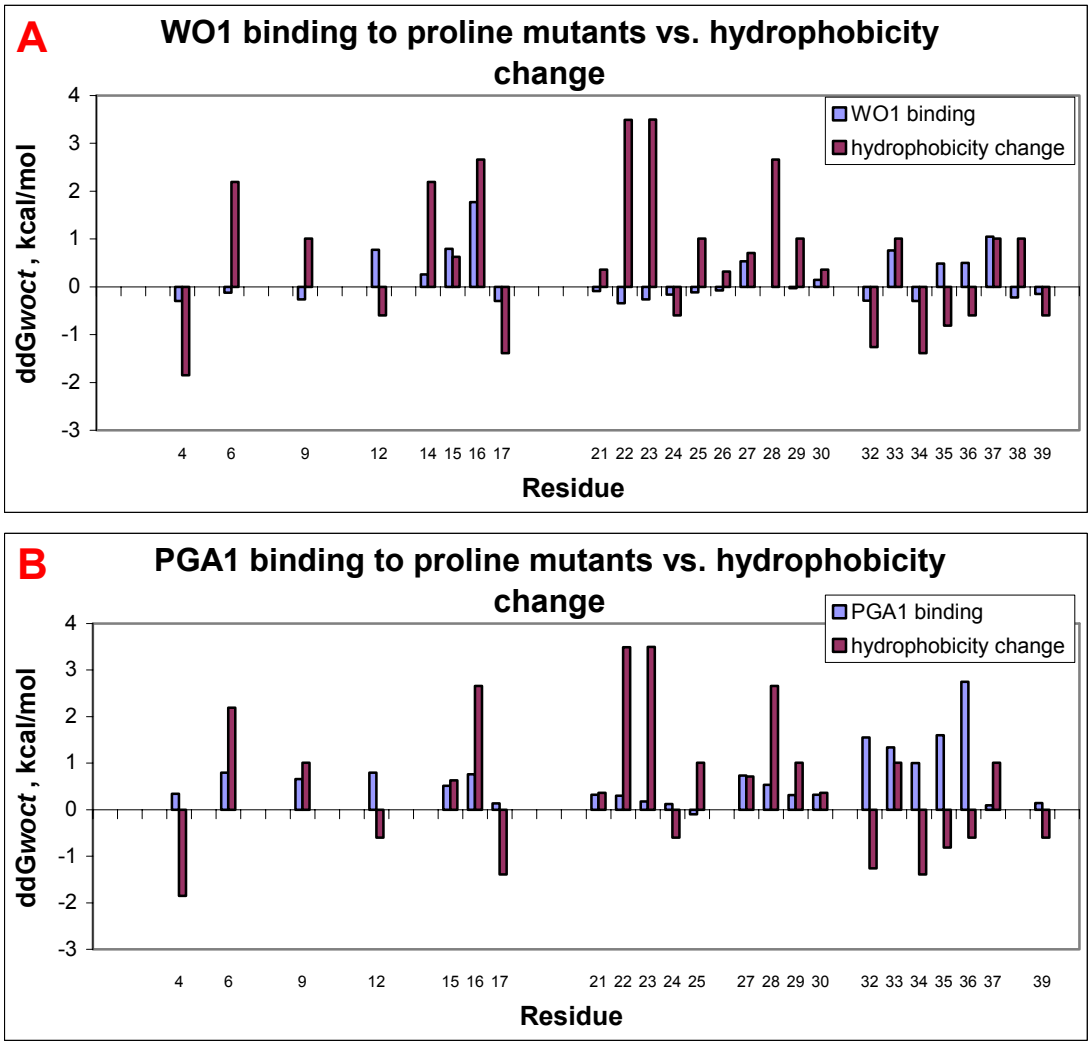


Figure 25. WO1 and PGA1 binding to proline and alanine mutant fibrils versus hydrophobicity change. The antibody binding data were plotted alongside hydrophobicity change data. The hydrophobicity change data are based on water/octanol partitioning of amino acids [46]. To calculate the change in hydrophobicity for each mutant, the hydrophobicity value for either proline or alanine was subtracted from that for the WT residue. A positive hydrophobicity change value indicates increased hydrophobicity. A positive $\Delta\Delta G_{app}$ value for antibody binding indicates the antibody bound more strongly to the mutant fibrils than to WT fibrils.

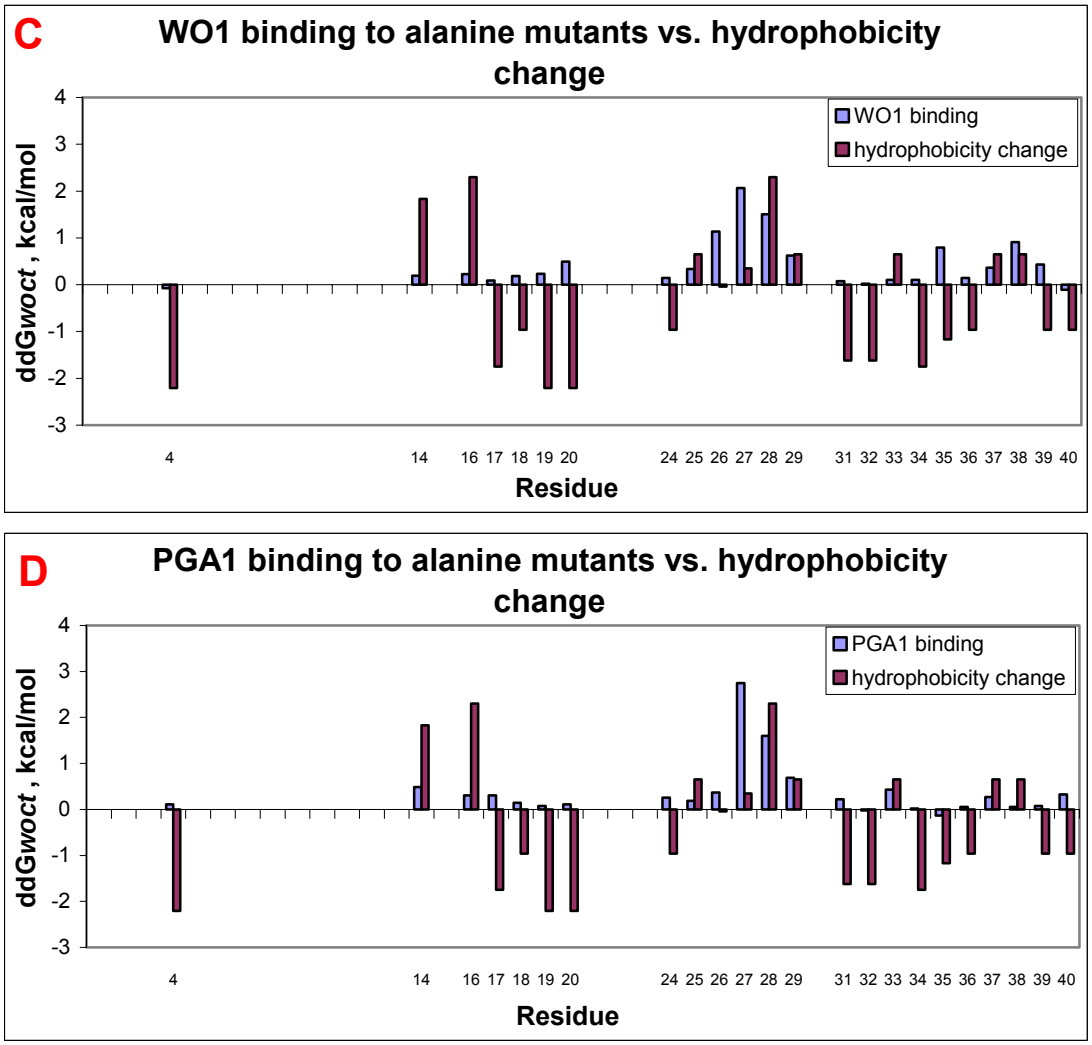


Figure 25. Continued.

change between the very flexible glycine and the rigid proline. The PGA1 binding data to the proline mutant fibrils coincides with the hydrophobicity change data at residues 16, 28, and 33 (Figure 25b). Residues 16 and 28 were expected to stand out since they are both lysines in wild-type fibrils. Residue 33 may stand out for the same reasons discussed for WO1 binding. These results are revealing, but the limitation that proline can substantially alter fibril structure must be considered for these fibrils.

A comparison of antibody binding to hydrophobicity changes for alanine mutant fibrils could be more informative since alanine should not cause substantial structural changes. The WO1 and PGA1 binding data to these fibrils coincides significantly with the hydrophobicity change data only at residue 28 (Figures 25c & d). This suggests that both antibodies bind more strongly to fibrils that are more hydrophobic at this residue. The PGA1 binding data to the cysteine and modified cysteine mutants at residue 28 support this notion (Table 3). There was enhanced PGA1 binding to the more hydrophobic K28C and K28C-MT fibrils, but not to the negatively charged K28C-CMT fibrils. These results are further supported by studies of accessibility of cysteine mutant fibrils to alkylation by iodoacetic acid (Dr. Shankaramma

Shivaprasad, unpublished data). These studies showed residue 28 to be inaccessible to solvent, suggesting it is buried in the amyloid core. If this is the case, a hydrophobic amino acid at this residue could potentially stabilize the epitopes recognized by the antibodies. Residues 16, 33, and 37 do not show a strong correlation as is seen with the proline mutants (Figures 25c & d). This suggests that the improved binding to the proline mutant fibrils at these residues may be due to structural changes rather than simply increased hydrophobicity. In the case of residue 16, it may be due to structural changes rather than the removal of the positive charge.

The results for PGA1 binding to several mutants at residue 28 initially seem to run counter to the salt and pH effects experiments (Figure 25, Table 3). The antibodies appear to prefer that residue 28 is hydrophobic. This would suggest that the antibodies bind through hydrophobic interactions. However, residue 28 appears to be buried in the amyloid core. Furthermore, PGA1 binding to mutants of residues 30 and 31 suggests electrostatic interactions are more important (Table 3). There was greatly enhanced PGA1 binding to the negatively charged A30C-CMT and I31C-CMT mutant fibrils, but not to the unmodified or MT-modified fibrils. These results suggest PGA1 may

rely more on electrostatic interactions. It is still likely that the binding of PGA1 to fibrils is not entirely dependant on electrostatic interactions. Nonetheless, PGA1 binding appears to be more dependant upon electrostatic interactions.

There are many cases of enhanced antibody binding not attributable to just charge or stability differences. These include WO1 binding to K16P and PGA1 binding to V36P fibrils (Figures 23 & 25). In these cases, charge was not found to be important and fibril stability was not drastically higher or lower than many mutant fibrils that were bound less strongly by the antibodies. There may be specific structural changes to these fibrils that make the antibody epitopes more accessible or more favorable to the antibodies. For K16P and V36P, one possible explanation is that the rigid proline could serve to secure the unstructured amino- or carboxy-terminus such that it cannot fold back onto the amyloid core. This may allow better antibody access to the fibril surface. The enhanced binding of WO1 and PGA1 to N27A fibrils was unexpected. It does not appear to be attributable to either a charge difference or a large stability difference (Figures 23 & 25). These fibrils are destabilized, but not appreciably more or less than many fibrils that were bound much less strongly by

the antibodies. It appears that both WO1 and PGA1 binding are very sensitive to changes at this residue. It could be that the structural change, however small, imparted by substituting alanine for asparagine stabilizes the epitopes recognized by the antibodies.

Another available set of data to which antibody binding can be compared is ThT binding. These data were collected during the monitoring of fibril growth progress for all of the mutant fibrils (Angela Williams) [34]. The level of ThT binding is measured to detect the amount of fibrils in a sample. Eventually, a maximal level of ThT binding is obtained. This value is corrected based on the starting and ending concentrations of Aβ monomer in a sample. The reason for this correction is that ThT is measured on a fibril suspension that contains varying percentages of fibrils, depending on the fibril stability conferred by the mutation. ThT signal can be attributed to multiple possible effects: ThT binding affinity, ThT binding site number, and/or ThT fluorescent yield. It may be a combination of these three factors affecting binding. This should be kept in mind when comparing the antibody and ThT binding data. These two sets of data were compared to look for any potential correlation between them (Figure 26, Table 6). Antibody binding data were plotted versus ThT binding data and

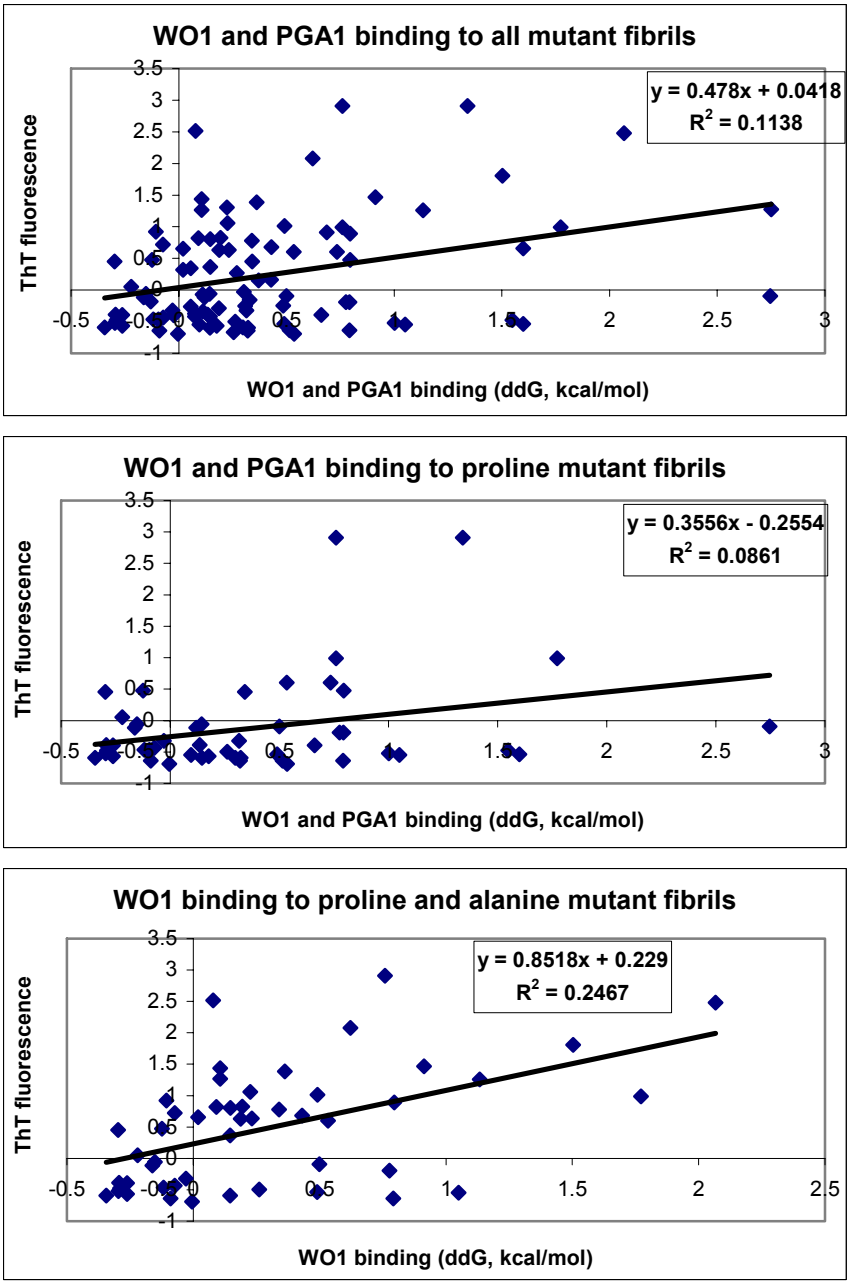


Figure 26. Comparison plots of antibody binding to ThT binding. These plots are examples of the comparisons done for antibody binding versus ThT binding. A best fit line was plotted for each set of data and a correlation coefficient (R^2) found. The first plot shown involves both WO1 and PGA1 binding to all the available proline and alanine mutant fibrils. The other two plots make more specific comparisons of subsets of the data.

Table 6. Comparison table of antibody binding to ThT binding. The first column lists all the different sets of antibody binding data compared to different sets of hydrophobicity change data. The second and third columns show the slope and correlation coefficient (R^2) from the best fit done for each set of data. The highest R^2 value was 0.42. None of the comparisons showed a strong correlation.

ThT fluorescence	Slope	R^2
WO1/PGA1 to pro/ala mutants	0.48	0.11
WO1/PGA1 to core pro/ala mutants (15-36)	0.54	0.15
WO1/PGA1 to pro mutants	0.36	0.086
WO1/PGA1 to ala mutants	0.62	0.21
WO1/PGA1 to core pro mutants (15-36)	0.47	0.13
WO1/PGA1 to core ala mutants (15-36)	0.61	0.22
WO1 to pro/ala mutants	0.85	0.25
PGA1 to pro/ala mutants	0.37	0.12
WO1 to core pro/ala mutants (15-36)	1.04	0.34
PGA1 to core pro/ala mutants (15-36)	0.38	0.13
WO1 to pro mutants	0.55	0.15
PGA to pro mutants	0.31	0.063
WO1 to ala mutants	0.62	0.32
PGA1 to ala mutants	0.54	0.39
WO1 to core pro mutants (15-36)	0.93	0.33
PGA to core pro mutants (15-36)	0.33	0.07
WO1 to core ala mutants (15-36)	0.61	0.29
PGA1 to core ala mutants (15-36)	0.55	0.42

best fit lines were determined (Figure 26). Many different comparisons were made, but no strong correlation was found for any of them (Table 6). However, overall the correlations were significantly better than for the other attempted comparisons. There also appeared to be correlation at certain residues. WO1 and ThT binding appeared to have numerous connections within the set of proline mutants (Figure 27a). The most prominent of these were at residues 16, 27, and 33. Likewise, residues 16, 27, and 33 stood out notably for PGA1 binding (Figure 27b). These residues were earlier suggested to be important for antibody binding due to possible structural changes rather than to charge or major stability differences. It is possible that ThT binding is similarly affected by these changes. WO1 and PGA1 binding to the alanine mutant fibrils appeared to overlap ThT binding, particularly at residues 27, 28, and 29 (Figure 27c & d). These alanine mutant fibrils are the most strongly bound by WO1 and PGA1. They also represent three of the four alanine mutants most strongly bound by ThT (Figure 27c & d). There are many parallels between the binding of the antibodies and ThT to the alanine mutant fibrils. As such, it is quite possible that the binding sites of the antibodies and ThT are related. It is also possible that ThT and antibody binding both correlate with an unknown third variable, such as fibril flexibility or

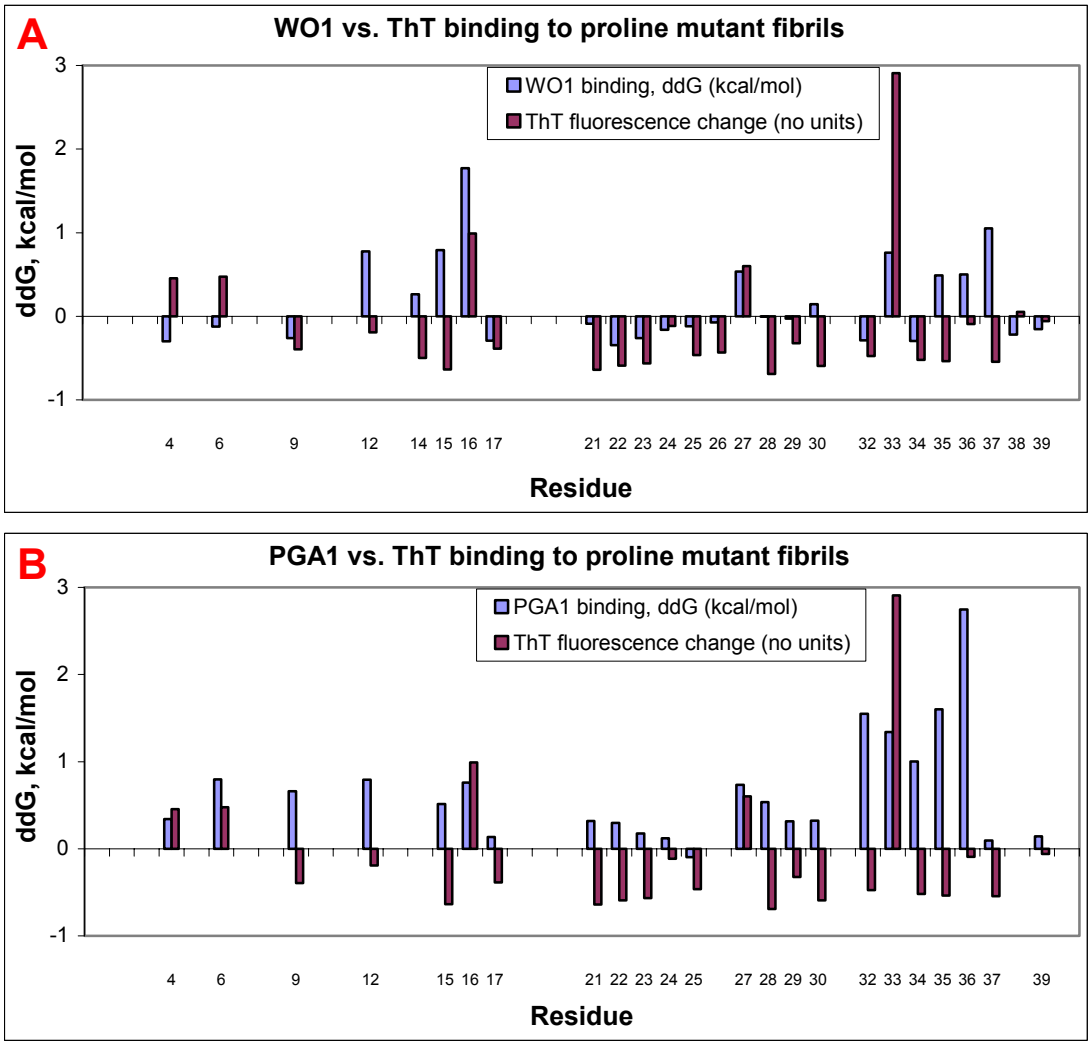


Figure 27. WO1 and PGA1 binding to proline and alanine mutant fibrils versus ThT binding. The antibody binding data were plotted alongside ThT binding data. The ThT binding data are derived from maximal corrected ThT fluorescence data obtained while monitoring fibril growth (Angela Williams) [34]. These ThT data were prepared for this comparison plot using the equation: (mutant ThT fluorescence – WT ThT fluorescence) / WT ThT fluorescence. The ThT data have no units. A positive ThT fluorescence change indicates greater ThT binding by the mutant versus WT fibrils. A positive $\Delta\Delta G_{app}$ value for antibody binding indicates the antibody bound more strongly to the mutant fibrils than to WT fibrils.

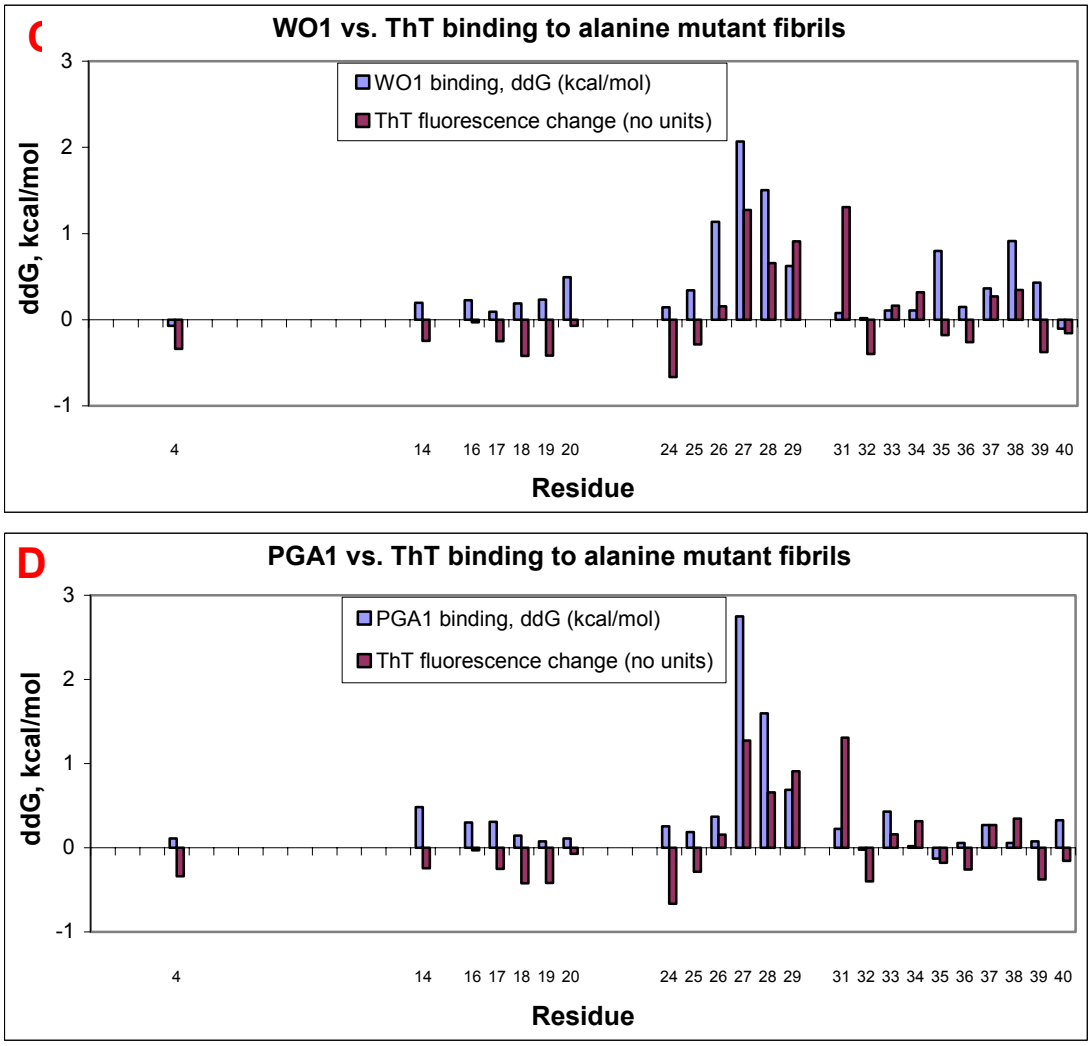


Figure 27. Continued.

motility. In any case, there appears to be some connection between the binding of the anti-amyloid antibodies and ThT to fibrils.

Antibody binding data were also compared to HD exchange data for proline mutant fibrils [34]. These data provide a measure of the amount of β-sheet structure since residues not involved in this structure are expected to be more susceptible to HD exchange [34]. Comparing the binding data to these data could give some insight into whether antibody binding correlates with the amount of β-sheet structure. These two sets of data were compared (Figure 28, Table 7). Antibody binding data were plotted versus HD exchange data and best fit lines were determined (Figure 28). Several comparisons were made, but no correlation was found for any of them (Table 7). This suggests that WO1 and PGA1 binding do not correlate with the amount of β-sheet structure implied by the HD exchange data.

After examining the antibody binding data and comparing it to several other bodies of data, the information was compared to our model of the amyloid protofilament (Figure 29a). In addition, it was compared to another model of fibril structure with many differences from our model [47] (Figure 29b). The Tycko model consists of Aβ

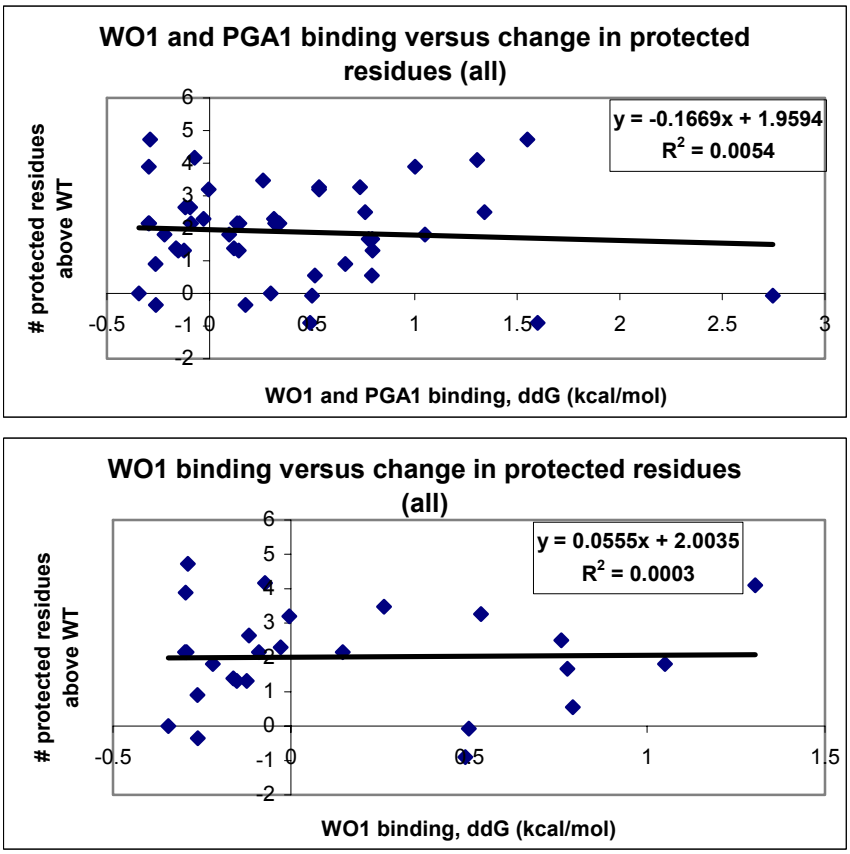


Figure 28. Comparison plots of antibody binding to difference in protected residues. These plots are examples of the comparisons done for antibody binding versus the number of protected residues above WT fibrils. These numbers were calculated from the data presented in [34] using the equation: (40 - # protected residues in mutant) - # protected residues in WT. A best fit line was plotted for each set of data and a correlation coefficient (R^2) found. The first plot shown involves both WO1 and PGA1 binding to all the available proline mutant fibrils. The second plot involves WO1 binding only.

Table 7. Comparison table of antibody binding to difference in protected residues. The first column lists all the different sets of antibody binding data compared to different sets of HD exchange data. The second and third columns show the slope and correlation coefficient (R^2) from the best fit done for each set of data. The highest R^2 value was 0.071. None of the comparisons showed any correlation.

HD exchange comparison	Slope	R^2
WO1/PGA1 to pro mutants	-0.17	0.0054
WO1/PGA1 to core pro mutants (15-36)	-0.38	0.024
WO1 to pro mutants	0.056	0.0003
PGA to pro mutants	-0.2	0.0087
WO1 to core pro mutants (15-36)	-1.14	0.071
PGA to core pro mutants (15-36)	-0.23	0.011

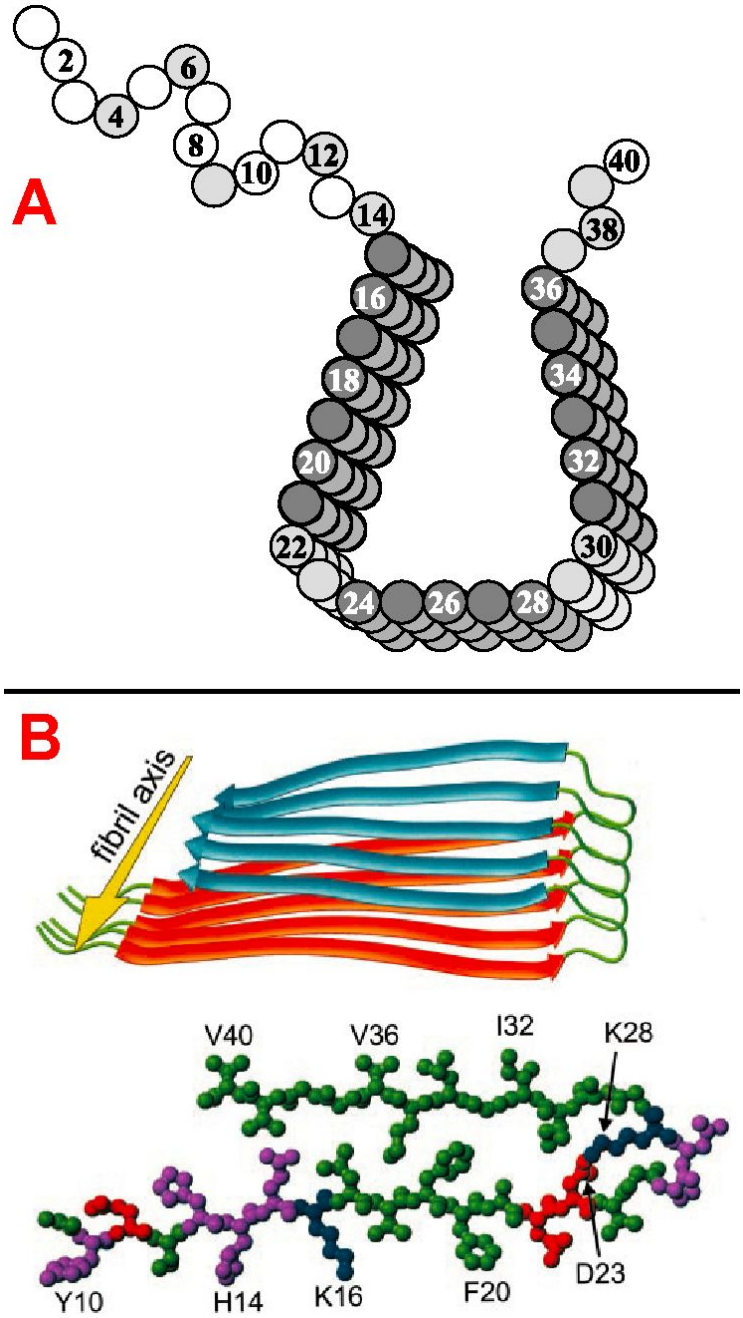


Figure 29. Two Aβ amyloid protofilament models. Our model is shown in figure A while the Tycko model [47] is shown in figure B. (Figure B adapted from Petkova, A.T., et al., *A structural model for Alzheimer's beta -amyloid fibrils based on experimental constraints from solid state NMR.* Proc Natl Acad Sci U S A, 2002. **99**(26): p. 16742-7.)

subunits in which there are two β-strands, residues 12 to 24 and 30 to 40. The amino terminus is unstructured and residues 25 to 29 comprise a bend in the sequence [47]. There is also a potential salt bridge between residues D23 and K28 in the core of the Tycko model (Figure 29b).

The possible explanation for the WO1 binding results to K16P could fit into either model. That is, the rigid proline could serve to secure the unstructured amino-terminus such that it does not fold back onto the fibril and impede the antibody from binding. In both cases, there is an unstructured amino-terminus, though this terminus stops around residues 10 to 12 in the Tycko model (Figure 29b). The results for PGA1 binding to V36P can be similarly explained as this residue is near the unstructured carboxy-terminus in our model (Figure 29a). They do not, however, fit as well into the Tycko model since it lacks an unstructured carboxy-terminus. It is possible that these results could hinge more on destabilization of the fibril. If that is case, they could fit the Tycko model.

The results for WO1 and PGA1 binding to N27A are less clear. The change from an asparagine to an alanine does not result in a

charge difference and should not cause large structural changes compared to wild-type. In our model, this residue is in the middle of a β-strand whereas in the Tycko model it is in the bend between the two β-strands (Figure 29). The results for residue 27 do not seem to exclude either model. However, they do not seem to clearly support one over the other either.

The results for PGA1 binding to the A30C-CMT mutant fibrils could fit into either model. Both models transition from turn to β-strand structure around this residue. Being near the turn region, charged residues may be tolerated or, as the binding data suggests, preferred. Residue 30 appears to be extremely accessible to solvent based on the cysteine mutant fibril alkylation studies (Dr. Shankaramma Shivaprasad, unpublished data). Those results are in agreement with both models [34, 47]. The PGA1 binding results to the A31C-CMT mutant fibrils are somewhat less clear. This residue appears to be inaccessible to solvent based on the aforementioned alkylation studies (Dr. Shankaramma Shivaprasad, unpublished data). Furthermore, it is buried in the core of the Tycko model [47]. The results do not seem to fit either model. These fibrils may possess an altered structure, such as incorporating residues 30 and 31 into an

extended turn, to accommodate a charge at this residue. It could also be the case that the residue is still in the fibril core at the cost of reduced fibril stability. The latter scenario takes into account that PGA1 appears to bind more strongly to destabilized fibrils.

The results for WO1 and PGA1 binding to K28A fibrils seem quite clear. Combined with the PGA1 binding results to modified cysteine mutant fibrils, it appears that the antibodies bind more strongly to fibrils in which residue 28 is hydrophobic. Residue 28 appears to be buried in the amyloid core, a hydrophobic environment unfavorable to lysine. A more hydrophobic amino acid at this position could potentially pack better into the amyloid core. This could stabilize the epitopes recognized by WO1 and PGA1. The Tycko model has the lysine at residue 28 in the amyloid core, but it may form a salt bridge with the aspartic acid at residue 23 [47] (Figure 29b). Residue 23 appears to be inaccessible to solvent based on the aforementioned alkylation studies (Dr. Shankaramma Shivaprasad, unpublished data). This lends some support to the Tycko model. However, the antibody binding results to the mutants at residue 28 seem to indicate that if a salt bridge exists, it is not critical to the structure of the fibril. A salt bridge may exist in wild-type fibrils, but the K28A mutant may prevent

it forming. This could alter fibril structure, possibly to the benefit of antibody binding.

Conclusions

Several characteristics of anti-amyloid antibody binding to fibrils were investigated. The salt and pH effects results suggest that electrostatic interactions are relatively important to WO1 binding and hydrophobic interactions are relatively unimportant. The WO1 and PGA1 binding results to the many different mutant fibrils looked more closely into amyloid fibril structure. There were several noteworthy findings. WO1 binding to K16P fibrils and PGA1 binding to V36P fibrils was greatly enhanced. Both WO1 and PGA1 binding to N27A and K28A fibrils were significantly enhanced. PGA1 binding to A30C-CMT and I31C-CMT fibrils was considerably enhanced while binding to K28C was somewhat enhanced.

Much more information was made clear through comparisons of the binding data to other available data. A comparison of the binding data to fibril stability showed no correlation. Fibril stability could play a role in antibody binding, but it does not appear to be the dominant factor. Antibody binding data were compared to hydrophobicity

change data, but no correlation was found. This suggests that WO1 and PGA1 binding do not correlate with the bulk hydrophobicity or hydrophilicity of amyloid fibrils. Antibody binding data were compared to HD exchange data to look for a relationship between the amount of β-sheet structure and binding. No correlation was found, suggesting that WO1 and PGA1 binding do not correlate with the amount of β-sheet structure implied by the HD exchange data. Comparing antibody and ThT binding data to fibrils revealed some weak correlation. This is the most interesting result to come from the correlation studies. It suggests there could be a relationship between binding of the anti-amyloid antibodies and ThT to fibrils.

With regard to certain residues, there appeared to be more correlation. Fibril stability appears to show some importance to antibody binding with regard to certain residues such as 16 and 36. Charge also appears to be important considering the results at residues 28, 30, and 31. In addition, some more specific structural features appear to be important based on the results at residues 16, 27, and 36. It looks as if the binding of these antibodies and ThT to amyloid fibrils are related based on some correlation in the data overall and some overlap in the binding results to specific mutants. It

does not appear that antibody binding correlates with the amount of β-sheet structure implied by the HD exchange data. Lastly, the binding results agree, for the most part, with our model of Aβ amyloid. Mutations in the Aβ sequence have a strong impact on binding of the anti-amyloid antibodies. The basis of these results is still not clear, but they could be important clues to the nature of fibril structure or at least the fibril epitopes recognized by the antibodies.

Chapter IV
Phage Display Results and Discussion

The available anti-amyloid antibodies are all of the IgM class (Figure 5e). As mentioned earlier, these are large, flexible, multivalent species not amenable to many structural studies. For example, the large size and flexibility of IgM molecules is very unfavorable to protein crystallography. Another example is the multivalent and cooperative nature of IgM binding to antigens complicates potential mutagenesis studies because a single mutation affects all ten binding sites. One potential option is to study fragments of these IgM antibodies. However, it was shown that monovalent fragments of WO2 do not bind any better to Aβ fibrils than to BSA (Figure 14). It would be preferable to study fragments with significant affinity for amyloid fibrils. Due to the limitations of the available antibodies, phage display experiments were carried out with the goal of producing anti-amyloid antibody fragments. Some progress was made to this end.

Verification of Phage Production and Anti-M13 Antibody Specificity

The phagemid clone received from the Barbas laboratory was transformed into XL1-Blue *E. coli* cells. A culture of the transformed cells was grown up and infected with helper phage to produce clonal phage particles. These were purified for use in a preliminary phage ELISA. This experiment was conducted to determine three things: if the phage production protocol generates a suitable phage titer, if the phage clone is bound by the chosen anti-M13 biotin secondary antibody, and if there is any significant background binding of the secondary antibody to Aβ amyloid. There appeared to be a suitable phage titer and strong binding by the secondary antibody. This is evidenced by the substantial binding curve for anti-M13 antibody to the phage clone (Figure 30). There is essentially no background binding of anti-M13 antibody to Aβ amyloid evidenced by a flat curve (Figure 30).

Phage Library Production

To generate the initial phage library, PCR random mutagenesis was carried out on the Fab genes within the phagemid clone. As stated earlier, 6 clones were selected for sequencing with the OMPSEQ

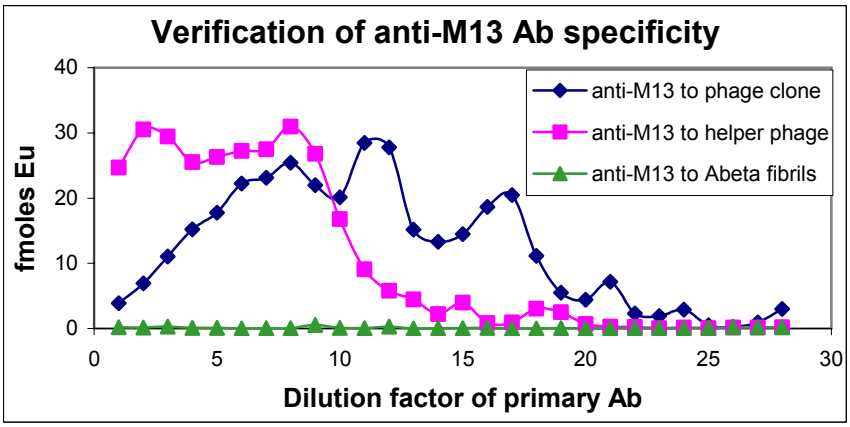


Figure 30. Verification of anti-M13 Ab specificity. The blue diamond marked curve shows that the purified phage clone is bound by the anti-M13 antibody. The magenta square marked curve is a positive control to verify the activity of the anti-M13 antibody on immobilized phage. The green triangle marked curve shows the lack of significant background binding by the anti-M13 antibody to amyloid fibrils.

primer (Table 2) to determine the rate of mutagenesis. The rate of base mutation was found to be roughly 1.5%. The phagemid library was transformed into XL1-Blue *E. coli* cells. Three rounds of selection against Aβ amyloid were conducted in hopes of enriching phage capable of binding the fibrils. The input and output phage titers at each stage of panning were determined. The phage titer after transformation of the starting library was 5*10^8 pfu/mL. For pan 1, the titers were 3*10^12 pfu/mL input and 2*10^7 pfu/mL output. For pan 2, the titers were 8*10^11 pfu/mL input and 8*10^2 pfu/mL output. For pan 3, the titer could not be determined since all of the plates were blank, including the input titer plates. Phage pools from each round of selection as well as a nonpanned, preselection pool were saved for a total of four phage pools.

To test the phage pools for the presence of Aβ amyloid binding clones, several phage ELISA experiments were performed. All four phage pools were tested using the anti-M13 phage antibody as the secondary antibody. These experiments were not meant to be used for determining binding activity, but just to confirm whether or not there is any significant binding at all. This is indicated by a higher, right-shifted curve for aggregate binding compared to background

binding to BSA. The phage ELISAs indicated that all the phage pools possessed the ability to bind Aβ amyloid (Figure 31). This was unexpected since even the nonpanned phage pool appeared to possess affinity to Aβ amyloid fibrils (Figure 31, top left). These results indicate that there are a large number of binders even before selection. Antigen-binding sites are normally formed from the CDRs, but random mutagenesis should not favor these regions over the rest of the sequence. The majority of the mutants are likely structurally altered with truncations and mutations in antibody framework regions. Considering the markedly better affinity of the nonpanned library for fibrils over BSA blocked wells, it is possible that much of the binding came from such structurally altered antibodies. This suggests there could be considerable nonspecific binding. Phage ELISAs were also conducted against polyglutamine aggregates and the phage pools were found to have an affinity for them as well (Figure 31, bottom). Again, this may be due to nonspecific binding. Clones were ultimately selected from all four pools and tested against both Aβ amyloid and polyglutamine aggregates.

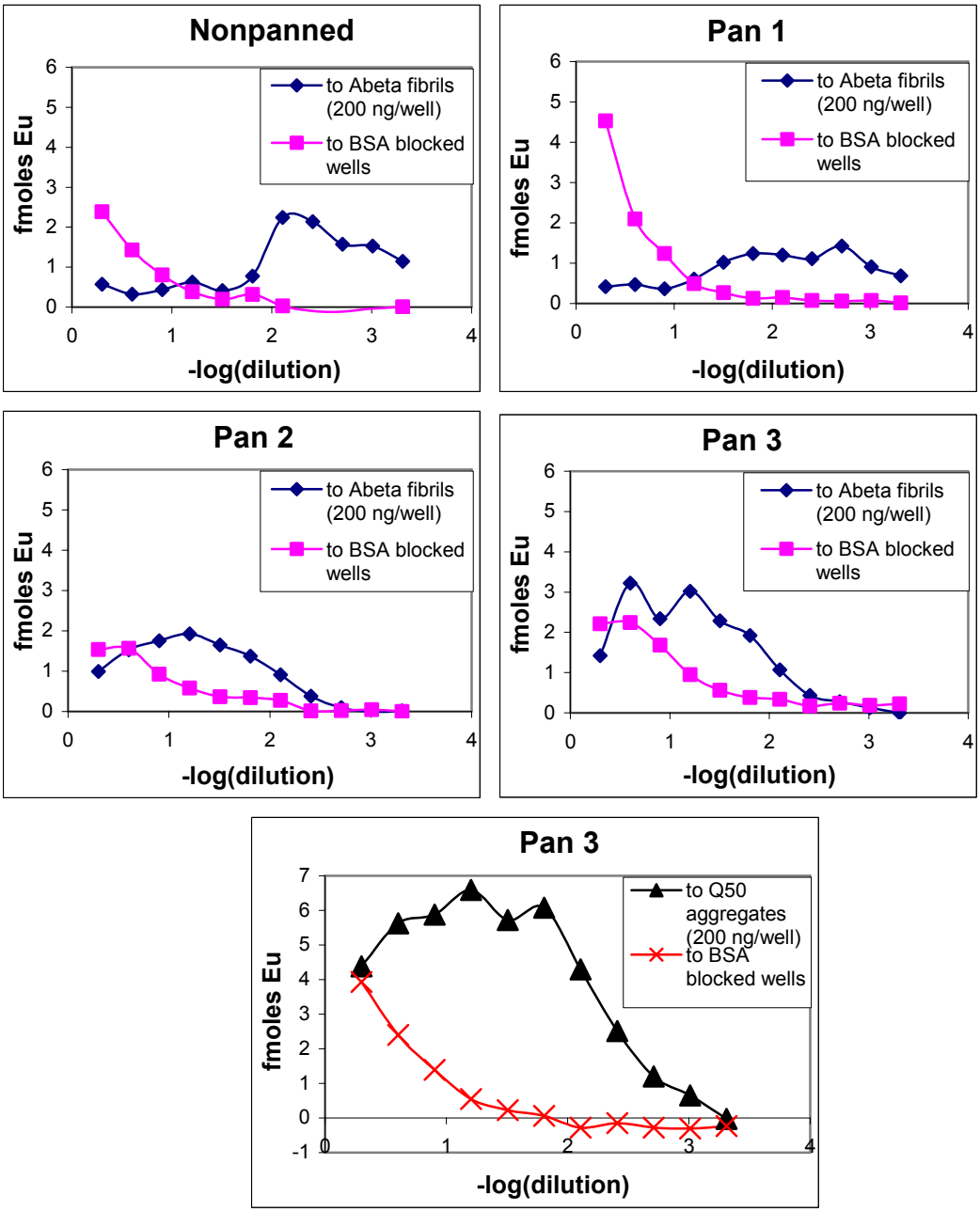


Figure 31. Phage pool ELISAs. ELISA binding assays were conducted using phage pools in place of the primary antibody. Even the nonpanned pool shows Aβ amyloid binding (top left). There is also binding to polyglutamine aggregates, even though the library was selected against Aβ amyloid (bottom).

Phage Clone Selection

The cultures from which the phage pools were collected were plated and several clones were selected from each. Cultures were inoculated with picked colonies and grown up to produce clonal phage particles. The same was done for the unmutated phage. Phage ELISAs were carried out for each to determine if any of these individual clones could bind Aβ amyloid. Including the unmutated clone, 25 clones were tested for Aβ amyloid binding and 6 clones for polyglutamine aggregate binding. 10 clones from the nonpanned pool, 10 from the first panning, 2 from the second panning, and 2 from the third panning were tested for binding to Aβ amyloid. 2 of 25 bound Aβ amyloid more strongly than BSA: clones 1-1 and 2-2 (Figure 32). 4 of 6 drawn from the same set of clones bound polyglutamine aggregates more strongly than BSA: clones 1-1, 2-1, 2-2, and 3-1 (Figure 33). The unmutated clone did not bind either aggregate very well, especially when compared to the clones in figure 33. The problem with most of the clones binding to Aβ amyloid was that their binding to BSA was comparable (Figure 32, bottom right). With the polyglutamine aggregates, this was not an issue. Four clones were selected for further work. These are designated 1-1, 2-1, 2-2, and 3-1. The first number stands for the pool from which the clone was

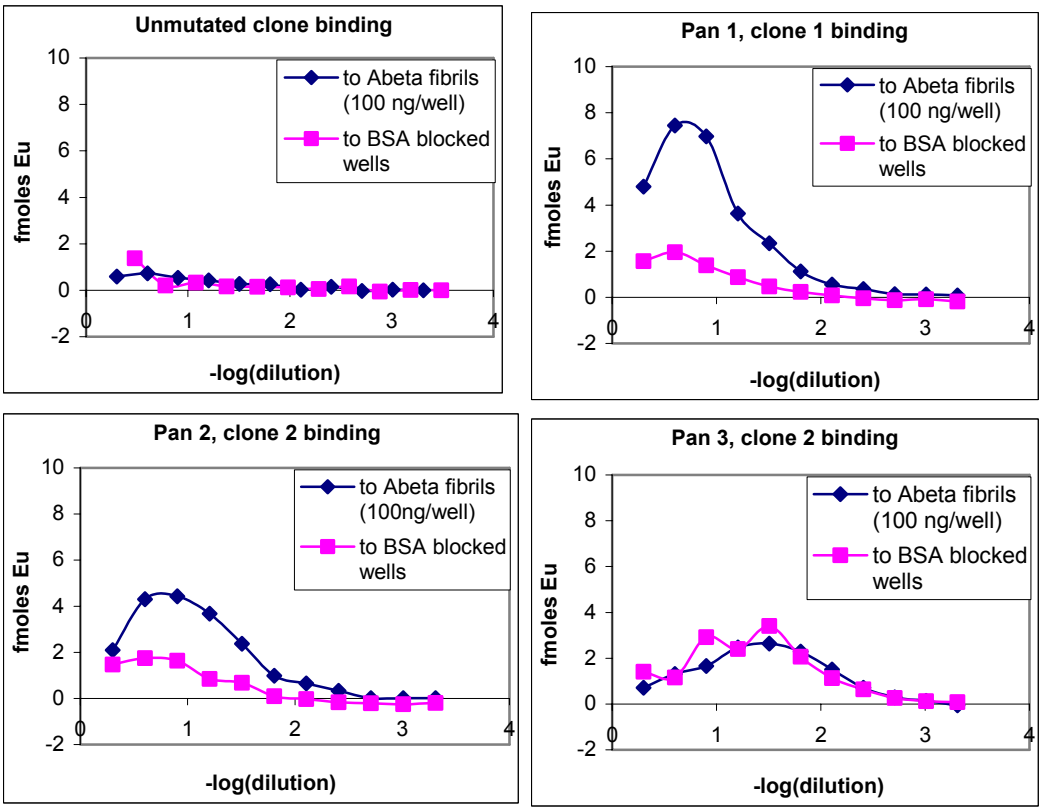


Figure 32. Phage clone binding to Aβ amyloid fibrils. The unmutated clone showed essentially no binding. Clones 1-1 and 2-2 are the only two positive clones obtained. Clone 3-2 is an example of one of the rejected clones. For this clone and most of the other negative clones there was often binding to Aβ amyloid, but there was also comparable binding to BSA.

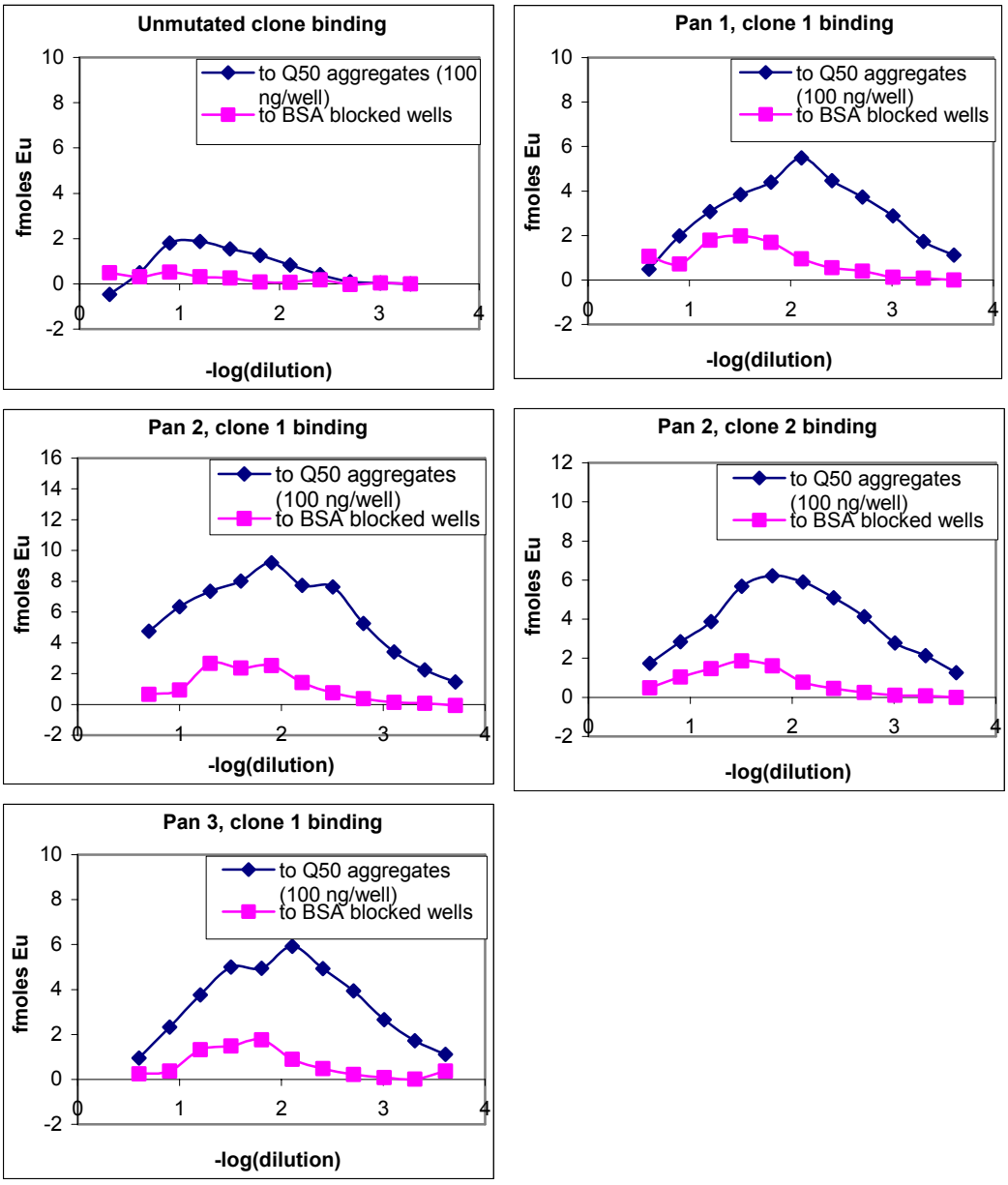


Figure 33. Phage clone binding to polyglutamine aggregates. ELISA binding curves using phage clones in place of the primary antibody. The top 3 curves are for Aβ amyloid binding and the bottom 5 are for polyglutamine aggregate binding.

taken. For example, clone 2-1 is from the second panning pool. Clones 1-1 and 2-2 bound to both Aβ amyloid and polyglutamine aggregates (Figures 32 and 33). Clones 2-1 and 3-1 bound to polyglutamine aggregates only (Figure 33). The amino acid sequences of these clones were examined to look for any differences from the original, unmutated clone.

Antibody Clone Sequences

Cultures were grown up for each clone, including the unmutated clone. Plasmid preparations were performed and the plasmids were sent off for sequencing using the OMPSEQ and PELSEQ primers (Table 2). The DNA sequences were translated to amino acid sequences. The heavy and light chain amino acid sequences for the clones are shown in tables 8 and 9, respectively. It is clear from the data that most of the clones are actually truncation mutants. The clone 2-1 heavy chain sequence is the only one besides the unmutated heavy and light chains that is not truncated (Tables 8 and 9). It actually has an identical amino acid sequence to that of the unmutated heavy chain. Two sequences were truncated as a result of a stop codon introduced by a substitution mutation: clone 1-1 heavy chain and clone 3-1 light chain. Three sequences were truncated as a result of

Table 8. Clone heavy chain sequences. Only the clone 2-1 heavy chain lacks a truncation mutation. Clone 2-2 appeared to actually be multiple clones by examining the electropherogram (data not shown). Therefore, the clone 2-2 sequence data could not be translated. Residues differing from unmutated are bold, italic, and highlighted in red.

Clone	Sequence	ORF length
Unmutated	MAEVQLLEQSGAEVKKPGSSVKVSCRASGGTF NNYAISWVRQAPGQGLEWMGGIFPFRNTAKY AQHFQGRVTITADESTGTAYMELSSLRSEDTAI YYCARGDTIFGVTMGYYAMDVWGQGTTVTVS AASTKGPSVFPLAPSSKSTSGGTAALGCLVKDY FPEPVTVSWNSGALTSGVHTFPAVLQSSGLYS LSSVVTVPSSSLGTQTYICNVNHKPSNTKVDK KVEPKSCDKTSGQAGQHHHHHHGAYPYDVPD YAS	258
1-1	MAEVQLLEQSGAEVKKPGSSVKVSCRASG***D***TF NNYAISWVRQAPGQGLEWMGG***F***FPF***LY***TAKY A	64
2-1	MAEVQLLEQSGAEVKKPGSSVKVSCRASGGTF NNYAISWVRQAPGQGLEWMGGIFPFRNTAKY AQHFQGRVTITADESTGTAYMELSSLRSEDTAI YYCARGDTIFGVTMGYYAMDVWGQGTTVTVS AASTKGPSVFPLAPSSKSTSGGTAALGCLVKDY FPEPVTVSWNSGALTSGVHTFPAVLQSSGLYS LSSVVTVPSSSLGTQTYICNVNHKPSNTKVDK KVEPKSCDKTSGQAGQHHHHHHGAYPYDVPD YAS	258
2-2	---	-
3-1	MAEVQLLEQSGAEVKKPG***F***SVKVSCRASGGT ***STIMPSAGCDRPLDKGLSGWEGSSLSVIQ QSTHNTSRAESPLPRTNPRAQPTWS***	85

Table 9. Clone light chain sequences. All the clones were apparently truncation mutants. Clone 2-2 appeared to actually be multiple clones (data not shown). Residues differing from unmutated are bold, italic, and highlighted in red.

Clone	Sequence	ORF length
Unmutated	MAGFATVAQAAELTQSPGTLSLSPGERATLSC RASHSVSRAYLAWYQQKPGQAPRLLIYGTSSR ATGIPDRFSGSGSGTDFTLTISRLEPEDFAVYY CQQYGGSPWFGQGTKVELKRTVAAPSVFIFPP SDEQLKSGTASVVCLLNNFYPREAKVQWKVD NALQSGNSQESVTEQDSKDSTYSLSSTLTLSK ADYEKHKVYACEVTHQGLSLPVTKSFNRGEC	223
1-1	MAGFATVAQAAELTQSPGTLSLSPGERA***PSPA GPVTVLAGPT***	42
2-1	MAGFATVAQAAELTQSPGTLSLSPGE***SHPLLQ GQSQC***	37
2-2	---	-
3-1	MAGFATVAQAAELTQSPGTLSLS***T***GERA***S***LSC ***W***AS***L***S***I***SRA	41

insertions or deletions causing frameshifts that subsequently led to premature stop codons: 3-1 heavy chain, 1-1 light chain, and 2-1 light chain. The clone 2-2 heavy and light chain sequences could not be accurately translated. An examination of the electropherograms of these two sequences revealed numerous occurrences of overlapping base peaks (data not shown). This suggests there is more than one clone in the clone 2-2 sample.

Unfortunately, not all the clone sequences appear to agree with the binding results. The clone 1-1 and 3-1 heavy chains are both truncated (Table 8). This has been verified by obtaining these sequences a second time. The downstream gp3 segment of these fusion proteins are, as a result, not expressed (Figure 11). Lacking this segment, the antibody fragment would not be associated with the phage particle and should not have an impact on phage selection. Since phage expressing these clones appeared to bind amyloid, it seems that the phage clones could be binding nonspecifically. Clones 1-1 and 3-1 are apparently false positives. Though the 2-1 light chain is truncated due to a frameshift mutation, the heavy chain is intact. This clone could be detected via an anti-HA western blot. Soluble

expression was attempted for all the clones including the unmutated clone.

Soluble Expression

Fresh *E. coli* cultures expressing each phagemid were grown up and plasmid preps were used to purify the clonal phagemid DNA. These phagemid were electroporated into TOP10 *E. coli* cells in order to carry out expression of soluble Fab protein. Whole protein extracts were taken from cultures of these clones and tested for the presence of Fab protein using western blots. Two monoclonal anti-HA antibodies were used in one set of western blot experiments and a polyclonal anti-human heavy and light chain antibody in another. The anti-HA western blot results lined up with the sequencing results (Figure 34). As expected, only the two clones possessing the HA tag, the unmutated clone and clone 2-1, showed up on these blots. Cultures expressing the clones were grown up for protein extraction and western blots several times, but these clones did not show strong bands on every blot. In figure 34, the umutated clone showed stronger bands in blot A while clone 2-1 showed a stronger band in blot B. It may be that the Fab fragments are not stably expressed under the culture conditions used. It is also possible that the HA tag

A

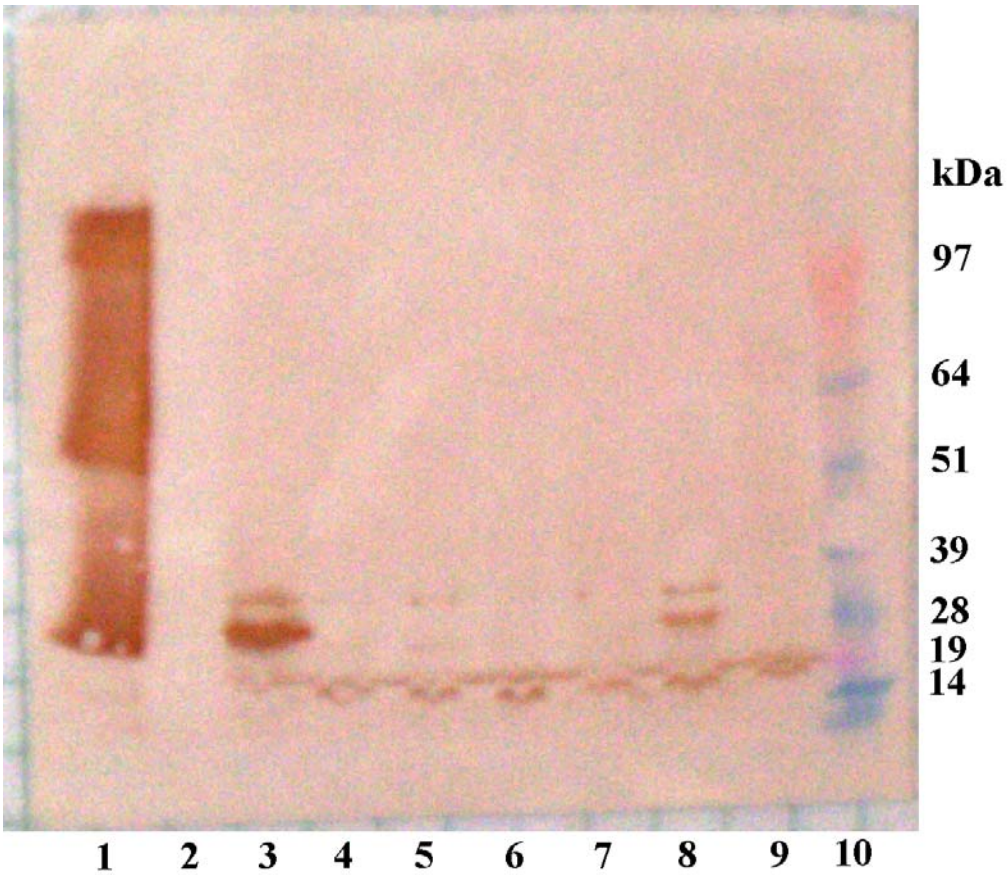


Figure 34. Anti-HA western blots. The lanes in western A are as follows: 1) anti-HA IgG, 2) blank, 3) unmutated, 4) clone 3-1, 5) clone 2-2, 6) clone 2-1, 7) clone 1-1, 8) unmutated from another culture, 9) untransformed, 10) Seeblue Plus 2 MW standard (Invitrogen). The lanes in western B are as follows: 1) clone 2-1, 2) unmutated, 3) human IgG, 4) clone 3-1, 5) clone 2-2, 6) clone 2-1, 7) clone 1-1, 8) unmutated from another culture, 9) same as lane 8, 10) Seeblue Plus 2 MW standard.

B

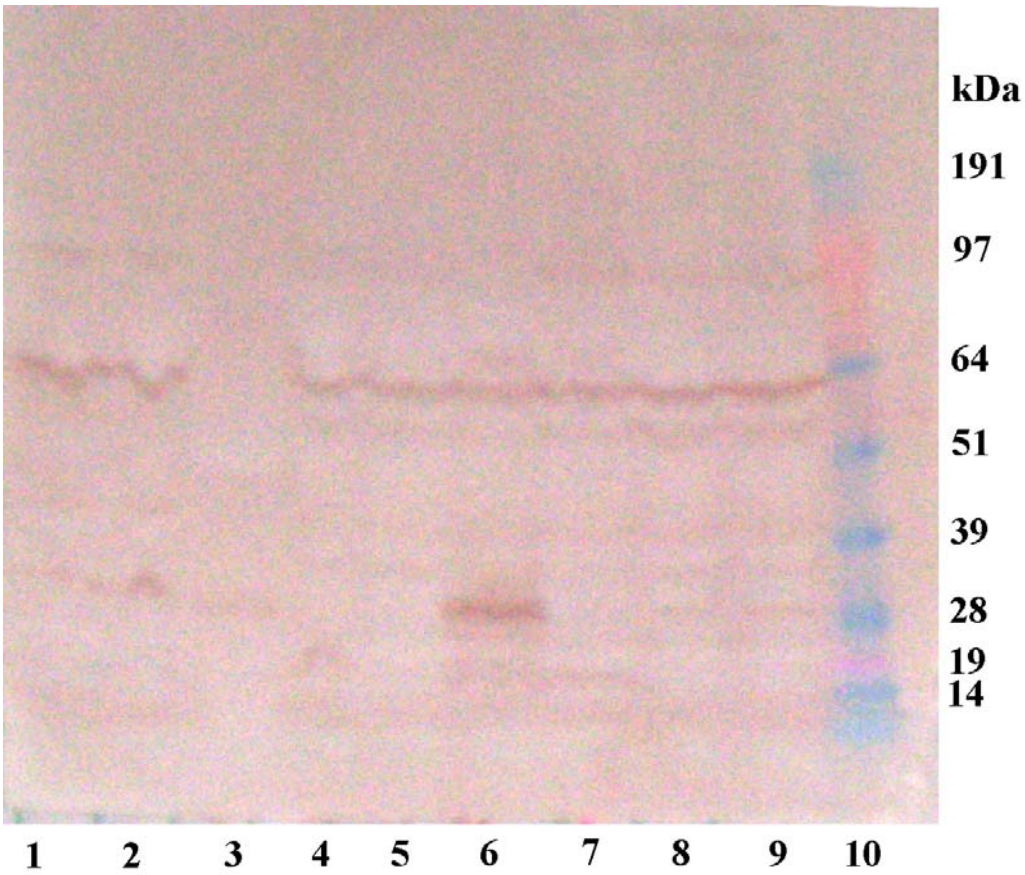


Figure 34. Continued.

located at the carboxy-terminus of the heavy chain could have been cleaved before loading the samples onto the gels. For the unmutated and 2-1 clones, the strong band was at approximately the correct molecular weight to represent a heavy chain Fd fragment, around 25 kDa (Figure 34). There were different background bands in each of these two blots. This may be due to the different anti-HA antibodies used.

The anti-human IgG (heavy and light chain specific) western blot showed bands around 25 kDa for some of the clones (Figure 35). There were also bands near the gel front for all the clones. The latter bands may represent truncated or partially degraded light and heavy chain fragments. The blot in figure 34b was run alongside that in figure 35, but the results were not consistent. The band near 25 kDa for clone 2-1 was very faint. Furthermore, this band was present for clone 3-1, a truncation mutant that should not have it. The anti-human IgG western blot results were not consistent. However, the anti-HA western blot results show that if an intact clone is available, expression can be achieved.

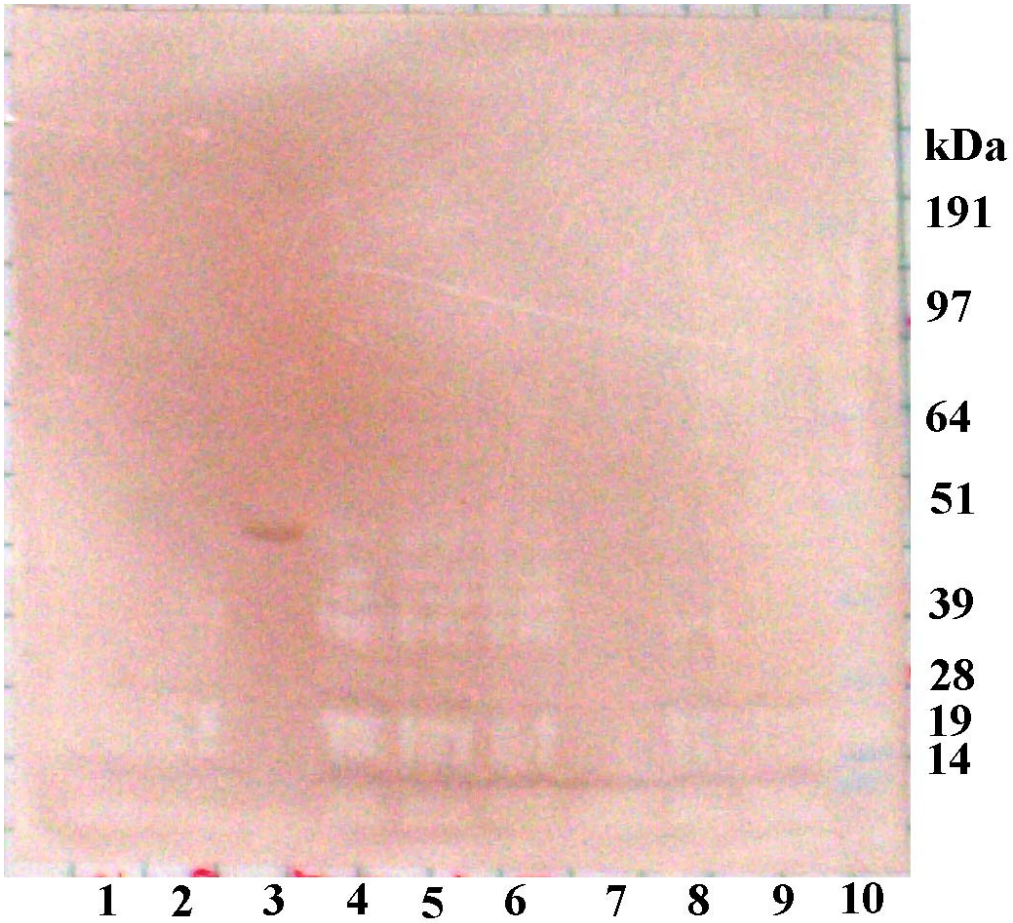


Figure 35. Anti-human IgG (heavy and light chain specific) western blot. The lanes in the western are as follows: 1) clone 2-1, 2) unmutated, 3) human IgG, 4) clone 3-1, 5) clone 2-2, 6) clone 2-1, 7) clone 1-1, 8) unmutated from another culture, 9) same as lane 8, 10) Seeblue Plus 2 MW standard.

Conclusions

Initial phage ELISA results suggested that the phage libraries, including nonpanned, had an affinity for amyloid fibrils. However, an examination of sequences of selected positive clones revealed that the phage selection procedure was ineffective. All the clones possessed truncations in the antibody heavy chain, the light chain, or both. This suggests that these clones were binding nonspecifically. The unmutated clone and clone 2-1 were expressed as soluble fragments, but were not purified for further analysis. Further work will need to be done to obtain anti-amyloid Fab fragments.

A successful strategy for obtaining truly positive clones could include a step to select for those phage presenting intact Fab fragments. One way to do this could be to include an additional selection step in which the phage are incubated in ELISA wells coated with anti-Fab antibodies. That is, after the selection step against amyloid, the library could be reamplified and subjected to Fab selection before continuing with the next round. This step could enrich the library with clones presenting intact Fab fragments and reduce the number of false positives during the screening process that follows selection.

List of References

List of References

1. *Alzheimer's Association.* http://www.alz.org.
2. Selkoe, D.J., *Alzheimer's disease: genotypes, phenotypes, and treatments.* Science, 1997. **275**(5300): p. 630-1.
3. Wolfe, M.S., *APP, Notch, and presenilin: molecular pieces in the puzzle of Alzheimer's disease.* Int Immunopharmacol, 2002. **2**(13-14): p. 1919-29.
4. Evin, G. and A. Weidemann, *Biogenesis and metabolism of Alzheimer's disease Abeta amyloid peptides.* Peptides, 2002. **23**(7): p. 1285-97.
5. Kowall, N.W., et al., *In vivo neurotoxicity of beta-amyloid [beta(1-40)] and the beta(25-35) fragment.* Neurobiol Aging, 1992. **13**(5): p. 537-42.
6. Seilheimer, B., et al., *The toxicity of the Alzheimer's beta-amyloid peptide correlates with a distinct fiber morphology.* J Struct Biol, 1997. **119**(1): p. 59-71.
7. McKee, A.C., et al., *The neurotoxicity of amyloid beta protein in aged primates.* Amyloid, 1998. **5**(1): p. 1-9.
8. Wang, J., et al., *The levels of soluble versus insoluble brain Abeta distinguish Alzheimer's disease from normal and pathologic aging.* Exp Neurol, 1999. **158**(2): p. 328-37.
9. Selkoe, D.J., *Amyloid beta-protein and the genetics of Alzheimer's disease.* J Biol Chem, 1996. **271**(31): p. 18295-8.
10. Geula, C., et al., *Aging renders the brain vulnerable to amyloid beta-protein neurotoxicity.* Nat Med, 1998. **4**(7): p. 827-31.
11. Hardy, J. and D.J. Selkoe, *The amyloid hypothesis of Alzheimer's disease: progress and problems on the road to therapeutics.* Science, 2002. **297**(5580): p. 353-6.
12. Braak, H. and E. Braak, *Diagnostic criteria for neuropathologic assessment of Alzheimer's disease.* Neurobiol Aging, 1997. **18**(4 Suppl): p. S85-8.
13. Kheterpal, I., et al., *Abeta protofibrils possess a stable core structure resistant to hydrogen exchange.* Biochemistry, 2003. **42**(48): p. 14092-8.
14. Walsh, D.M., et al., *Amyloid beta-protein fibrillogenesis. Detection of a protofibrillar intermediate.* J Biol Chem, 1997. **272**(35): p. 22364-72.
15. Nybo, M., S.E. Svehag, and E. Holm Nielsen, *An ultrastructural study of amyloid intermediates in A beta1-42 fibrillogenesis.* Scand J Immunol, 1999. **49**(3): p. 219-23.

16. Harper, J.D., et al., *Observation of metastable Abeta amyloid protofibrils by atomic force microscopy.* Chem Biol, 1997. **4**(2): p. 119-25.
17. Nilsberth, C., et al., *The 'Arctic' APP mutation (E693G) causes Alzheimer's disease by enhanced Abeta protofibril formation.* Nat Neurosci, 2001. **4**(9): p. 887-93.
18. Virchow, V.R., Verh Phys Med Ges Wurzburg, 1851(2): p. 51-4.
19. Virchow, V.R., Virchows Arch Pathol Anat, 1854(6): p. 135-8.
20. Bennhold, H., Muench Med Wochenschr, 1922: p. 1537-8.
21. Divry, P. and M. Florkin, C R Soc Biol, 1927(97): p. 1808-10.
22. Sunde, M. and C. Blake, *The structure of amyloid fibrils by electron microscopy and X-ray diffraction.* Adv Protein Chem, 1997. **50**: p. 123-59.
23. Sipe, J.D. and A.S. Cohen, *Review: history of the amyloid fibril.* J Struct Biol, 2000. **130**(2-3): p. 88-98.
24. Harper, J.D., et al., *Assembly of A beta amyloid protofibrils: an in vitro model for a possible early event in Alzheimer's disease.* Biochemistry, 1999. **38**(28): p. 8972-80.
25. Walsh, D.M., et al., *Amyloid beta-protein fibrillogenesis. Structure and biological activity of protofibrillar intermediates.* J Biol Chem, 1999. **274**(36): p. 25945-52.
26. Sipe, J.D., *Amyloidosis.* Annu Rev Biochem, 1992. **61**: p. 947-75.
27. Koo, E.H., P.T. Lansbury, Jr., and J.W. Kelly, *Amyloid diseases: abnormal protein aggregation in neurodegeneration.* Proc Natl Acad Sci U S A, 1999. **96**(18): p. 9989-90.
28. Kapurniotu, A., *Amyloidogenicity and cytotoxicity of islet amyloid polypeptide.* Biopolymers, 2001. **60**(6): p. 438-59.
29. Selkoe, D.J., *Alzheimer's disease: genes, proteins, and therapy.* Physiol Rev, 2001. **81**(2): p. 741-66.
30. Taylor, J.P., J. Hardy, and K.H. Fischbeck, *Toxic proteins in neurodegenerative disease.* Science, 2002. **296**(5575): p. 1991-5.
31. Kheterpal, I., et al., *Abeta amyloid fibrils possess a core structure highly resistant to hydrogen exchange.* Proc Natl Acad Sci U S A, 2000. **97**(25): p. 13597-601.
32. Kheterpal, I., et al., *Structural features of the Abeta amyloid fibril elucidated by limited proteolysis.* Biochemistry, 2001. **40**(39): p. 11757-67.
33. Kheterpal, I., R. Wetzel, and K.D. Cook, *Enhanced correction methods for hydrogen exchange-mass spectrometric studies of amyloid fibrils.* Protein Sci, 2003. **12**(3): p. 635-43.

34. Williams, A.D., et al., *Mapping abeta amyloid fibril secondary structure using scanning proline mutagenesis.* J Mol Biol, 2004. **335**(3): p. 833-42.
35. Wood, S.J., et al., *Prolines and amyloidogenicity in fragments of the Alzheimer's peptide beta/A4.* Biochemistry, 1995. **34**(3): p. 724-30.
36. Chou, P.Y. and G.D. Fasman, *Empirical predictions of protein conformation.* Annu Rev Biochem, 1978. **47**: p. 251-76.
37. Lifson, S. and C. Sander, *Antiparallel and parallel beta-strands differ in amino acid residue preferences.* Nature, 1979. **282**(5734): p. 109-11.
38. Kuby, J., *Immunology*. 3rd Edition ed. 1997.
39. Davies, D.R., E.A. Padlan, and S. Sheriff, *Antibody-antigen complexes.* Annu Rev Biochem, 1990. **59**: p. 439-73.
40. O'Nuallain, B. and R. Wetzel, *Conformational Abs recognizing a generic amyloid fibril epitope.* Proc Natl Acad Sci U S A, 2002. **99**(3): p. 1485-90.
41. Hoess, R.H., *Protein design and phage display.* Chem Rev, 2001. **101**(10): p. 3205-18.
42. Barbas, C.F., 3rd, et al., *Phage Display: A Laboratory Manual*. 2002.
43. Barbas, C.F., 3rd, et al., *Assembly of combinatorial antibody libraries on phage surfaces: the gene III site.* Proc Natl Acad Sci U S A, 1991. **88**(18): p. 7978-82.
44. Kay, B.K., J. Winter, and J. McCafferty, *Phage Display of Peptides and Proteins: A Laboratory Manual.* 1996.
45. Chen, S., et al., *Amyloid-like features of polyglutamine aggregates and their assembly kinetics.* Biochemistry, 2002. **41**(23): p. 7391-9.
46. White, S.H., Wimley, W.C., *Membrane protein folding and stability: physical principles.* Annu Rev Biophys Biomol Struct, 1999. **28**: p. 319-65.
47. Petkova, A.T., Ishii, Y., Balbach, J.J., Antzutkin, O.N., Leapman, R.D., Delaglio, F., Tycko, R., *A structural model for Alzheimer's beta -amyloid fibrils based on experimental constraints from solid state NMR.* Proc Natl Acad Sci U S A, 2002. **99**(26): p. 16742-7.

Appendices

Appendix I

1% BSA in 1xPBS:

1 g	BSA (Sigma)
100 mL	1xPBS (Fisher)

For 3% or 5% BSA, add 3 g or 5 g of BSA, respectively.

1xPBS:

140 mM NaCl, 10 mM Na_2PO_4, 2.2 mM KH_2PO_4, 2.7 mM KCl

Order from Fisher as a pre-weighed powder. Mix into 1L water and filter for a 10x stock solution. Dilute to 1x in water and filter before use.

cell suspension buffer:

2.5 mL	0.2 M EDTA, pH 8.0 (Sigma)
2.5 mL	1.0 M Tris, pH 7.5 (Sigma)
95 mL	water

ELISA blocking solution:

1 g	BSA
100 mL	1xPBS
50 µL	Tween20 (Fisher)

ELISA wash buffer:

500 mL	1xPBS
250 µL	Tween20

LB agar:

8 g Difco LB agar (Beckton Dickinson)

Add water to 250 mL final volume. Autoclave for 20 minutes at 15 psi. Let cool to about 45°C. Pour about 25 mL into each plate and allow the agar to set for at least 2 hours before use.

LB agar+tetracycline:

Prepare LB agar, but do not immediately pour into plates after cooling to 45°C. Add tetracycline (Sigma) to a final concentration of 12 µg/mL, 600 µL of 5 mg/mL tetracycline, and rotate gently to mix. Pour plates.

LB agar+carbenicillin:

Prepare LB agar, but do not immediately pour into plates after cooling to 45°C. Add carbenicillin (Sigma) to a final concentration of 50 µg/mL, 125 µL of 100 mg/mL carbenicillin, and rotate gently to mix. Pour plates.

25% PEG-8000 / 15% NaCl:

25 g PEG-8000 (Sigma)
15 g NaCl

Add water to 100 mL final volume. Stir on a hot plate to dissolve solids. Autoclave for 20 minutes at 15 psi.

SB medium:

5 g MOPS (Sigma)
15 g tryptone (Fisher)
10 g yeast extract (Beckton Dickinson)

Add water to 500 mL final volume. Adjust pH to 7.0 with sodium hydroxide. Autoclave for 20 minutes at 15 psi.

SOC medium:

1 g	tryptone
0.25 g	yeast extract
0.025 g	NaCl
9.3 mg	KCl

Add water to 50 mL final volume. Adjust pH to 7.0 with sodium hydroxide. Autoclave for 20 minutes at 15 psi.

Vita

Israel Jerome Huff was born in Hamblen County, Tennessee in October of 1979. He attended school in Morristown, Tennessee and graduated from Morristown Hamblen High School West in 1997. From there he attended the University of Tennessee at Knoxville and earned a Bachelor of Science in Biochemistry, Cellular, and Molecular Biology in 2001. After graduation he continued in the Biochemistry, Cellular, and Molecular Biology Department and earned a Master of Science degree in 2005.